

AD-A259 020



AFIT/GE/ENG/92D-07

**AUTOMATED CONTROL OF AIRCRAFT
IN FORMATION FLIGHT**

THESIS

**Louis E. Buzogany
Captain, USAF**

AFIT/GE/ENG/92D-07

**DTIC
ELECTE
JAN 08 1993
S E D**

93-00074



Approved for public release; distribution unlimited

93 1 4 016

**AUTOMATED CONTROL OF AIRCRAFT
IN FORMATION FLIGHT**

THESIS

Presented to the Faculty of the School of Engineering

of the Air Force Institute of Technology

Air University

In Partial Fulfillment of the

Requirements for the Degree of

Master of Science in Electrical Engineering

Louis E. Buzogany, B.S. Electrical Engineering

Captain, USAF

Accession For	
NTIS CRA&I	<input checked="checked" type="checkbox"/>
DTIC TAB	<input type="checkbox"/>
Unannounced	<input type="checkbox"/>
Justification	
By	
Distribution /	
Availability Codes	
Dist	Avail and/or Special
A-1	

December, 1992

DTIC QUALITY INSPECTED 1

Approved for public release; distribution unlimited

Preface

The purpose of this study was to develop a control system capable of controlling a formation of aircraft. Special attention was placed on the analytical analysis of the control problem and the development of accurate, yet simple models of the formation aircraft. Motivated to improve the mission effectiveness of the Air Force Special Operations Forces, the C-130H aircraft was chosen as the primary formation aircraft.

The analytical analysis was performed on the formation flight control problem clearly indicates the necessity of integral control in the design of the automated formation flight control system. This analysis also revealed the interrelationship of the formation geometry, aircraft models and controller parameters on system stability. Further investigation led to the design of a three dimensional formation control system, two wing aircraft simulations and the development of a visualization tool in evaluating the formation flight control system.

In performing the research and writing this thesis, I have had a great deal of help from others. I am deeply indebted to my thesis advisors, Dr. Meir Pachter, Dr. John J. D'Azzo and Dr. C. Houppis. Their continued guidance and technical assistance proved invaluable during difficult times. Specifically, I am grateful for their mathematical and literary expertise. I am also grateful for the long-distance support and encouragement given by my parents throughout this endeavor. Their concern and interest was extremely beneficial.

Louis E. Buzogany

Table of Contents

	Page
Preface	ii
Table of Contents	iii
List of Figures	viii
List of Tables	xii
List of Symbols	xiii
Abstract	xviii
I. Introduction	1-1
1.1 Overview of the Thesis	1-1
1.2 Background	1-1
1.3 Problem Statement	1-5
1.4 Summary of Current Knowledge	1-6
1.5 Research Objective	1-7
1.6 Research Questions	1-7
1.7 Assumptions	1-8
1.8 Scope	1-9
1.9 Standards	1-9
1.10 Approach/Methodology	1-9
1.11 Benefits of the Research	1-10
1.12 Literature Review	1-10
1.12.1 Equation of Coriolis	1-10
1.12.2 Porter's Design Method	1-11
1.12.3 Large Aircraft Flying Qualities	1-12
1.13 Materials and Equipment	1-13

	Page
II. Simulation Development	2-1
2.1 Aircraft and Autopilot Models	2-2
2.1.1 First Order Models	2-2
2.1.2 Second Order Models	2-3
2.2 Aircraft Sensor Measurements	2-5
2.3 Formation Coordinate System	2-6
2.4 Kinematic Equations	2-6
2.5 Formation Controller Strategy	2-10
2.5.1 Closed Loop Control Using a PI Controller .	2-10
2.5.2 Closed Loop Control Using a Linear Mixer and a PI Controller	2-12
2.6 Measures of Merit	2-14
 III. Lead Aircraft's Trajectory in Wing Aircraft's Rotating Reference Frame	 3-1
3.1 Lead Aircraft's Trajectory using Lissajous Figures . .	3-1
3.2 Performance Evaluation using Lissajous Figures . . .	3-2
3.2.1 Diamond Formation Heading Change	3-2
3.2.2 Trail Formation Heading Change	3-5
3.3 Summary	3-7
 IV. Two Wing Aircraft Formation Flight Control	 4-1
4.1 Two Wing Formation Controller Implementation . . .	4-1
4.2 Inertial Calculations	4-2
4.3 Performance Evaluations	4-5
4.3.1 Trail Formation Heading Change	4-5
4.3.2 Diamond Formation Heading Change	4-8
4.4 Summary	4-11

	Page
V. Analytical Formation Flight Controller Synthesis	5-1
5.1 Theoretical Development	5-1
5.1.1 Y-Channel	5-6
5.1.2 X-Channel	5-9
5.2 Pole Placement through Controller Gain Adjustment: Residues of the Step Response for Preliminary Identifi- cation of Dominant Dynamics	5-12
5.2.1 Y-Channel Gains	5-15
5.2.2 X-Channel Gains	5-16
5.3 Performance Evaluations	5-17
5.3.1 Diamond Formation Heading Change	5-18
5.3.2 Diamond Formation Velocity Change	5-18
5.4 Summary	5-19
VI. Energy Conserving Maneuvers	6-1
6.1 Theoretical Development	6-1
6.2 X-Channel Controller Gain Adjustment	6-5
6.3 Performance Evaluations	6-5
6.3.1 Diamond Formation Side Step Maneuver	6-6
6.3.2 Diamond Formation 90 Degree Heading Change and Formation Transposition	6-7
6.4 Summary	6-10
VII. Automated Formation Flight Control Simulation using Second- Order C-130 Aircraft Models	7-1
7.1 Initial Performance Evaluation	7-1
7.1.1 Velocity Change Performance Evaluation	7-1
7.1.2 Heading Change Performance Evaluation	7-2
7.1.3 Altitude Change Performance Evaluation	7-4

	Page
7.2 Performance Evaluation using Modified PI Controller and Linear Mixer Gains	7-5
7.2.1 Velocity Change Performance Evaluation . . .	7-5
7.2.2 Heading Change Performance Evaluation . . .	7-6
7.2.3 Altitude Change Performance Evaluation . . .	7-7
7.3 Summary	7-7
VIII. Analysis and Conclusions	8-1
8.1 Analysis of Results	8-1
8.2 Display of Lead Aircraft's Trajectory as a Means of Evaluating the Formation Flight Control System's Per- formance	8-1
8.3 Two Wing Aircraft Formation Flight Control	8-1
8.4 Analytical Formation Flight Controller Synthesis . . .	8-2
8.5 Energy Conservation of Wing Aircraft	8-2
8.6 Computer Simulation of Formation Flight Control Sys- tem using Second-Order Aircraft Models	8-3
8.7 Conclusions	8-4
8.8 Recommendations for Further Study	8-5
8.9 Summary	8-5
Appendix A. Second-Order Aircraft Models and Large Aircraft Fly- ing Qualities	A-1
A.1 Theoretical Background	A-1
A.2 Design Example	A-4
A.3 Summary	A-7
Appendix B. C-130 Aircraft Models and Longitudinal and Lateral Autopilots	B-1
B.1 Longitudinal Autopilot and Reduced Order Models .	B-2

	Page
B.2 Lateral Autopilot and Reduced Order Model	B-6
B.3 Summary	B-9
Bibliography	BIB-1
Vita	VITA-1

List of Figures

Figure	Page
1.1. Trail Formation	1-2
1.2. Diamond Formation	1-3
1.3. Diamond Formation Heading Change Maneuver	1-4
1.4. Trail Formation Altitude Change Maneuver	1-4
1.5. Trail to Diamond Formation Change	1-5
1.6. Diamond Formation, 90 Degree Heading Change using Energy Conservation and Formation Transposition	1-6
1.7. Inertial and Rotating Frames of Reference	1-11
2.1. Block Diagram of Formation Control System Simulation	2-1
2.2. C-130B Aircraft Autopilot Models Time Response Comparison	2-5
2.3. Inertial Reference Frame and Separation Distances	2-7
2.4. Wing's Rotating Reference Frame and Separation Distances	2-8
2.5. Relative Motion Diagram	2-9
2.6. Formation Control System utilizing a PI Controller	2-11
2.7. Formation Control System utilizing a Linear Mixer and PI Controller	2-13
3.1. Example of Lead Aircraft's Trajectory Lissajous Figure	3-2
3.2. Diamond Formation, ± 30 Degrees Heading Change Time Response	3-3
3.3. Diamond Formation, +30 Degrees Heading Change (top), and -30 Degrees Heading Change (bottom), Lead Trajectory Lissajous Figures	3-4
3.4. Trail Formation, ± 30 Degrees Heading Change Time Response	3-5
3.5. Trail Formation, +30 Degrees Heading Change (top), and -30 Degrees Heading Change (bottom), Lead Trajectory Lissajous Figures	3-6
4.1. Two Wing Aircraft Formation Geometry	4-2

Figure	Page
4.2. Trail Formation, Two Wing Aircraft, +30 Degrees Heading Change Time Response	4-6
4.3. Trail Formation, Two Wing Aircraft, +30 Degrees Heading Change, Separation Distances	4-7
4.4. Lissajous Figure of Wing ₂ 's Trajectory in Wing ₁ 's Reference Frame, for a +30 Degrees Heading Change in Trail Formation	4-7
4.5. Diamond Formation, Two Wing Aircraft, +30 Degrees Heading Change Time Response	4-8
4.6. Trail Formation, Two Wing Aircraft, +30 Degrees Heading Change, Separation Distances	4-9
4.7. Lissajous Figure of Wing ₂ 's Trajectory in Wing ₁ 's Reference Frame, for a +30 Degree Heading Change in Diamond Formation	4-9
4.8. Diamond Formation, +30 Degrees Heading Change, Inertial Flight Paths	4-10
5.1. Formation Geometry	5-2
5.2. Comparison of Linear and Rate-Limited Velocity Responses	5-14
5.3. Y-Channel, Wing's Heading Step Response, Poles and Residues versus Controller Gains, $\frac{k_{yz}}{k_{yi}} = 100$	5-15
5.4. X-Channel, Wing's Velocity Step Response, Poles and Residues versus Controller Gains, $\frac{k_{yz}}{k_{yi}} = 100$	5-17
5.5. Diamond Formation, 10 Degrees Heading Change, Time Response Comparison	5-18
5.6. Diamond Formation, 375 to 400 fps Velocity Change, Time Response Comparison	5-19
6.1. X-Channel Design for Energy Conservation, Wing's Velocity Step Response, Poles and Residues versus Controller Gains, $\frac{k_{xyz}}{k_{xii}} = 100$	6-6
6.2. Diamond Formation 10 Degree Side Step Heading Change	6-7
6.3. Diamond Formation 90 Degree Heading and Formation Change utilizing Energy Conservation, Flight Path Illustration	6-8
6.4. Diamond Formation 90 Degree Heading and Formation Change Utilizing Energy Conservation; Time Responses	6-9

Figure	Page
6.5. Diamond Formation 90 Degree Heading and Formation Change Utilizing Energy Conservation, Flight Path in Inertial Frame	6-9
6.6. Diamond Formation 90 Degree Heading and Formation Change Utilizing Energy Conservation; 3-D Flight Path in Inertial Frame	6-10
7.1. Time Response Plots to a 400 fps Velocity Command, 1st and 2nd Order Aircraft, Initial Gains	7-3
7.2. Time Response Plots to a 30 Degrees Heading Command, 1st and 2nd Order Aircraft, Initial Gains	7-3
7.3. Time Response Plots for a 550 feet Altitude Change Command, 1st and 2nd Order Aircraft, Initial Gains	7-4
7.4. Time Response plots of a 400 fps Velocity Command, Diamond Formation, 1st and Second Order Models and Initial Controller Gains	7-6
7.5. Time Response plots of a 30 Degree Heading Command, Diamond Formation, 1st and Second Order Models and Modified Controller Gains	7-7
7.6. Time Response plots of a 550 feet Altitude Command, Diamond Formation, 1st and Second-Order Models and Initial Controller Gains	7-8
A.1. Overdamped Second Order Step Response, $a=2$, $b=1$	A-2
A.2. Overdamped Function OR x OD	A-4
A.3. C-130 Time Response Step Altitude Change	A-6
A.4. C-130 Altitude Time Response Comparison	A-7
B.1. C-130 Mach-Hold Autopilot Design	B-3
B.2. Mach-Hold Autopilot response to 10 fps Command Input	B-3
B.3. Time Response Comparison of Mach-Hold Autopilot and First-Order Approximation	B-4
B.4. Altitude-Hold Autopilot Control System Design	B-4
B.5. Time Response of the Altitude-Hold Autopilot to a 10 feet Step Altitude Command	B-5
B.6. Time Response Comparison of Altitude-Hold Autopilot and Second Order Approximation	B-6

Figure	Page
B.7. Lateral Directional Autopilot Control System Design	B-7
B.8. Time Response of the Lateral Directional Autopilot to a 10 Degree Heading Command	B-8
B.9. Time Response Comparison of Lateral Directional Autopilot and Second-Order Model Heading Response	B-8
B.10. MatrixX System Build Diagram of C-130 Autopilots	B-10

List of Tables

Table	Page
2.1. Aircraft Rate Limits and Model Time Constants	2-4
5.1. Y-Channel Routhian Array	5-8
5.2. X-Channel Routhian Array	5-12
5.3. Formation and Aircraft Parameters	5-14
5.4. PI Controller Gains	5-17
6.1. X-Channel Routhian Array	6-4
6.2. PI Controller Gains	6-6
7.1. Initial Performance Evaluation Parameters	7-2
7.2. Adjusted PI Controller and Mixer Performance Parameters	7-5
A.1. C-130 Altitude Response 2nd Order Parameters	A-5
B.1. Aircraft Flight Conditions and Parameters	B-2
B.2. Altitude-Hold 2nd Order Parameters	B-5

List of Symbols

Symbol		Page
$\dot{\mathbf{R}}_i$	velocity of object in frame i	1-10
$\dot{\mathbf{R}}_p$	velocity of object in frame p	1-10
ω_{ip}	angular velocity of frame p with respect to frame i	1-10
\mathbf{R}_p	position of object in frame p	1-11
t	time	1-12
$\dot{\mathbf{x}}(t)$	state vector	1-12
\mathbf{A}	state transition matrix	1-12
\mathbf{B}	input matrix	1-12
$\mathbf{u}(t)$	input vector	1-12
$\mathbf{y}(t)$	output vector	1-12
\mathbf{C}	output matrix	1-12
V_L	inertial velocity of lead aircraft	2-1
ψ_L	inertial heading of lead aircraft	2-1
h_L	inertial altitude of lead aircraft	2-1
V_{Lc}	inertial velocity command of lead aircraft	2-1
ψ_{Lc}	inertial heading command of lead aircraft	2-1
h_{Lc}	inertial altitude command of lead aircraft	2-1
V_W	inertial velocity of wing aircraft	2-1
ψ_W	inertial heading of wing aircraft	2-1
h_W	inertial altitude of wing aircraft	2-1
V_{Wc}	inertial velocity command of wing aircraft	2-1
ψ_{Wc}	inertial heading command of wing aircraft	2-1
h_{Wc}	inertial velocity command of wing aircraft	2-1
x^W	x separation distance	2-1
y^W	y separation distance	2-1

Symbol		Page
z^W	z separation distance	2-1
x_c^W	x separation distance command	2-1
y_c^W	y separation distance command	2-1
z_c^W	z separation distance command	2-1
V	aircraft's velocity	2-3
V_c	aircraft's velocity command	2-3
τ_V	velocity time constant of first-order aircraft model	2-3
ψ	aircraft's heading	2-3
ψ_c	aircraft's heading command	2-3
τ_ψ	heading time constant of first-order aircraft model	2-3
h	aircraft's altitude	2-3
h_c	aircraft's altitude command	2-3
τ_h	altitude time constant of first-order aircraft model	2-3
a_ψ	second order real pole, heading channel	2-4
b_ψ	second order real pole, heading channel	2-4
a_h	second order real pole, altitude channel	2-4
b_h	second order real pole, altitude channel	2-4
V_{WL}^W	lead's velocity with respect to the wing, expressed in wing's frame	2-7
V_L^W	lead's inertial velocity in wing's frame	2-7
ω_W^W	angular velocity of wing's frame expressed in wing's frame . . .	2-7
R_{WL}^W	position of lead with respect to wing expressed in wing's frame	2-8
V_W^W	wing's velocity expressed in its own frame of reference	2-8
C_L^W	direction cosine matrix, lead to wing transformation	2-8
ψ_E	$\psi_L - \psi_W$, heading error between lead and wing	2-8
x	$x_c^W - x^W$, x separation error	2-12
y	$y_c^W - y^W$, y separation error	2-12
z	$z_c^W - z^W$, z separation error	2-12

Symbol		Page
k_{xp}	x-channel proportional gain	2-12
k_{xi}	x-channel integral gain	2-12
k_{yp}	y-channel proportional gain	2-12
k_{yi}	y-channel integral gain	2-12
k_{zp}	z-channel proportional gain	2-12
k_{zi}	z-channel integral gain	2-12
V_E	$V_L - V_W$, velocity error signal	2-14
k_V	velocity error signal mixer gain	2-14
k_ψ	heading error signal mixer gain	2-14
k_X	x-separation error signal mixer gain	2-14
k_Y	y-separation error signal mixer gain	2-14
X_L^I	lead's inertial position along X^I axis	4-3
Y_L^I	lead's inertial position along Y^I axis	4-3
$X_{W_1}^I$	wing ₁ 's inertial position along Y^I axis	4-3
$Y_{W_1}^I$	wing ₁ 's inertial position along Y^I axis	4-3
ψ_{W_1}	wing ₁ 's inertial heading	4-3
$X_{W_2}^I$	wing ₂ 's inertial position along Y^I axis	4-3
$Y_{W_2}^I$	wing ₂ 's inertial position along Y^I axis	4-3
ψ_{W_2}	wing ₂ 's inertial heading	4-3
$R_{W_1L}^I$	lead-wing ₁ inertial separation	4-4
$R_{W_2L}^I$	lead-wing ₂ inertial separation	4-4
$R_{W_1W_2}^I$	wing ₂ -wing ₁ inertial separation	4-4
$C_{W_n}^I$	direction cosine matrix, nth wing to inertial frame of reference (f.o.r.)	4-4
ψ_{W_n}	nth wing aircraft's inertial heading	4-4
x_n	nth wing x-separation in its f.o.r.	4-4
y_n	nth wing y-separation in its f.o.r.	4-4

Symbol		Page
z_n	nth wing z-separation in its f.o.r.	4-4
$R_{W_n L}^{W_n}$	lead's position with respect the nth wing aircraft	4-4
x_o	nominal x-separation	5-2
y_o	nominal y-separation	5-2
α	separation angle	5-2
τ_{V_W}	wing's first order velocity time constant	5-3
τ_{ψ_W}	wing's first order heading time constant	5-3
l	characteristic length, nominal formation separation	5-4
\bar{t}	characteristic time	5-4
V_o	nominal formation velocity	5-4
\hat{x}	non-dimensional x-separation error	5-4
\hat{y}	non-dimensional y-separation error	5-4
\hat{x}_o	non-dimensional nominal x-separation	5-4
\hat{y}_o	non-dimensional nominal y-separation	5-4
\hat{V}_W	non-dimensional wing velocity	5-4
\hat{V}_{Wc}	non-dimensional wing velocity command	5-4
$\hat{\tau}_{V_W}$	non-dimensional wing velocity time constant	5-4
$\hat{\tau}_{\psi_W}$	non-dimensional wing heading time constant	5-4
\hat{V}_L	non-dimensional lead velocity	5-5
D	disturbance input matrix	5-5
Γ	disturbance input vector	5-5
\hat{k}_{yp}	non-dimensional, y-separation error, proportional gain	5-6
\hat{k}_{yi}	non-dimensional, y-separation error, integral gain	5-6
X_y	augmented y-channel state vector	5-7
A_y	augmented y-channel state transition matrix	5-7
Γ_y	augmented y-channel disturbance input matrix	5-7
D_y	augmented y-channel disturbance input vector	5-7

Symbol		Page
Y_y	augmented y-channel output vector	5-7
C_y	augmented y-channel output matrix	5-7
\hat{k}_{xp}	non-dimensional, x-separation error, proportional gain	5-10
\hat{k}_{xi}	non-dimensional, x-separation error, integral gain	5-10
X_x	augmented x-channel state vector	5-10
A_x	augmented x-channel state transition matrix	5-10
Γ_x	augmented x-channel disturbance input matrix	5-10
D_x	augmented x-channel disturbance input vector	5-10
Y_x	augmented x-channel output vector	5-10
C_x	augmented x-channel output matrix	5-11
g	acceleration of gravity	6-1
e_w	wing aircraft's specific energy	6-1
ξ	altitude to velocity proportionality constant	6-2
\hat{k}_{xzp}	non-dimensional, 3-D x-separation error, proportional gain	6-2
\hat{k}_{xzi}	non-dimensional, 3-D x-separation error, integral gain	6-2
X_{xz}	augmented x-channel state vector	6-3
A_{xz}	augmented x-channel state transition matrix	6-3
Γ_{xz}	augmented x-channel disturbance input matrix	6-3
D_{xz}	augmented x-channel disturbance input vector	6-3
Y_{xz}	augmented x-channel output vector	6-3
C_{xz}	augmented x-channel output matrix	6-3
ω_n	undamped natural frequency	A-3
ζ	damping ratio	A-3
OR	onset rate	A-5
OD	onset delay	A-5
$h(t)$	altitude response of the C-130 to a step input	A-5
t^*	time of the maximum rate of change of $h(t)$	A-5

Abstract

In this study, an automated formation control system for an aircraft formation comprised of one lead and multiple wing aircraft is analyzed. Second-order models of the C-130 aircraft are developed in order to accurately model the flying qualities of large aircraft. This automated formation control system is capable of controlling the C-130 aircraft in maneuvering formation flight, thus reducing the wing's pilot workload.

During formation flight, the wing aircraft continuously measures the lead aircraft's relative position with an ideal on-board position sensor. This information, in addition to Proportional Plus Integral feedback control, is used to maintain the aircraft in formation. The control of each wing aircraft is assumed to be independent of other wing aircraft. Other than for nominal formation separation commands, no continuous communication is assumed between the formation aircraft.

An analytical analysis of the formation control problem reveals that integral control is needed to achieve zero steady state error in the separation distances (after a formation maneuver is executed). This conclusion is confirmed using computer simulations. An analytical method of selecting the Proportional Plus Integral parameters is developed by identifying the dominant system dynamics and residues of the step response. In an attempt to reduce the fuel consumption of the wing aircraft during formation heading change maneuvers, an alternate control system is designed to conserve the energy of the wing aircraft. Thus, an altitude change is used to control the wing aircraft's velocity, minimizing the use of the throttles during a heading change maneuver.

The resulting automated formation control system effectively maintains the formation of aircraft through a combination of velocity, heading, and altitude changes. There is zero steady state error for all maneuver and separation distance change responses. Additionally, the separation transients are such that no collisions occur between the aircraft. Both analytical equations and computer simulation generated time responses are provided for reference.

AUTOMATED CONTROL OF AIRCRAFT IN FORMATION FLIGHT

I. Introduction

1.1 Overview of the Thesis

The introduction and general background information relevant to the formation flight control problem is provided in Chapter I. The simulation development, aircraft autopilot models, and formation controller design is presented in Chapter II. A method of evaluating the transient response of the formation flight control system by displaying the lead aircraft's trajectory in the wing aircraft's reference frame is presented in Chapter III. A two wing aircraft formation and performance simulation is presented in Chapter IV. A detailed derivation of a linear and parametrized Multi-Input Multi-Output (MIMO) plant used to analytically determine the optimal Proportional Plus Integral (PI) control parameters for the formation flight control problem is presented in Chapter V. Chapter VI presents the theoretical analysis and computer simulation of an 3-Dimensional (3D) formation flight control system based on energy conservation of the wing aircraft. A performance evaluation of the formation flight control system incorporating second-order aircraft models is presented in Chapter VII. The method used to obtain second-order aircraft models is presented in Appendix A. The design and computer simulation of longitudinal and lateral autopilots developed around the C-130 aircraft is included in Appendix B. Conclusions and areas requiring further study are presented in Chapter VIII.

1.2 Background

Military pilots are required to fly many missions that require extended periods of formation flight. During these periods, the pilot's attention is divided between monitoring the instruments of his aircraft, and maintaining the correct separation distance to the adjacent aircraft. The denser the formation of aircraft, the more time the pilot spends on maintaining the formation. As other conditions, such as visibility, navigation and enemy

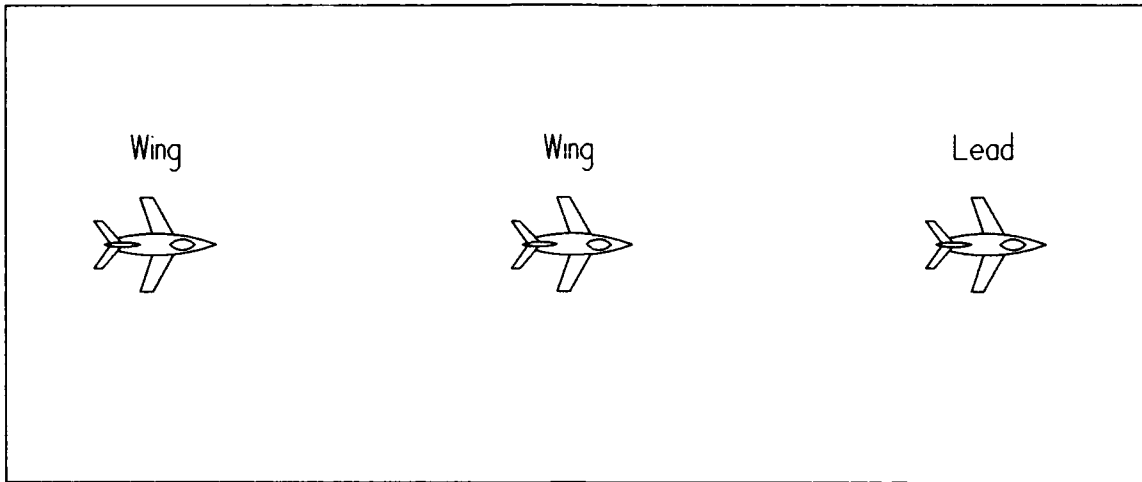


Figure 1.1. 'Trail Formation

threat begin to require more of the pilot's attention, the more difficult it is for him to maintain the formation(2)[1-2].

An automated formation flight control system is developed to relieve the strain on military pilots during formation flight. This system is analogous to an autopilot used on a single aircraft, except that this "autopilot" is used to control a formation of aircraft.

The Air Force Special Operations Forces (SOF) perform missions involving extended periods of formation flight that place heavy workloads on the pilots. SOF pilots are tasked to conduct overt, clandestine, or covert missions which can range from routine training missions to highly sensitive missions of national importance(2)[1-2]. Many times these missions require close formation flight at low altitudes, using similar or dissimilar aircraft. The C-130 aircraft are predominantly used during these missions.

The C-130 aircraft, models C-130A and C-130B, fly several typical formations, including the trail and diamond formations. The trail formation is shown in Figure 1.1, while the diamond formation is shown in Figure 1.2. The trail formation is important since a minimum amount of land mass is overflown by the formation aircraft, translating to a reduced probability of detection by ground forces. The diamond formation maintains good visibility between the various aircraft.

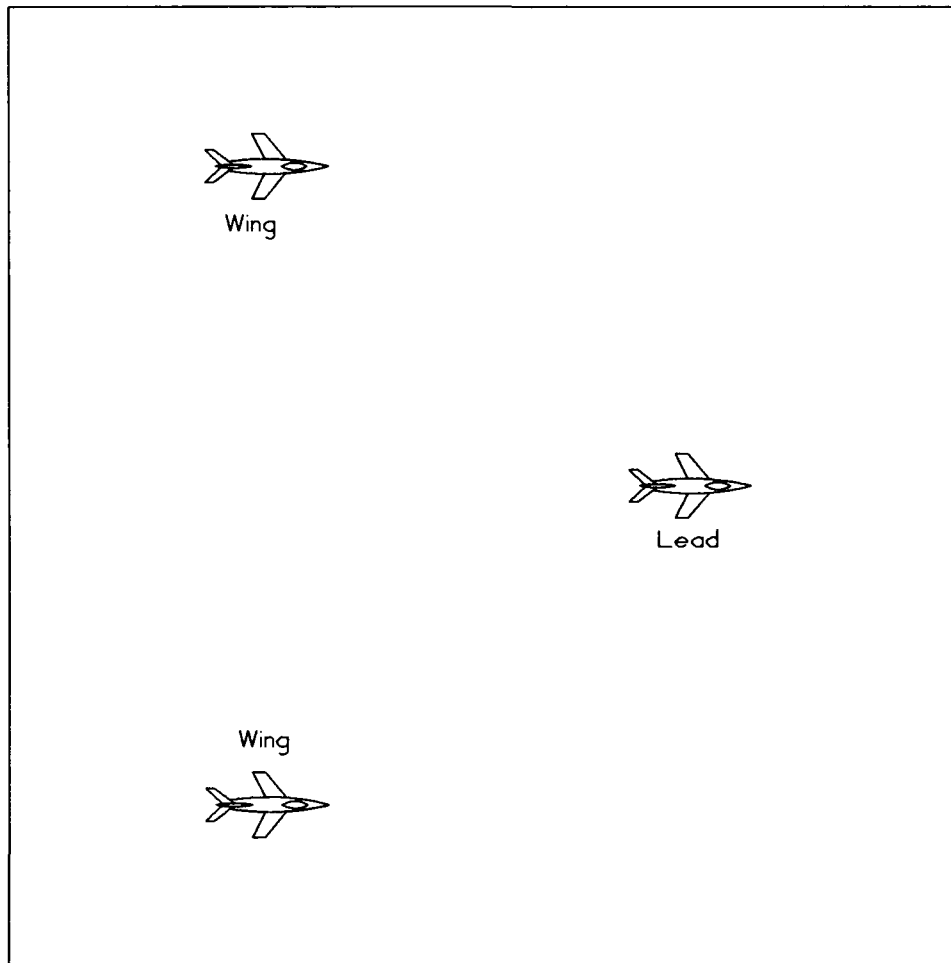


Figure 1.2. Diamond Formation

Various maneuvers are performed while the aircraft are flying in formation. These maneuvers are initiated by the lead aircraft, without prior knowledge of the wing aircraft. The lead aircraft may initiate a change in velocity, heading, altitude, or a combination of the three. Figure 1.3 shows a heading change maneuver and Figure 1.4 shows an altitude change maneuver. These maneuver's are executed from a diamond formation and a trail formation respectively. Depending on varying conditions and mission requirements, the formation used by SOF aircraft may change throughout the flight. A change from trail formation to diamond formation is shown in Figure 1.5.

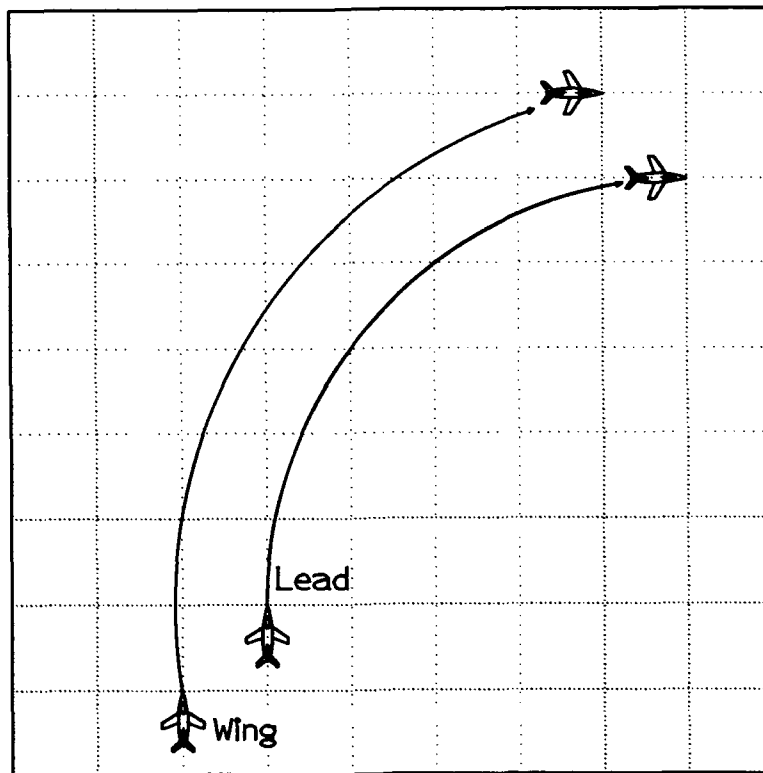


Figure 1.3. Diamond Formation Heading Change Maneuver

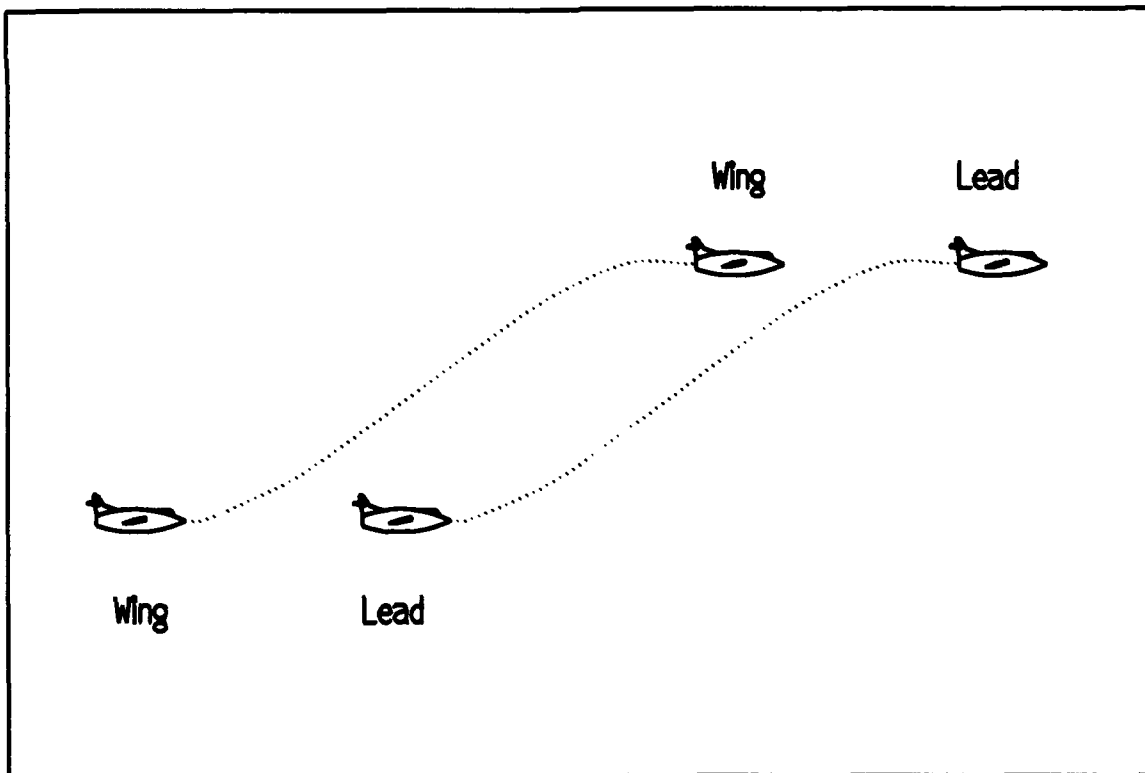


Figure 1.4. Trail Formation Altitude Change Maneuver

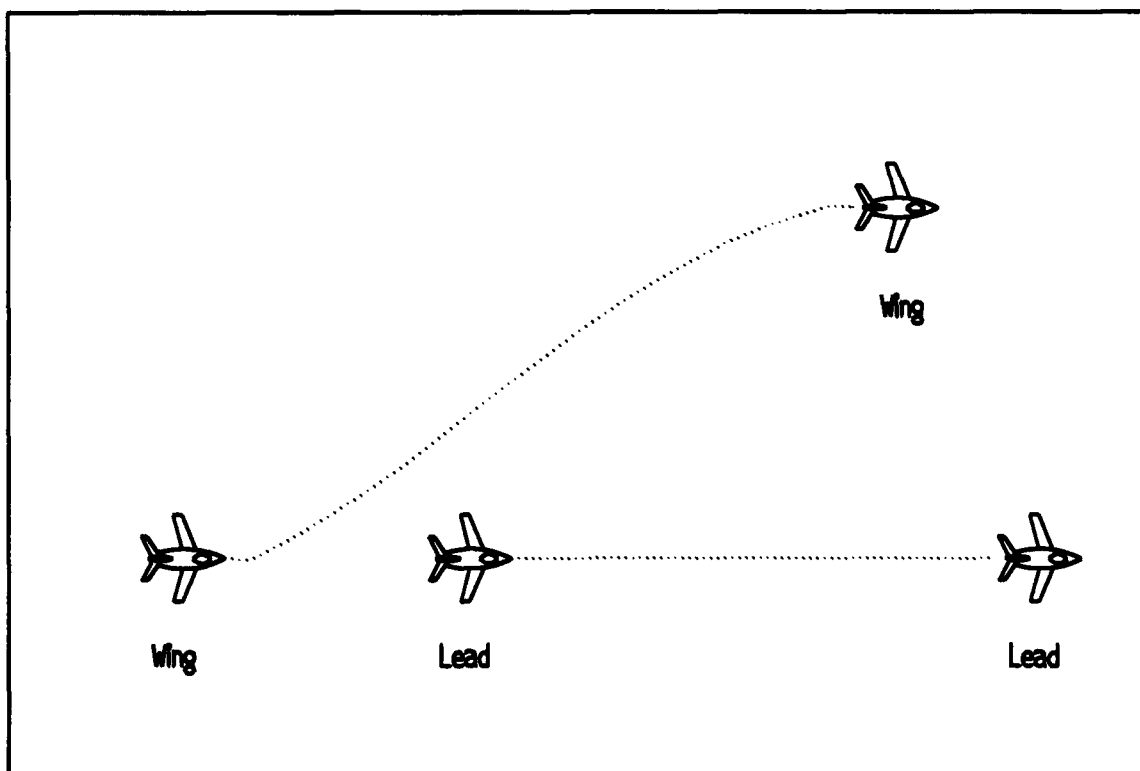


Figure 1.5. Trail to Diamond Formation Change

The most difficult maneuver for the wing aircraft is a large heading change in a diamond formation. This type of maneuver is shown in Figure 1.3. The wing aircraft must initially increase its velocity and traverse the outside path in order to track the lead aircraft, following which the wing aircraft will reduce its speed. This modulation of the velocity results in increased fuel consumption. In an attempt to save fuel, it is customary for the pilot of the wing aircraft to initially descend to increase his velocity during the maneuver, and then to ascend to bleed off any excess airspeed. Considering a single wing aircraft formation, the wing's pilot may also initiate an altitude change in addition to a heading change. An example of such a maneuver is shown in Figure 1.6. This type of maneuver is addressed in detail in Chapter VI.

1.3 Problem Statement

The problem of improving SOF mission effectiveness through the implementation of an automated formation flight control system is addressed in this thesis. The automated

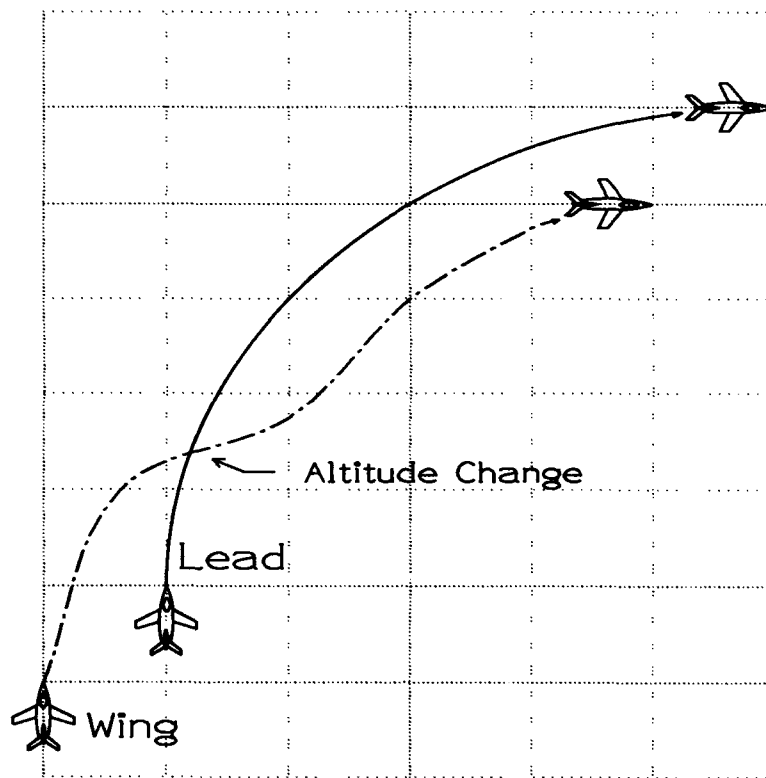


Figure 1.6. Diamond Formation, 90 Degree Heading Change using Energy Conservation and Formation Transposition

formation flight control system will both relieve pilot fatigue and allow the performance of other tasks during the formation flight. Accurate aircraft models and thorough control system analysis directly impacts the validity of the final results. Thus, the purpose of this thesis is to develop models and methods needed to design an automated formation flight control system to control a formation of aircraft.

1.4 Summary of Current Knowledge

Two previous theses research efforts by Capt Paul Rohs and Capt John Dargan at the Air Force Institute of Technology (AFIT) investigated the development of an automated formation flight control system. Both used a digital computer simulation for development and evaluation. Capt Rohs developed a control system capable of controlling a formation of similar or dissimilar aircraft through three separate maneuvers(9). These maneuvers included a heading change, a terrain avoidance altitude change, and a formation change.

Aircraft position was measured using a Cartesian reference system. It was assumed that perfect lead aircraft position information was available to each wing aircraft control system. First order mathematical models of different aircraft were used in the simulations. Capt Dargan continued Capt Roh's research and developed a control system composed of a PI controller and a linear mixer. Formations consisting of one lead and one wing aircraft were used for simulation and evaluation. First order models of C-130 aircraft were also used. The results of this research showed that a PI controller can be developed for an automated formation flight control system that maintains formation, without collisions, and provides satisfactory transient behavior with zero steady state error(2)[6-5].

1.5 Research Objective

The objective of this research is to continue the development of an automated formation flight control system through an analytical analysis of the formation flight control problem and computer simulations using more realistic aircraft models.

1.6 Research Questions

The following questions are answered in this thesis.

1. Can second-order aircraft models be developed in order to more accurately model the flight performance of the C-130 aircraft?
2. What is the effect of second-order aircraft models on the response of the formation flight control system.
3. Can the current formation control system containing the PI controller and linear mixer be used to address the two wing aircraft formation flight control problem?
4. Can the derivation of a linear and parametrized MIMO plant be used to analytically determine the optimal control gains for the formation flight control problem.?
5. Can a flight control system be developed to perform 3-Dimensional maneuvers in order to reduce the fuel consumption of the wing aircraft during heading change maneuvers?

6. Can a tool for evaluating the formation flight control system be developed by graphically displaying the trajectory of the lead aircraft with respect to the wing?

1.7 Assumptions

In support of the thesis objectives, and questions listed earlier, the following assumptions are made:

The lead aircraft is piloted by a human pilot, while the wing aircraft are controlled by the formation control system. The formation of aircraft is referenced to the lead aircraft. Thus all formation maneuvers are initiated by the pilot of the lead aircraft with no prior knowledge of the maneuvers given to the wing aircraft. Each wing aircraft contains the formation flight control system avionics, independent of the system mounted on the other aircraft in the formation.

Each wing aircraft is assumed to possess an on-board sensor capable of providing precise position information relative to the wing aircraft⁽²⁾[1-12]. This sensor measurement data is used to track the lead aircraft.

Each aircraft in the formation contains an automated flight control system capable of maintaining or changing the aircraft's velocity, heading and altitude. Thus, each aircraft is endowed with an Mach-Hold autopilot, capable of adjusting the aircraft's forward velocity to control separation along the flight path, a Heading-Hold autopilot for performing coordinated turns for lateral separation control, and an Altitude-Hold autopilot for climbing or ascending for vertical separation control. The mathematical autopilot models used in this simulation are based on the performance of the C-130 aircraft. Both first and second order aircraft/autopilot models are used. The first order models are used in analytical analyses and for performance comparison against previous research.

The initial conditions for all formation maneuvers are straight and level flight in a constant formation. Formation maneuvers are executed one at a time; however, simultaneous heading change maneuvers and formation transpositions are considered.

1.8 Scope

The objective of this research is to develop a mathematical control law capable of controlling a formation of aircraft under realistic (simulation) conditions. The system designed for this research is developed through the use of the MATRIX_x CAD tool. Even though two different models of the C-130 are available, the C-130B is used as the primary formation aircraft. Under the assumption that perfect position information is available, position sensor models are not used. This research is not intended to result in the hardware fabrication of the formation control system. Hence, hardware specifications such as power, weight and size requirements are not addressed(2)[1-13].

1.9 Standards

Conventional control system analysis and design standards are used in this research. Control system responses to input commands are analyzed with respect to stability, transient behavior and steady state values. Time-response specifications of rise time, settling time, peak overshoot and steady state error is emphasized (7:90). While simulation tools are available that are capable of measuring these time response specifications, the primary means of evaluating the transient response is the shape of the output waveform.

1.10 Approach/Methodology

The formation control systems developed by Captains Rohs and Dargan serve as a foundation for this research. The PI controller developed by Capt Dargan is verified through simulation on the digital computer. Upon verification, this system is used as a starting point, and modified as needed during the design process.

The premise of using Dargan's formation control system as a starting point is justified since his research showed that the system worked under the given assumptions. Therefore, since a system has been previously designed and has been shown to work, it is not necessary to start over and design a completely new system. This system is used for the majority of the simulations and theoretical analyses.

1.11 Benefits of the Research

This research provides a method of designing a control system able to maintain a formation during maneuvers and able to command separation distances. Related research is being conducted by the Intra Formation Positioning System (IFPS) program at the Flight Dynamics Laboratory. This thesis provides an additional approach to the formation flight control problem. The ideas and information from this research may be used in the IFPS program to help solve a real world problem.

1.12 Literature Review

The following technical literature dealing with the application of control theory to aircraft formation flight is reviewed. This review includes the equation of Coriolis, Porter's Method for controller design, and large aircraft flying qualities. This review, in addition to the previous research by Dargan and Rohs, gives the background information needed to develop the simulation model of a formation control system.

1.12.1 Equation of Coriolis The equation of Coriolis is needed when the motion of one object, relative to another object in a different rotating reference frame, is desired. The motion of this object, as viewed from the rotating reference frame, consists of the motion as seen from its moving frame, plus the motion resulting from the relative angular velocity of the moving frame with respect to the inertial reference frame(1)[489]. This situation is illustrated in Figure 1.7. The equation of Coriolis is

$$\dot{\mathbf{R}}_i = \dot{\mathbf{R}}_p + \omega_{ip} \times \mathbf{R}_p \quad (1.1)$$

where

$\dot{\mathbf{R}}_i$ = velocity of object in frame i

$\dot{\mathbf{R}}_p$ = velocity of object in frame p

ω_{ip} = angular velocity of frame p with respect to frame i

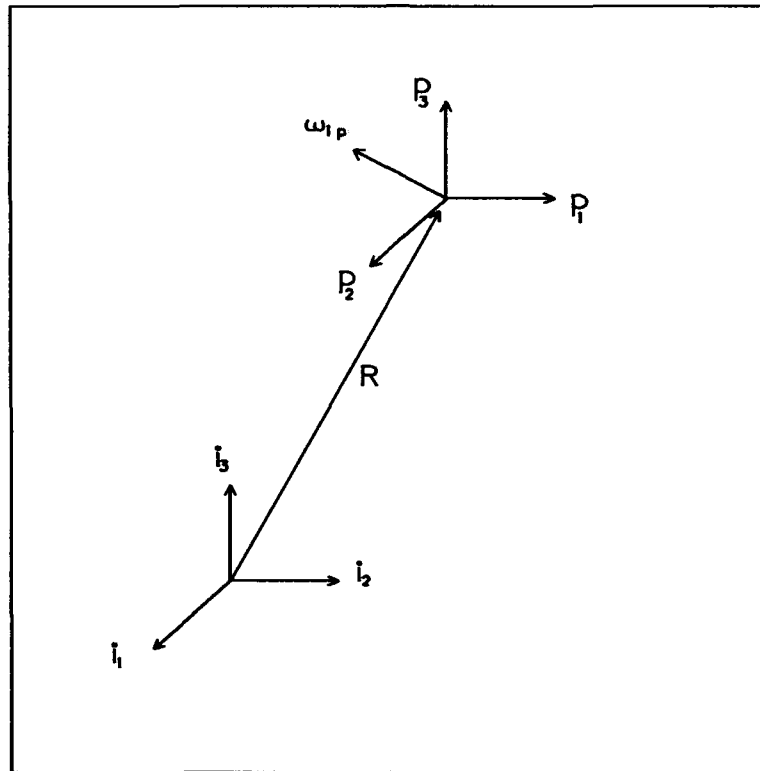


Figure 1.7. Inertial and Rotating Frames of Reference

R_p = position of object in frame p

The equation of Coriolis is also referred to as the velocity transformation law. This equation is useful in expressing the lead aircraft's velocity in the wing aircraft's rotating reference frame.

1.12.2 Porter's Design Method The decoupling of the outputs is an essential requirement in many multi-input multi-output (MIMO) control systems. Some design methods require that all the states must be fed back in order to achieve output decoupling. Depending upon the dimension of the state vector, it may not be physically possible to include enough sensors which will measure all of the states. It may be necessary in this case to use a state estimator or observer to reconstruct the states, and then feed back these estimated states. However, a control design method which uses only output feedback to generate an error vector avoids the requirement for measuring or reconstructing the entire state vector. One such method is that developed by Brian Porter (7) (8). His method

of designing a high gain proportional plus integral controller produces output decoupling and leads to very fast tracking of the command input by the output. The MIMO plant is represented by the standard state and output equations, of the respective forms:

$$\dot{\mathbf{x}}(t) = \mathbf{A}\mathbf{x}(t) + \mathbf{B}\mathbf{u}(t) \quad (1.2)$$

$$\mathbf{y}(t) = \mathbf{C}\mathbf{x}(t) \quad (1.3)$$

where

t = time

$\dot{\mathbf{x}}(t)$ = state vector

\mathbf{A} = state transition matrix

\mathbf{B} = input matrix

$\mathbf{u}(t)$ = input vector

$\mathbf{y}(t)$ = output vector

\mathbf{C} = output matrix

A requirement for Porter's design method is that the matrix product \mathbf{CB} have full rank. When \mathbf{CB} has full rank the plant is described as "regular". When \mathbf{CB} does not have full rank the plant is described as "irregular". In the case of regular plants the controller implements a proportional plus integral control law in the forward path of the control system. In the case of irregular plants, the proportional plus integral control is augmented with an inner-loop which provides extra measurements for control purposes (3:660-661).

1.12.3 Large Aircraft Flying Qualities Flying qualities are defined as those characteristics of an aircraft that govern the ease and precision with which a pilot is able to perform his mission (5)[456]. There are significant differences in the flying capabilities between large and relatively small aircraft. These differences are reflected in the short period frequency in the longitudinal mode, the time to bank in the lateral mode, and the time delay for all axes. Of special importance, in terms of modelling the flying performance of the aircraft, is the time delay.

The time delay is measured as the time from the initiation of a step control input, until the first indication of the overall aircraft response (5)[459]. Even though time delays degrade the flying qualities rating of the aircraft, and may result in Pilot Induced Oscillations (PIOs), time delays greater than 1 second have been measured (5)[460]. The presence of these delays, especially in large aircraft, reinforces the motivation to develop second order models for the formation control system simulation.

1.13 Materials and Equipment

The following equipment and materials are required for this research:

- The MATRIX_x Computer Aided Design tool. Both the Unix Open Windows and the IBM PC compatible versions are used.
- The Sun SPARC workstation computers located in the AFIT/ENG computer lab in room 133 in building 640.
- Both personal and AFIT/ENG IBM compatible personal computers.
- Generic CADD 5.0 computer-aided drafting software, personal copy.
- Latex document preparation software, Unix and IBM PC versions.

II. Simulation Development

A block diagram representing the computer simulation used to model the formation flight control system is shown in Figure 2.1. The lead aircraft is totally independent of the wing aircraft. The information about the lead aircraft available to the wing aircraft is acquired by its external sensors. The external sensors, kinematic calculations, formation control law and formation separation commands are implemented in the wing aircraft block/module. Thus additional aircraft can be added to the formation simulation by duplicating the Wing Aircraft block. This is explained in detail in Chapter IV.

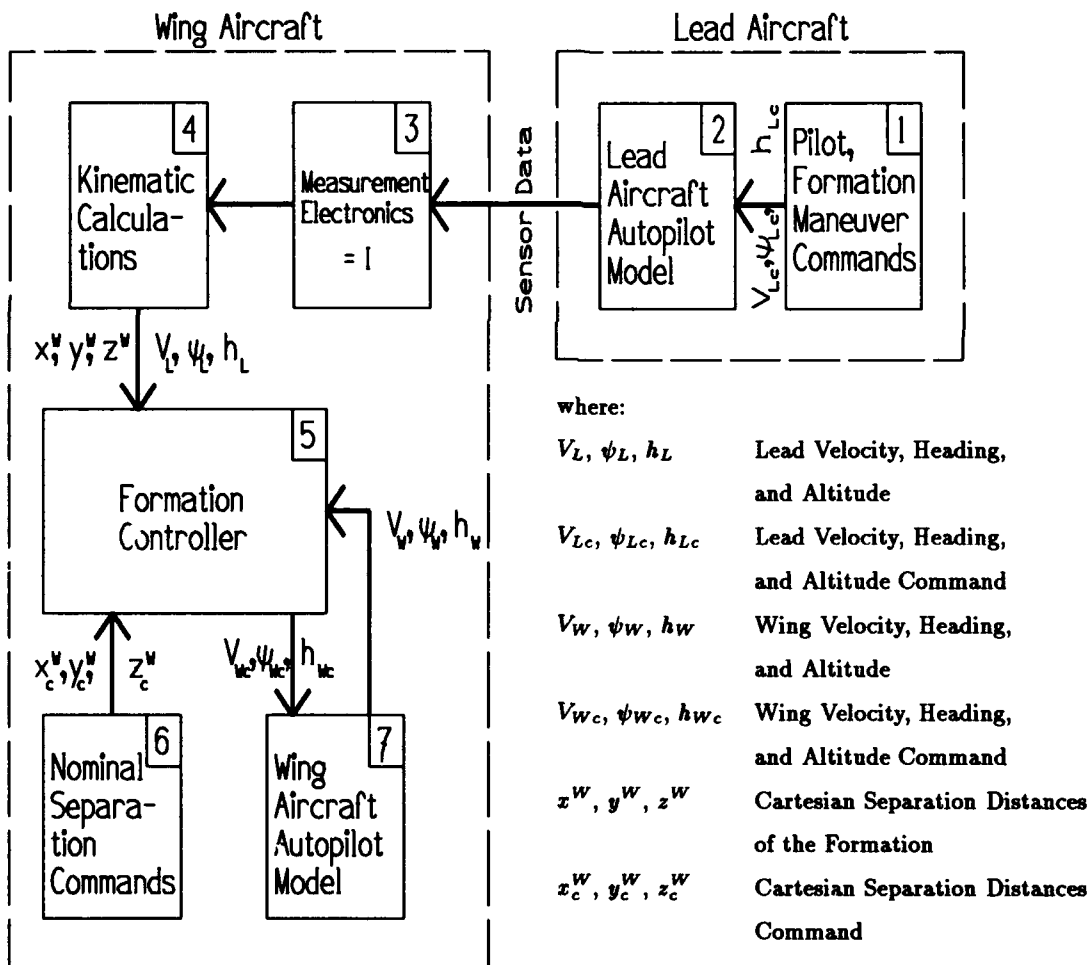


Figure 2.1. Block Diagram of Formation Control System Simulation

The following steps describe in detail the simulation of a typical formation maneuver initiated by the lead aircraft:

1. The pilot of the lead aircraft, block 1, commands a velocity, heading, or altitude change. The lead aircraft, block 2, responds to this command.
2. The sensors on the wing aircraft, block 3, relay the lead aircraft's positional data to the kinematics calculations, block 4. This block calculates the actual separation distances and the lead aircraft's position, velocity, and heading. This information is relayed to the formation controller.
3. The formation controller, block 5, receives nominal separation information from block 6, and kinematic information from block 4. An error signal is constructed by extracting the difference between the commanded and actual separation parameters.
4. The formation controller implements a Proportional Plus Integral control law, commanding the wing aircraft, block 7, in order to null the error signal.
5. This process continues as long as the formation control system is engaged.

If a formation separation change is required, then block 6, the nominal separation commands, would send this information to the formation controller. The following sections describe in detail, the key blocks comprising the formation control system simulation.

2.1 Aircraft and Autopilot Models

2.1.1 First Order Models A major component of the formation control system simulation are the aircraft and autopilot models, blocks 2 and 7 in Figure 2.1. Previous research by Dargan(2) and Rohs(9) developed first-order transfer functions modelling the response of autopilot equipped C-130H aircraft. The lateral and longitudinal autopilots were divided into three separate channels, velocity, (magnetic) heading, and altitude. The transfer functions for these channels are shown in Eqs (2.1) to (2.3) (2)[3-3].

$$\frac{V(s)}{V_c(s)} = \frac{\frac{1}{\tau_v}}{s + \frac{1}{\tau_v}} \quad (2.1)$$

$$\frac{\psi(s)}{\psi_c(s)} = \frac{\frac{1}{\tau_\psi}}{s + \frac{1}{\tau_\psi}} \quad (2.2)$$

$$\frac{h(s)}{h_c(s)} = \frac{\frac{1}{\tau_h}}{s + \frac{1}{\tau_h}} \quad (2.3)$$

where

V = aircraft's velocity

V_c = aircraft's velocity command

τ_V = velocity time constant of first-order aircraft model

ψ = aircraft's heading

ψ_c = aircraft's heading command

τ_ψ = heading time constant of first-order aircraft model

h = aircraft's altitude

h_c = aircraft's altitude command

τ_h = altitude time constant of first-order aircraft model

The performance variation between the three channels dynamics is due to the differences in their first-order time constants τ_V , τ_ψ and τ_h , respectively. Additionally, two models of the C-130, the C-130A and the C-130B, are simulated. While the same linear transfer functions are used for both aircraft, they differ in their velocity, heading and climb rate limits(2)[3-2]. Table 2.1 displays the time constants and rate limits for each aircraft.

2.1.2 Second Order Models Second Order Aircraft models are based on second order linear transfer functions that incorporate a time delay and a maximum rate of change. These transfer functions can better model physical systems that exhibit an appreciable amount of delay in their time response. Additionally, a second-order transfer function can model both an underdamped or an overdamped time response.

A major difficulty in deriving second order autopilot models of the C-130 aircraft is the acquisition of accurate flight performance data. Consequently, the second order

Table 2.1. Aircraft Rate Limits and Model Time Constants

Aircraft and Parameter	Lower Limit	Upper Limit	τ_v	τ_ψ	τ_h
C-130A					
Constants			.333 secs	1.5 secs	2 s
Velocity	304 ft/s	422 ft/s			
Heading	-3 deg/s	3 deg/s			
Altitude	-42 ft/s	8.5 ft/s			
C-130B					
Constants			.333 secs	1.5 secs	2 secs
Velocity	304 ft/s	422 ft/s			
Heading	-4.7 deg/s	4.7 deg/s			
Altitude	-42 ft/s	33 ft/s			

transfer functions are developed from computer simulations of linear bare aircraft state space models, equipped with basic autopilots. The theoretical method for synthesizing the augmented transfer functions is contained in Appendix A. Appendix B describes in detail, the autopilot design and second order transfer function derivation. The new transfer functions for the C-130 are shown below:

$$\frac{V(s)}{V_c(s)} = \frac{\frac{1}{\tau_v}}{s + \frac{1}{\tau_v}} = \frac{0.1}{(s + 0.1)} \quad (2.4)$$

$$\frac{\psi(s)}{\psi_c(s)} = \frac{a_\psi b_\psi}{(s + a_\psi)(s + b_\psi)} = \frac{0.296}{(s + 0.544)(s + 0.544)} \quad (2.5)$$

$$\frac{h(s)}{h_c(s)} = \frac{a_h b_h}{(s + a_h)(s + b_h)} = \frac{0.211}{(s + 1.625)(s + 0.13)} \quad (2.6)$$

where

a_ψ = second order real pole, heading channel

b_ψ = second order real pole, heading channel

a_h = second order real pole, altitude channel

b_h = second order real pole, altitude channel

Of special note is the velocity channel transfer function, Eq (2.4). This channel is best modeled by a first order transfer function similar to Eq (2.1), except that now the (realistic) time constant is 10 seconds, as opposed to 0.333 seconds. The same rate limiters distinguishing the C-130A from the C-130B models are used with the second order transfer functions. A comparison of the new and previous autopilot models time responses to a step input is shown in Figure 2.2. The time responses of the new autopilot models are

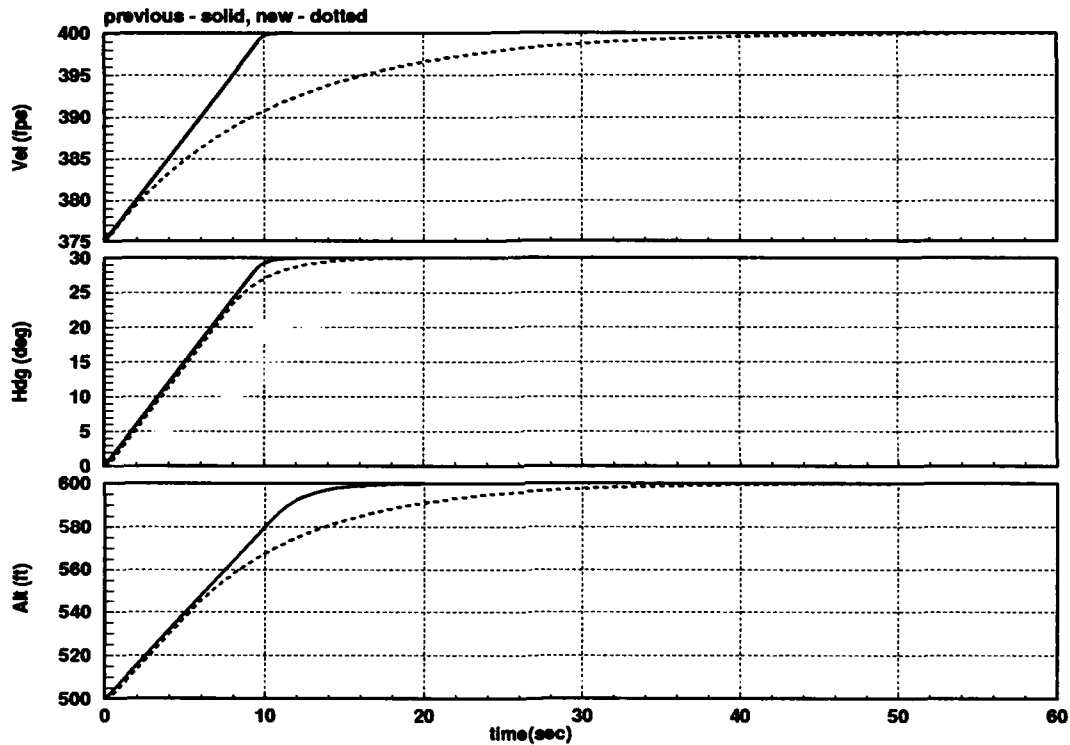


Figure 2.2. C-130B Aircraft Autopilot Models Time Response Comparison

slower than the previous models. Consequently, the controller parameters determined in previous research need to be reevaluated. The first order models are used, due to their simplicity, for theoretical analysis and performance comparison against previous research. The new models are used to validate the final control system parameters.

2.2 Aircraft Sensor Measurements

An on-board sensor capable of providing relative position and velocity information of the lead aircraft with respect to the wing is needed (2)[3-8]. A Kalman Filter can be used

to process the available measurements in order to estimate non-measured parameters and improve the accuracy of the measured data. For the purposes of the computer simulation, perfect measurement data is assumed.

2.3 Formation Coordinate System

Two coordinate reference frames, an inertial and a rotating reference frame centered on the wing aircraft, are used in this research(2)[3-8].

The inertial reference frame has a stationary origin, with latitude, longitude, and altitude as its axes(2)[3-9]. During computer simulation, the lead aircraft begins all maneuvers on the inertial axis, at an altitude of 500 feet, and a zero degrees magnetic heading. This somewhat simplifies the kinematic calculations. Figure 2.3 depicts the lead and wing aircraft separation distances using the inertial frame of reference.

The rotating reference frame origin is aligned with the wing aircraft, with the x-axis aligned to the aircraft's direction of flight, y-axis out the right wing, and the z-axis down toward the earth(2)[3-9]. The reference frame rotates with respect to the inertial reference frame, as the wing aircraft changes heading. An example of the wing's rotating reference frame is shown in Figure 2.4. The orthogonal separation distances between the wing and lead aircraft are directly provided by this coordinate system.

Both reference frames are used extensively throughout this research. Kinematic equations are developed in the next section utilizing these coordinate systems.

2.4 Kinematic Equations

The kinematic equations are used to represent the relative positions/distances between the lead and wing aircraft. The distances are expressed using a Cartesian coordinate system affixed to the inertial reference frame or the wing's rotating reference frame. In previous research by Dargan, the separation distances between the two aircraft with respect to the wing was derived(2)[3-12 to 3-21]. The lead-wing separation distances, referred to as the inertial reference frame, is derived in Chapter IV. The lead-wing separation distances, referred to as the wing aircraft, is reviewed in the following paragraphs. Given the inertial

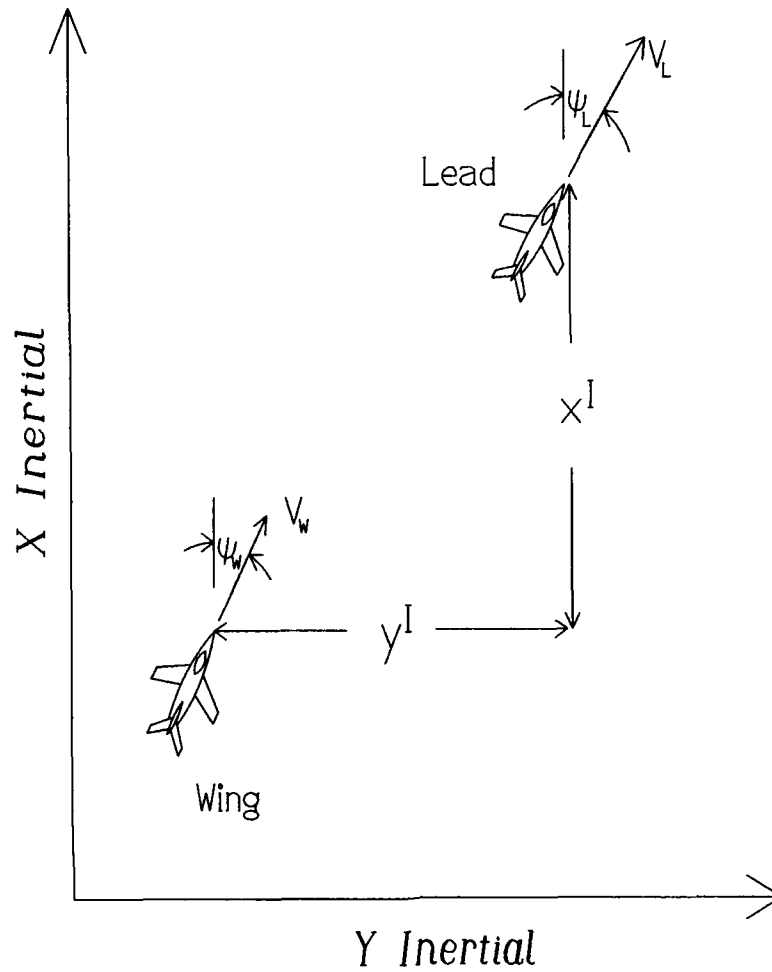


Figure 2.3. Inertial Reference Frame and Separation Distances

velocity, heading and altitude of each aircraft, an equation which relates the position of the lead aircraft with respect to the wing is desired. Using the Equation of Coriolis, the velocity of lead aircraft with respect to the wing is shown below(2)[Equation (3.12)]:

$$V_{WL}^W = V_L^W - \omega_W^W \times R_{WL}^W - V_W^W \quad (2.7)$$

where

V_{WL}^W = lead's velocity with respect to the wing, expressed in wing's frame

V_L^W = lead's inertial velocity in wing's frame

ω_W^W = angular velocity of wing's frame expressed in wing's frame

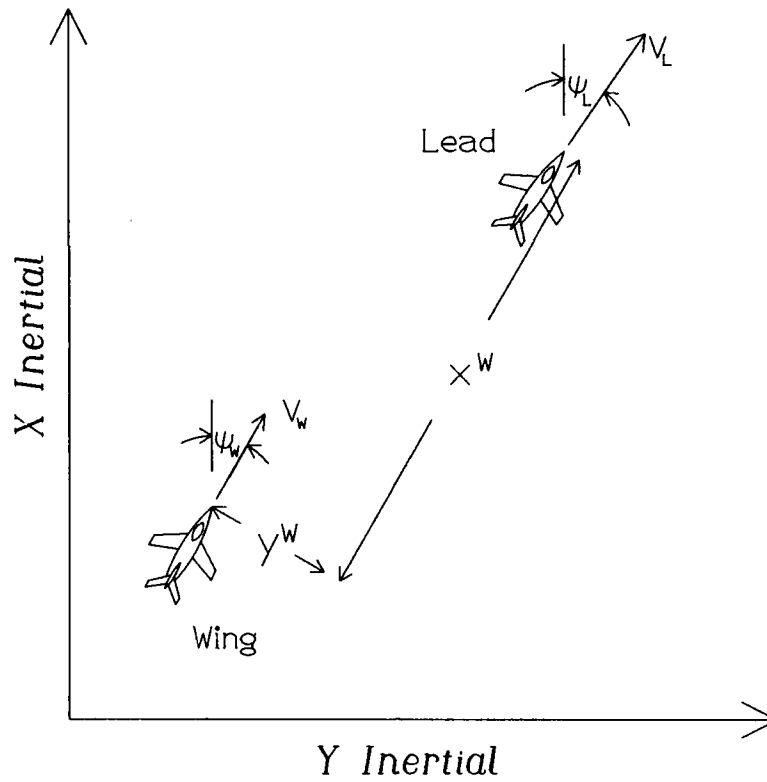


Figure 2.4. Wing's Rotating Reference Frame and Separation Distances

R_{WL}^W = position of lead with respect to wing expressed in wing's frame

V_W^W = wing's velocity expressed in its own frame of reference

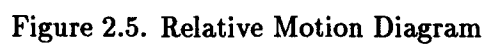
and,

$$V_L^W = C_L^W V_L^L = \begin{bmatrix} \cos \psi_E & -\sin \psi_E & 0 \\ \sin \psi_E & \cos \psi_E & 0 \\ 0 & 0 & 1 \end{bmatrix} \begin{bmatrix} V_L \\ 0 \\ 0 \end{bmatrix} = \begin{bmatrix} V_L \cos \psi_E \\ V_L \sin \psi_E \\ 0 \end{bmatrix} \quad (2.8)$$

where

C_L^W = direction cosine matrix, lead to wing transformation

$\psi_E = \psi_L - \psi_W$, heading error between lead and wing


$$\omega_W^w = \begin{bmatrix} 0 \\ 0 \\ \psi_w \end{bmatrix}, \quad R_{wL}^w = \begin{bmatrix} x^w \\ y^w \\ z^w \end{bmatrix}, \quad V_w^w = \begin{bmatrix} V_w \\ 0 \\ 0 \end{bmatrix} \quad (2.9)$$
$$\mathbf{V}_{WL}^w = \begin{bmatrix} V_L \cos \psi_E \\ V_L \sin \psi_E \\ 0 \end{bmatrix} - \begin{bmatrix} -\dot{\psi}_W y^w \\ \dot{\psi}_W x^w \\ 0 \end{bmatrix} - \begin{bmatrix} V_W \\ 0 \\ 0 \end{bmatrix} \quad (2.10)$$

Separating the above equation into the x , y , and z components yields:

$$\dot{x}^W = V_L \cos \psi_E + \dot{\psi}_W y^W - V_W \quad (2.11)$$

$$\dot{y}^W = V_L \sin \psi_E - \dot{\psi}_W x^W \quad (2.12)$$

$$\dot{z}^W = 0 \quad (2.13)$$

In the computer simulation, the above equations are integrated to get the separation distances as a function of time.

2.5 Formation Controller Strategy

In this research, a two tiered control strategy is employed(2)[3-11]. The upper tier is the control of the formation as a whole, and the lower tier is for the control of the individual aircraft within the formation. In Figure 2.1, the upper tier formation commands are directed by the pilot in the lead aircraft, while the lower tier commands are directed by the formation controller located on each wing aircraft. This section describes the design of the formation controller.

In previous research by Dargan, two types of formation controllers utilizing proportional plus integral feedback were designed. The first type utilized only a PI controller, while the second type included both a PI controller and a linear mixer. Both types of formation controllers are used in this research.

2.5.1 Closed Loop Control Using a PI Controller The PI controller operates on the error between the commanded separation and the actual separation distances. The proportional and integral action is used to drive this error to zero. A block diagram of the Formation Control System utilizing the PI Controller is shown in Figure 2.6.

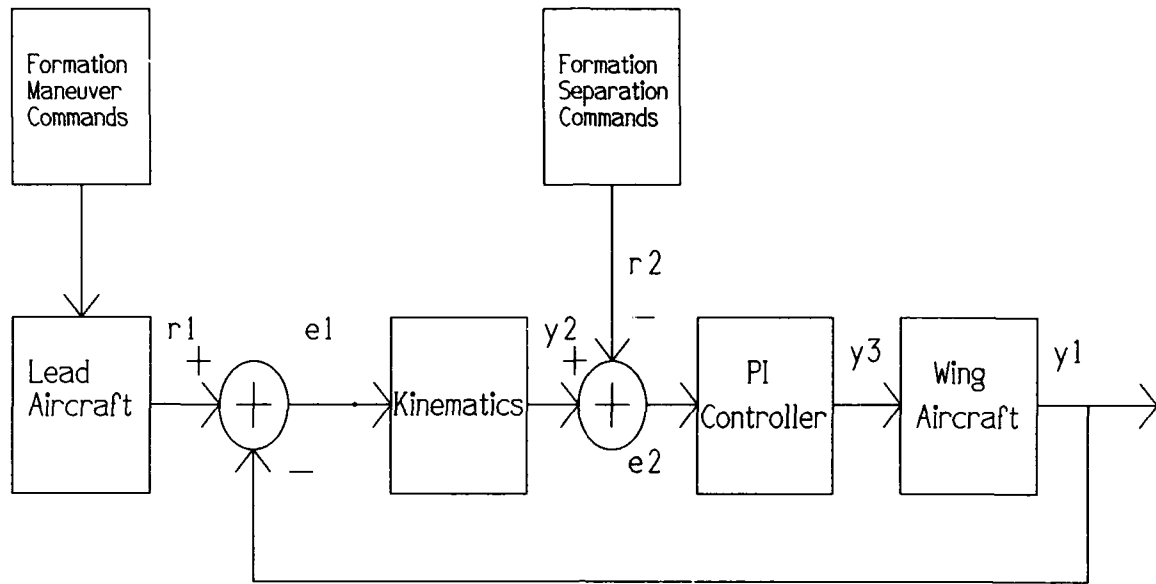


Figure 2.6. Formation Control System utilizing a PI Controller

where

$$\begin{aligned}
 r1 &= \begin{bmatrix} \text{Lead Velocity} \\ \text{Lead Heading} \\ \text{Lead Altitude} \end{bmatrix} & r2 &= \begin{bmatrix} \text{X Separation} \\ \text{Y Separation} \\ \text{Z Separation} \end{bmatrix} \\
 y1 &= \begin{bmatrix} \text{Wing Velocity} \\ \text{Wing Heading} \\ \text{Wing Altitude} \end{bmatrix} & y2 &= \begin{bmatrix} \text{Wing X Position} \\ \text{Wing Y Position} \\ \text{Wing Z Position} \end{bmatrix} \\
 y3 &= \begin{bmatrix} \text{Wing Velocity Command} \\ \text{Wing Heading Command} \\ \text{Wing Altitude Command} \end{bmatrix} & e1 &= r1 - y1 = \text{Maneuver Errors} \\
 & & e2 &= r2 - y2 = \text{Separation Errors}
 \end{aligned} \tag{2.14}$$

A large command is supplied to the wing aircraft when either the magnitude or integral of the error is large(2)[4-1]. The key to this controller's operation is the proportional plus integral gains in the PI controller. The following equations define the relationship

between the longitudinal and lateral separation errors and the command inputs to the wing aircraft.

$$V_{Wc}(t) = k_{xp}x + k_{xi} \int_0^t x dt \quad (2.15)$$

$$\psi_{Wc}(t) = k_{yp}y + k_{yi} \int_0^t y dt \quad (2.16)$$

$$h_{Wc}(t) = k_{zp}z + k_{zi} \int_0^t z dt \quad (2.17)$$

$$(2.18)$$

where

$x = x_c^W - x^W$, x separation error

$y = y_c^W - y^W$, y separation error

$z = z_c^W - z^W$, z separation error

k_{xp} = x-channel proportional gain

k_{xi} = x-channel integral gain

k_{yp} = y-channel proportional gain

k_{yi} = y-channel integral gain

k_{zp} = z-channel proportional gain

k_{zi} = z-channel integral gain

The proportional and integral controller gains are optimized in order to produce the best time response. The previous research by Dargan showed that this type of formation control system produced adequate transient responses and zero steady state error (2)[4-13].

2.5.2 Closed Loop Control Using a Linear Mixer and a PI Controller The following formation control system is similar to the previous one, except a linear mixer is added. The mixer is used to combine the separation errors (x and y spacing errors) as well as the maneuver errors (velocity and heading errors). The PI controller operates on this

combined error, by commanding the wing aircraft to drive this error to zero. The addition of the velocity and heading error signal improves the transient response of the system. The key parameters to the controller operation are the gains used in both the mixer and the PI controller. Only velocity and heading channels are controlled using this formation control system. A block diagram of the Formation Control System utilizing the mixer and the PI Controller is shown in Figure 2.7.

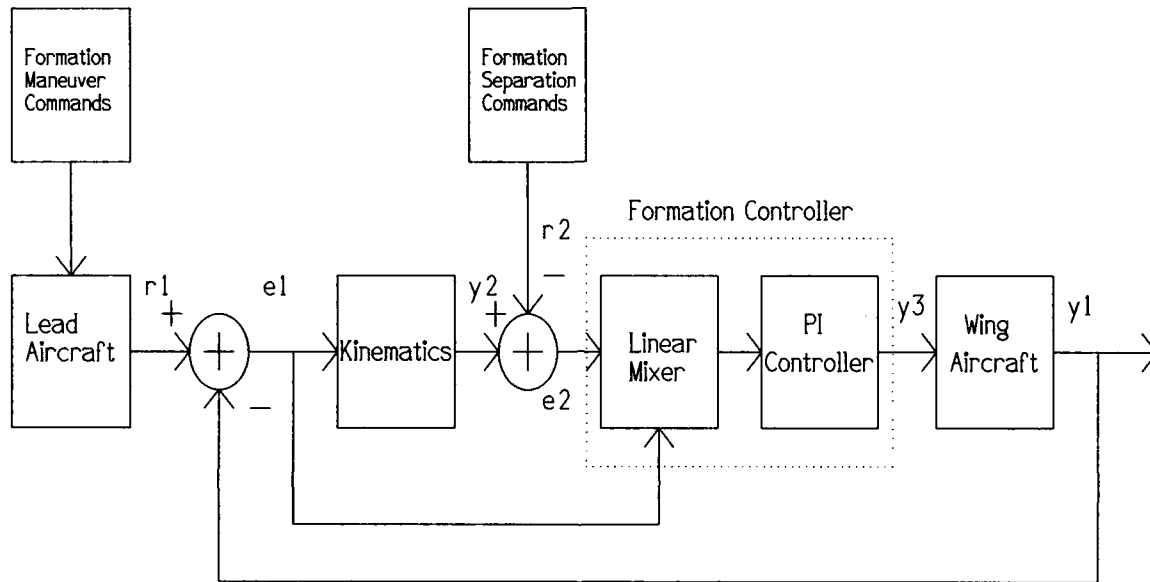


Figure 2.7. Formation Control System utilizing a Linear Mixer and PI Controller

where

$$\begin{aligned}
 r1 &= \begin{bmatrix} \text{Lead Velocity} \\ \text{Lead Heading} \end{bmatrix} & r2 &= \begin{bmatrix} \text{X Separation} \\ \text{Y Separation} \end{bmatrix} \\
 y1 &= \begin{bmatrix} \text{Wing Velocity} \\ \text{Wing Heading} \end{bmatrix} & y2 &= \begin{bmatrix} \text{Wing X Position} \\ \text{Wing Y Position} \end{bmatrix} \\
 y3 &= \begin{bmatrix} \text{Wing Velocity Command} \\ \text{Wing Heading Command} \end{bmatrix} & e1 &= r1 - y1 = \text{Maneuver Errors} \\
 & & e2 &= r2 - y2 = \text{Separation Errors}
 \end{aligned} \tag{2.19}$$

The following equations define the relationship between the longitudinal and lateral separation errors and the command inputs to the wing aircraft.

$$V_{Wc}(t) = k_{xp}[k_V V_E + k_X x] + k_{xi} \int_0^t [k_V V_E + k_X x] dt \quad (2.20)$$

$$\psi_{Wc}(t) = k_{yp}[k_\psi \psi_E + k_Y y] + k_{yi} \int_0^t [k_\psi \psi_E + k_Y y] dt \quad (2.21)$$

where

$V_E = V_L - V_W$, velocity error signal

k_V = velocity error signal mixer gain

k_ψ = heading error signal mixer gain

k_X = x-separation error signal mixer gain

k_Y = y-separation error signal mixer gain

The mixer and PI controller gains are again optimized in order to produce the best time response. The use of the mixer provides a better transient response behavior for the longitudinal channel but there is little improvement in the lateral channel (2)[4-22].

2.6 Measures of Merit

The measures of merit are based on the formation control system's transient behavior and steady state error performance. The formation control system is considered to perform satisfactorily if it is able to track all commanded inputs with zero steady state error, and if its transient behavior is such that "collisions" between the lead and the wing aircraft are avoided during the transients(2)[3-36]. An important consideration is the stability of the control system. Large formation maneuver command inputs, such as a 90 degree step heading change, can produce unstable responses for large value of controller gains, due to the deleterious effects of the system's nonlinearities. The ability of the formation control system to handle large command inputs is also used as a figure of merit.

III. Lead Aircraft's Trajectory in Wing Aircraft's Rotating Reference Frame

The performance of the formation control system is determined by analyzing the time responses of the wing aircraft. The wing aircraft's velocity and heading formation separation distances, as well as altitude is monitored. These distances are of special concern since they determine how well the formation is maintained during maneuvers and how well formation geometry change commands are executed. While the time response plots provide valuable information on the transient and steady state behavior of the formation control system, they fail to provide insight into the spatial trajectory of the wing aircraft. Presenting the wing or lead aircraft's trajectory with respect to the other aircraft provides a visualization tool in evaluating the performance of the formation control system.

3.1 Lead Aircraft's Trajectory using Lissajous Figures

The x and y separation distances between the lead and wing aircraft are obtained as a function of time, with respect to the wing's rotating reference frame. These distances are presented in Eqs (2.11) and (2.12). Using this information, the lead aircraft's trajectory, which is given in parametric form, is plotted using a Cartesian coordinate system. Figure 3.1 illustrates a two dimensional trajectory. The wing aircraft is located at the origin of the diagram. The solid line in Figure 3.1 is the trajectory of the lead aircraft in the wing aircraft's reference frame. The trajectory is a closed path since the original formation is maintained after the maneuver is complete. This would not be the case during a formation change maneuver. The dotted circle represents a minimum formation separation distance which is established as a safety region. If the solid line were to penetrate this circle, then the minimum separation distance specification is violated.

This presentation of the lead aircraft's trajectory is analogous to Lissajous figures used to visualize two-dimensional oscillations. The shape of this figure provides insight in the response of the formation control system. A small figure indicates a tight and fast control system with little deviation from the original formation. A large and wide figure indicates a sluggish response with wide swings in the formation.

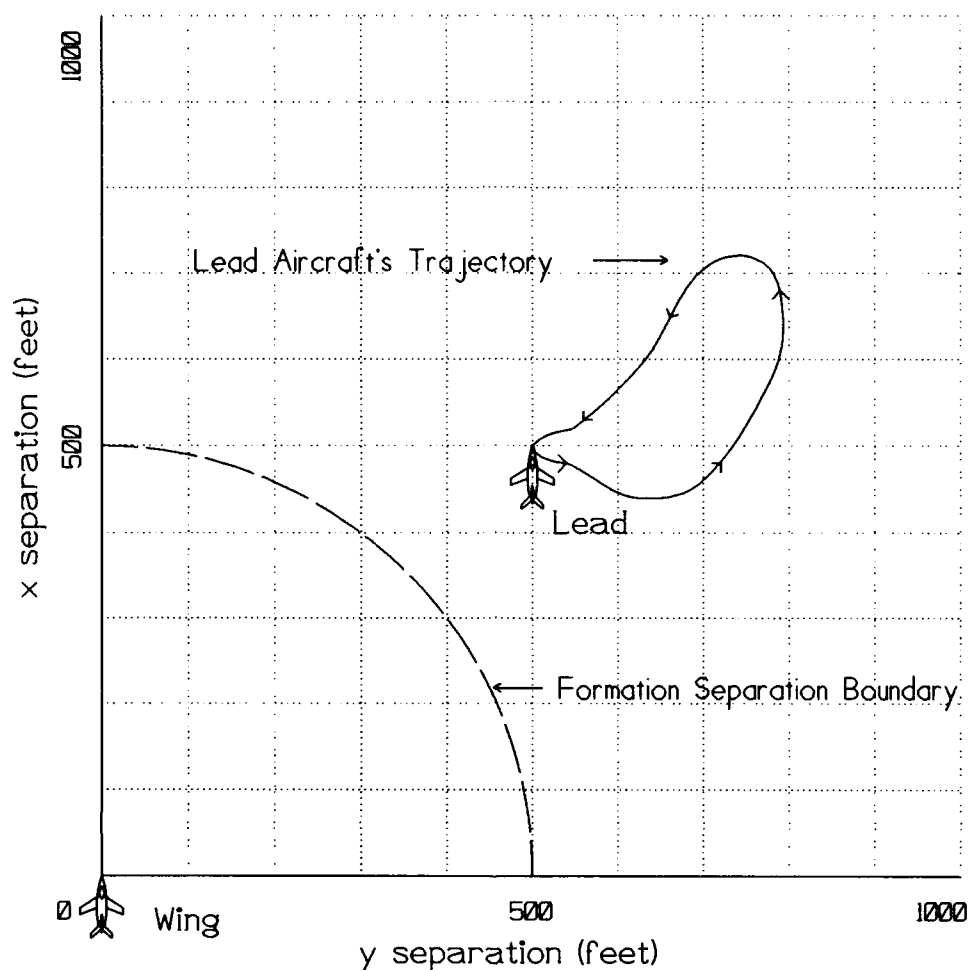


Figure 3.1. Example of Lead Aircraft's Trajectory Lissajous Figure

3.2 Performance Evaluation using Lissajous Figures

3.2.1 Diamond Formation Heading Change The time response plots of a single wing aircraft formation through a plus and minus 30 degree heading change maneuver is shown in Figure 3.2. Two separate simulations are included in the figure. The solid lines represent the plus 30 degree heading change, while the dotted lines are the negative 30 degree heading change. This information suffices to simulate a symmetric three aircraft diamond formation's heading change. The corresponding Lissajous figures are shown in Figure 3.3. In both maneuvers, the lead aircraft's trajectory is a closed path since the formation is maintained after the maneuver. The dotted line represents a 600 feet separation boundary between the two aircraft. The lead aircraft is commanded inward toward the

wing during the minus 30 degree heading maneuver, consequently its trajectory approaches closer to the 600 ft boundary.

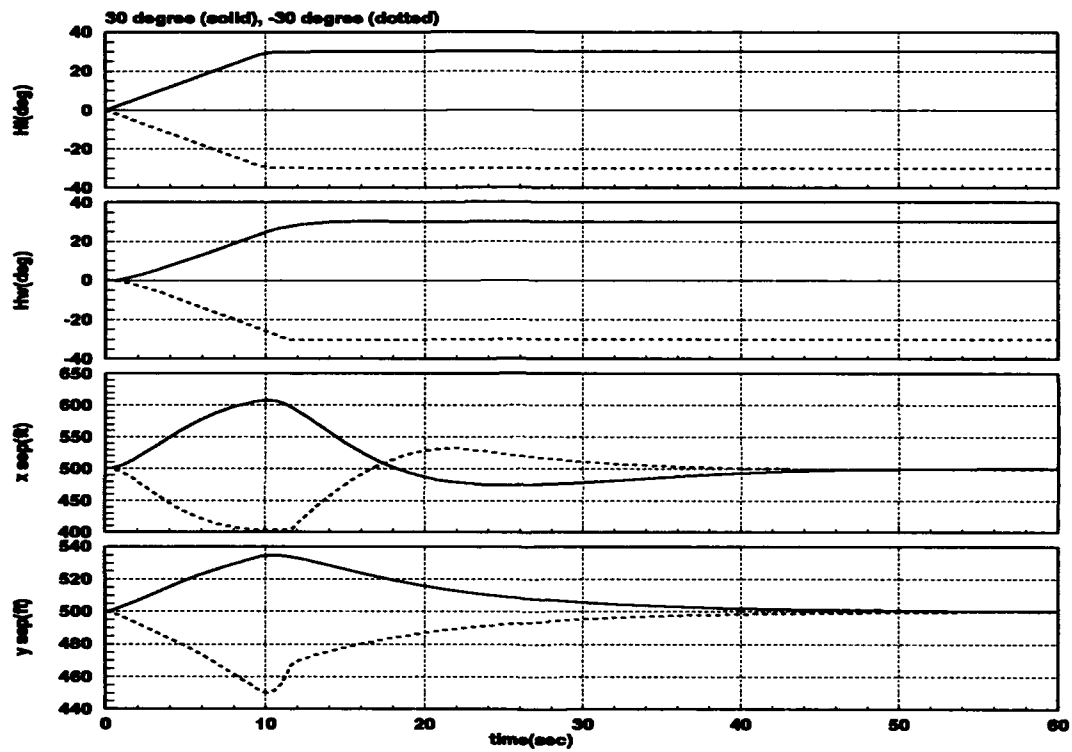


Figure 3.2. Diamond Formation, ± 30 Degrees Heading Change Time Response

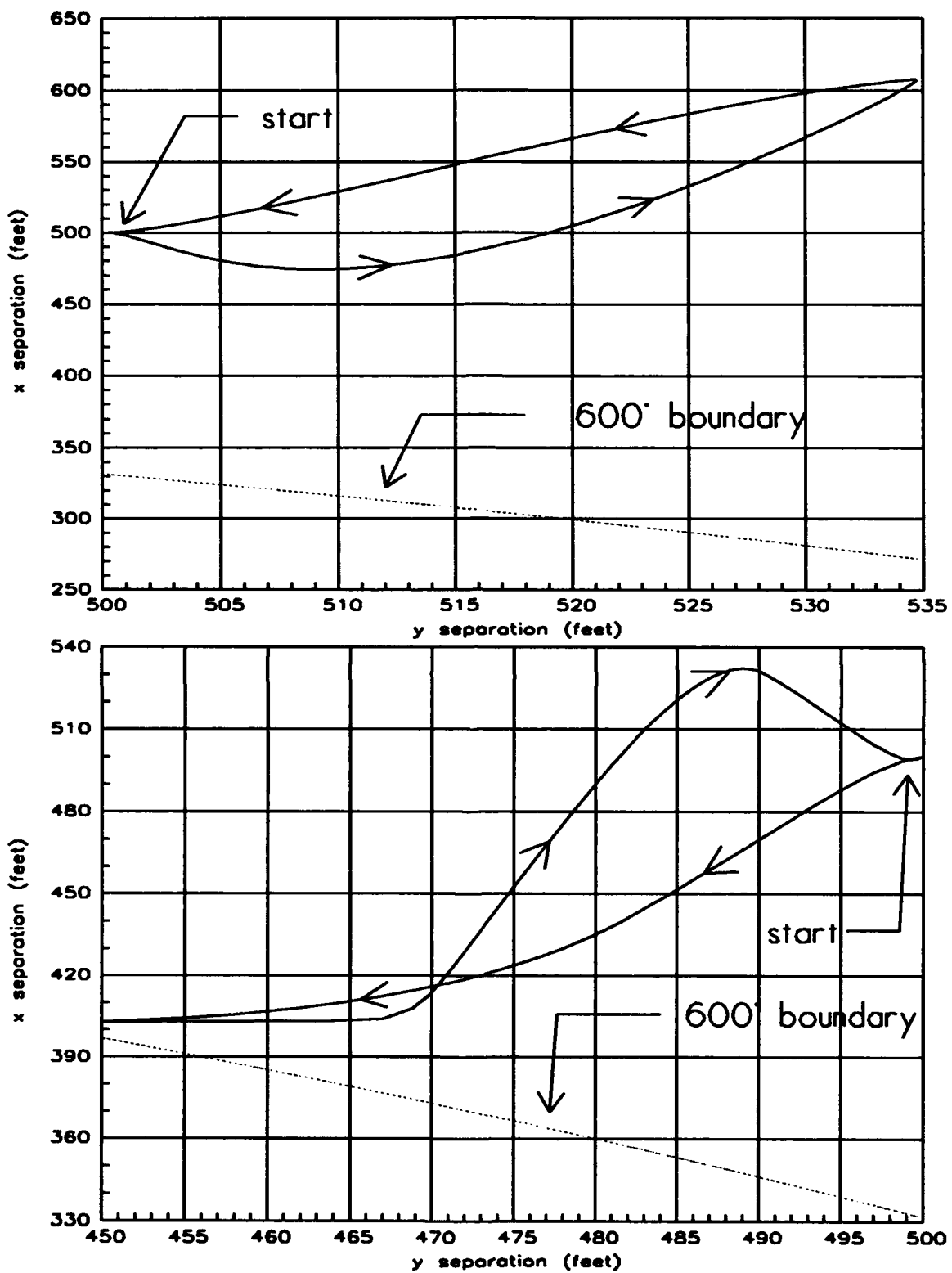


Figure 3.3. Diamond Formation, +30 Degrees Heading Change (top), and -30 Degrees Heading Change (bottom), Lead Trajectory Lissajous Figures

3.2.2 Trail Formation Heading Change The previous simulations are repeated for two aircraft in a trail formation. The plus and minus 30 degree heading change time response plots of the two aircraft are shown in Figure 3.4. The lead aircraft's trajectories are shown in Figure 3.5. As for the case for the diamond formation heading change, the lead aircraft's trajectory is a closed path, since the formation is maintained after the maneuver. A 500 feet boundary is established for this maneuver. As seen in Figure 3.5, the boundary is crossed during both heading changes. Even though the boundary is violated, the magnitude of the crossing is less than one foot. As expected, the Lissajous figures for both are identical, but are reflected about the x axis.

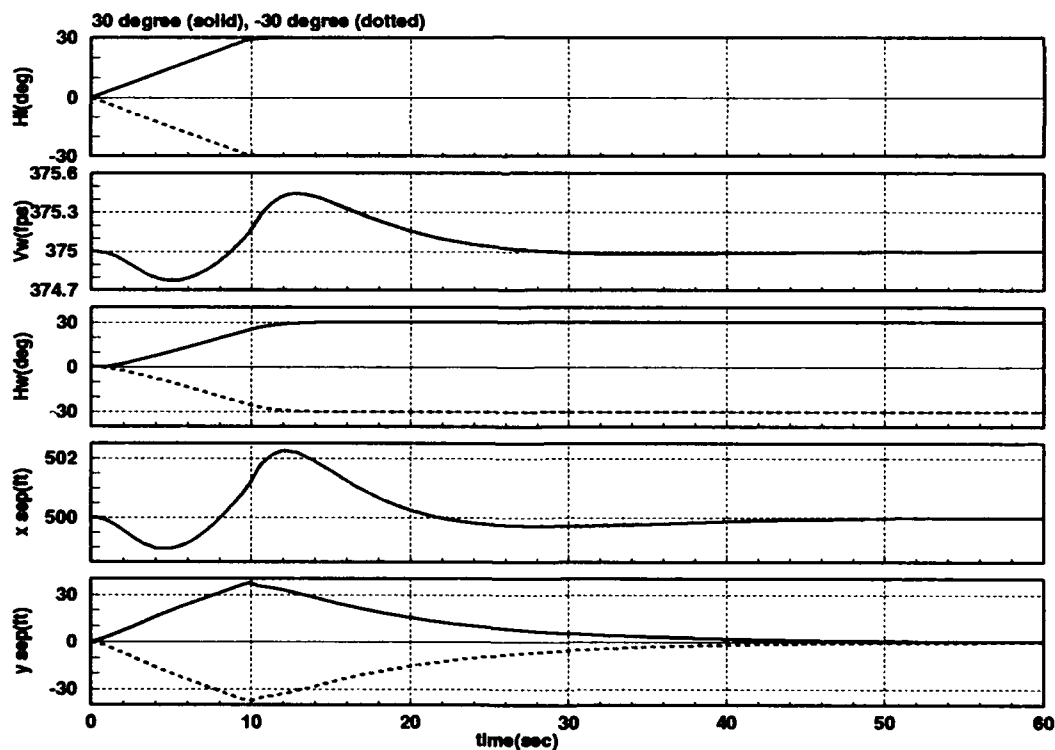


Figure 3.4. Trail Formation, ± 30 Degrees Heading Change Time Response

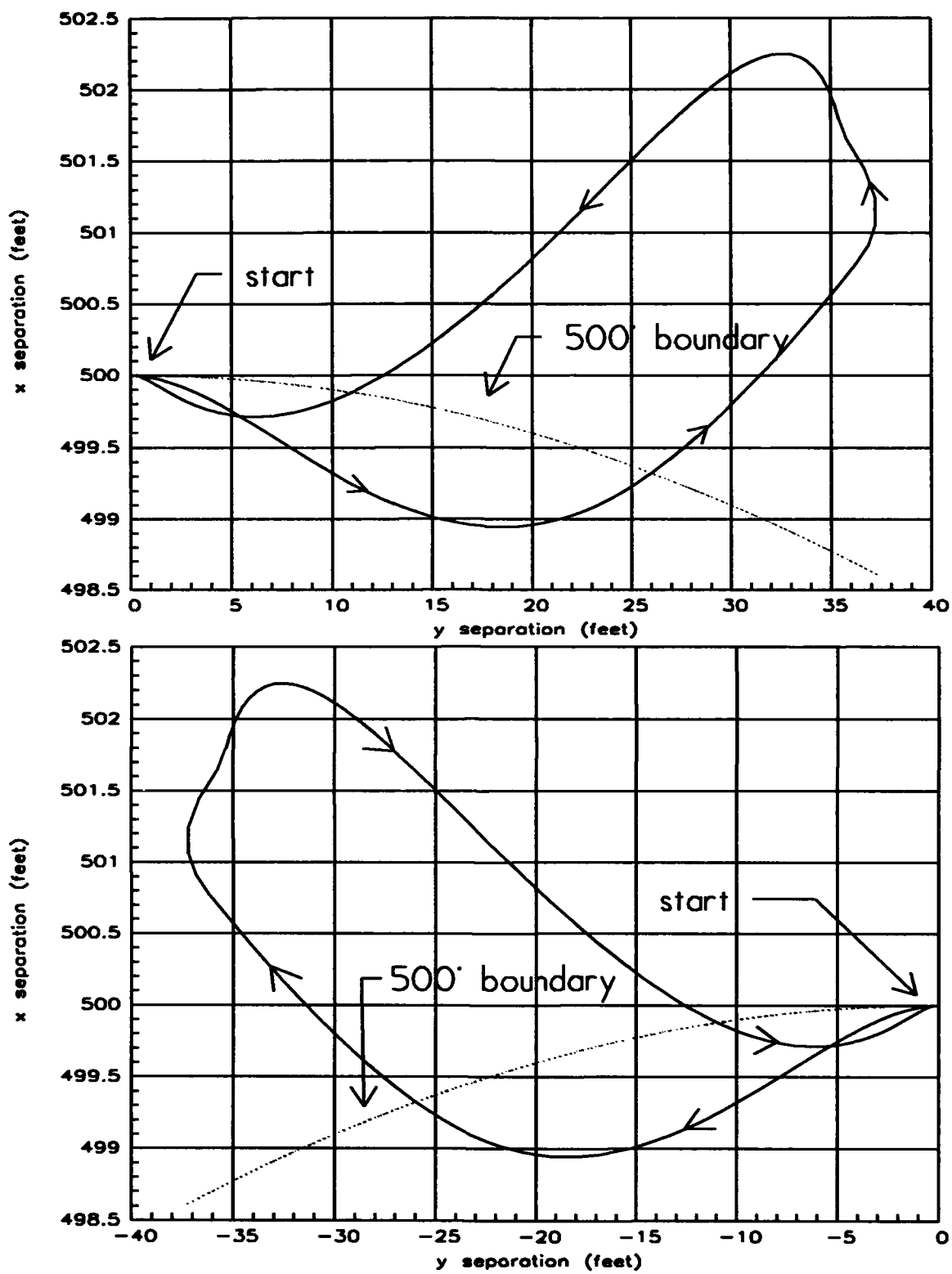


Figure 3.5. Trail Formation, +30 Degrees Heading Change (top), and -30 Degrees Heading Change (bottom), Lead Trajectory Lissajous Figures

3.3 Summary

The Lissajous figure representation of the lead aircraft's trajectory in the wing aircraft's rotating reference frame is a valuable tool for visualizing the performance of the formation control system. It provides a graphical means of verifying any violation of the minimum distance between the two aircraft. The size and shape of the lead aircraft's trajectory is used to evaluate the tightness of the formation and speed of the control system.

IV. Two Wing Aircraft Formation Flight Control

A degree of complexity is added to the formation flight control problem for formations including two wing aircraft. The two wing aircraft not only must independently and successfully track the lead aircraft, but they must also avoid a collision between themselves. The current formation control concept stipulates that each wing aircraft, through the use of its sensors, tracks the lead aircraft by measuring the lead-wing separation distances. The separation distance between the two wing aircraft is not measured, but it is computed analytically for this report. Furthermore, no communication nor coordination between the wing aircraft is envisioned. However, the formation control simulation is used to ensure no collision occurs between the two wing aircraft during a formation maneuver or a formation geometry change. This is the primary motivation for the implementation of the two wing formation flight control system simulation.

4.1 Two Wing Formation Controller Implementation

The Two Wing Formation Flight Control Problem is simplified through the use of the following assumptions.

- Each wing aircraft is equipped with a formation flight control system capable of independently tracking the lead aircraft with an established tracking error.
- The separation distances determining the geometry of the formation are established in accordance with the tracking error of each wing aircraft. For example, a heavier aircraft with a high tracking error requires larger separation distances.
- These assumptions can be used in establishing multiple wing aircraft formations.

The diagram in Figure 4.1 outlines the geometry of a two wing aircraft formation. In this diagram, a diamond formation is illustrated. The addition of a second wing aircraft requires the use of a common inertial reference frame, and the calculation of the inertial positions of each aircraft. This common reference frame is used to obtain the separation distances between the three aircraft during simulations. The calculations are presented in the next section.

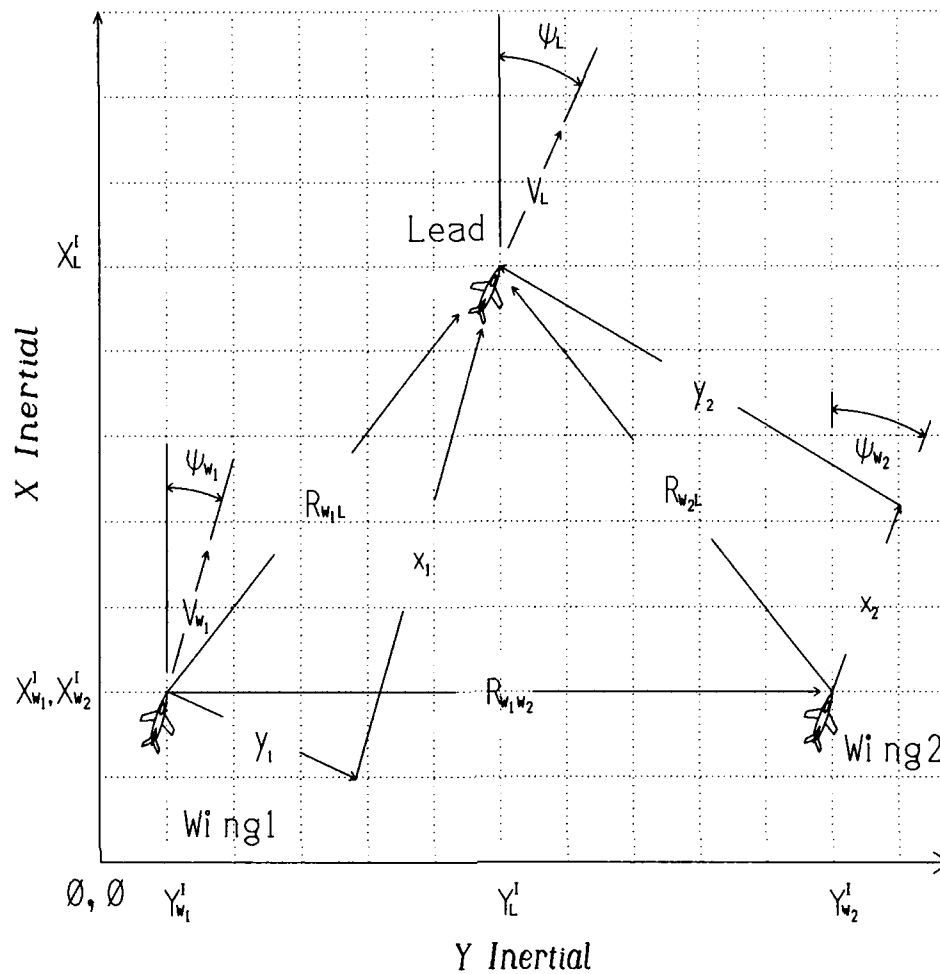


Figure 4.1. Two Wing Aircraft Formation Geometry

4.2 Inertial Calculations

The inertial position of each aircraft is needed in order to calculate the separation distance between two aircraft. Depending on the information available, the inertial separation distance between aircraft can be calculated in two different ways. In the computer simulation, the inertial velocity of each aircraft, resolved in its own reference frame, and the inertial headings are known. Additionally, the initial inertial position of each aircraft is known. Without loss of generality, the initial position of the lead aircraft is assumed to be the inertial origin. Equations (4.2) to (4.6) generate the positions of each aircraft. The separation distances between the aircraft is the difference between these values. Since the Z^W axis of each aircraft is aligned with the Z^I axis, no conversion is necessary. The

inertial separation between the two wing aircraft is shown in Eq (4.9).

$$X_L^I = \int_{t_0}^t V_L^L \cos \psi_L + X_L^I(0) \quad (4.1)$$

$$Y_L^I = \int_{t_0}^t V_L^L \sin \psi_L + Y_L^I(0) \quad (4.2)$$

$$X_{W_1}^I = \int_{t_0}^t V_{W_1}^{W_1} \cos \psi_{W_1} + X_{W_1}^I(0) \quad (4.3)$$

$$Y_{W_1}^I = \int_{t_0}^t V_{W_1}^{W_1} \sin \psi_{W_1} + Y_{W_1}^I(0) \quad (4.4)$$

$$X_{W_2}^I = \int_{t_0}^t V_{W_2}^{W_2} \cos \psi_{W_2} + X_{W_2}^I(0) \quad (4.5)$$

$$Y_{W_2}^I = \int_{t_0}^t V_{W_2}^{W_2} \sin \psi_{W_2} + Y_{W_2}^I(0) \quad (4.6)$$

where

X_L^I = lead's inertial position along X^I axis

Y_L^I = lead's inertial position along Y^I axis

$X_{W_1}^I$ = wing₁'s inertial position along Y^I axis

$Y_{W_1}^I$ = wing₁'s inertial position along Y^I axis

ψ_{W_1} = wing₁'s inertial heading

$X_{W_2}^I$ = wing₂'s inertial position along Y^I axis

$Y_{W_2}^I$ = wing₂'s inertial position along Y^I axis

ψ_{W_2} = wing₂'s inertial heading

$$\mathbf{R}_{W_1 L}^I = \begin{bmatrix} X_L^I - X_{W_1}^I \\ Y_L^I - Y_{W_1}^I \\ Z_L^I - Z_{W_1}^I \end{bmatrix} \quad (4.7)$$

$$\mathbf{R}_{W_2 L}^I = \begin{bmatrix} X_L^I - X_{W_2}^I \\ Y_L^I - Y_{W_2}^I \\ Z_L^I - Z_{W_2}^I \end{bmatrix} \quad (4.8)$$

$$\mathbf{R}_{W_1 W_2}^I = \mathbf{R}_{W_1 L}^I - \mathbf{R}_{W_2 L}^I \quad (4.9)$$

where

$\mathbf{R}_{W_1L}^I$ = lead-wing₁ inertial separation

$\mathbf{R}_{W_2L}^I$ = lead-wing₂ inertial separation

$\mathbf{R}_{W_1W_2}^I$ = wing₂-wing₁ inertial separation

An alternative method of calculating the inertial separations between the aircraft uses the separation distance between the wing and the lead aircraft referenced to the wing's rotating reference frame. In an actual implementation, this information is available to the each wing aircraft. The inertial separation between the two aircraft is calculated using the direction cosine matrix in Eq (4.10). Equations (4.11) to (4.12) implement the steps needed to calculate the inertial separations.

$$C_{W_n}^I = \begin{bmatrix} \cos \psi_{W_n} & -\sin \psi_{W_n} & 0 \\ \sin \psi_{W_n} & \cos \psi_{W_n} & 0 \\ 0 & 0 & 1 \end{bmatrix} \quad \mathbf{R}_{W_nL}^{W_n} = \begin{bmatrix} x_n \\ y_n \\ z_n \end{bmatrix} \quad (4.10)$$

where

$C_{W_n}^I$ = direction cosine matrix, nth wing to inertial frame of reference (f.o.r.)

ψ_{W_n} = nth wing aircraft's inertial heading

x_n = nth wing x-separation in its f.o.r.

y_n = nth wing y-separation in its f.o.r.

z_n = nth wing z-separation in its f.o.r.

$\mathbf{R}_{W_nL}^{W_n}$ = lead's position with respect the nth wing aircraft

and

$$\mathbf{R}_{W_1L}^I = C_{W_1}^I \mathbf{R}_{W_1L}^{W_1} = \begin{bmatrix} x_1 \cos \psi_{W_1} - y_1 \sin \psi_{W_1} \\ x_1 \sin \psi_{W_1} + y_1 \cos \psi_{W_1} \\ z_1 \end{bmatrix} \quad (4.11)$$

$$\mathbf{R}_{W_2L}^I = C_{W_2}^I \mathbf{R}_{W_2L}^{W_2} = \begin{bmatrix} x_2 \cos \psi_{W_2} - y_1 \sin \psi_{W_2} \\ x_2 \sin \psi_{W_2} + y_1 \cos \psi_{W_2} \\ z_2 \end{bmatrix} \quad (4.12)$$

The inertial separation between the two wing aircraft is the same as Eq (4.9). The distance can be transformed to wing₁'s reference frame using the direction cosine matrix. The transformation from the inertial reference frame to wing₁'s reference frame is shown in Eq (4.13).

$$\mathbf{R}_{W_1W_2}^{W_1} = C_I^{W_1} \mathbf{R}_{W_2W_1}^I \quad (4.13)$$

This distance is useful in plotting wing₂'s trajectory with respect to wing₁. A Lissajous figure showing this trajectory is included in the next section.

4.3 Performance Evaluations

The lead aircraft is commanded a 30 degree heading change while the wing aircraft are in both trail and diamond formations. During these simulations, no altitude change is commanded, so the z coordinate is ignored. The separation distance between all three aircraft is observed in order to meet minimum separation requirements.

4.3.1 Trail Formation Heading Change The time response plots of a two wing aircraft trail formation through a 30 degree heading change maneuver is shown in Figure 4.2. All aircraft are initially separated by 500 feet. Wing₁ is directly behind the lead aircraft, and wing₂ is 500 feet behind wing₁. See Figure 1.1 for reference. The time responses of both wing aircraft are included in this figure. The separation distances shown in Figure 4.2 are with respect to each wing aircraft.

The inertially resolved separation distances between all three aircraft during the 30 degree heading change are shown in Figure 4.3. The closest distance between any two aircraft, for this maneuver, is between the wing₁ and wing₂. The separation distance between these two aircraft decreases from a nominal 500 ft to 494 ft. Even though there is no direct control of this parameter, the individual formation control system on each

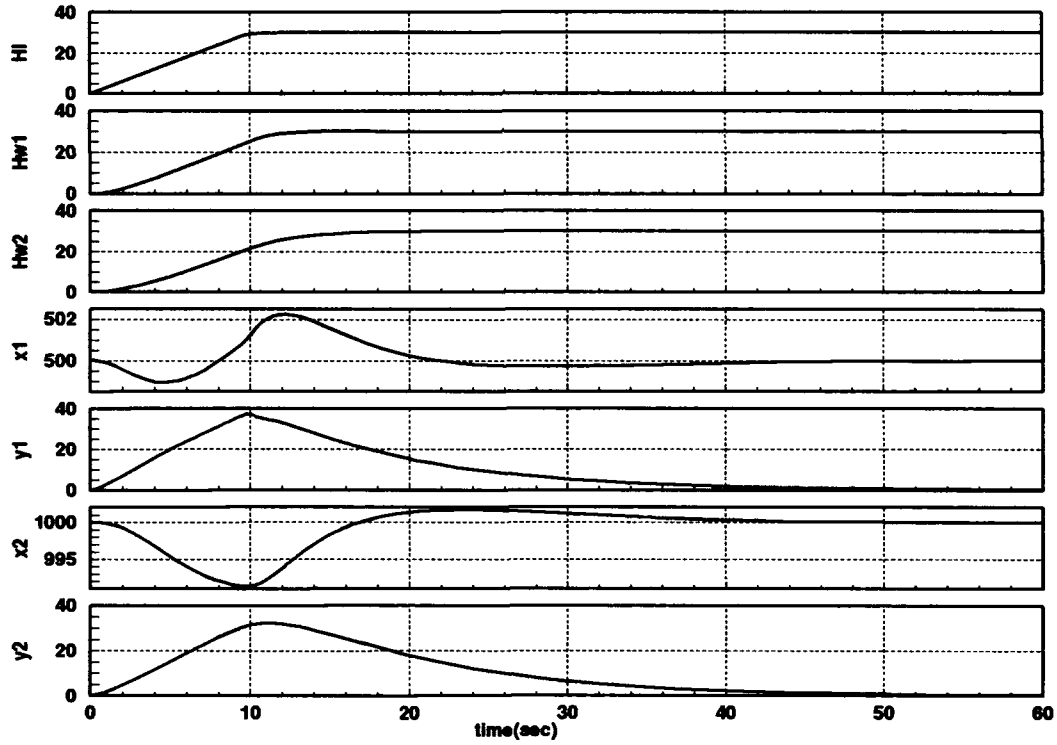


Figure 4.2. Trail Formation, Two Wing Aircraft, +30 Degrees Heading Change Time Response

aircraft is able to maintain the commanded separation. Figure 4.4 displays a Lissajous figure containing wing₂'s trajectory in wing₁'s reference frame.

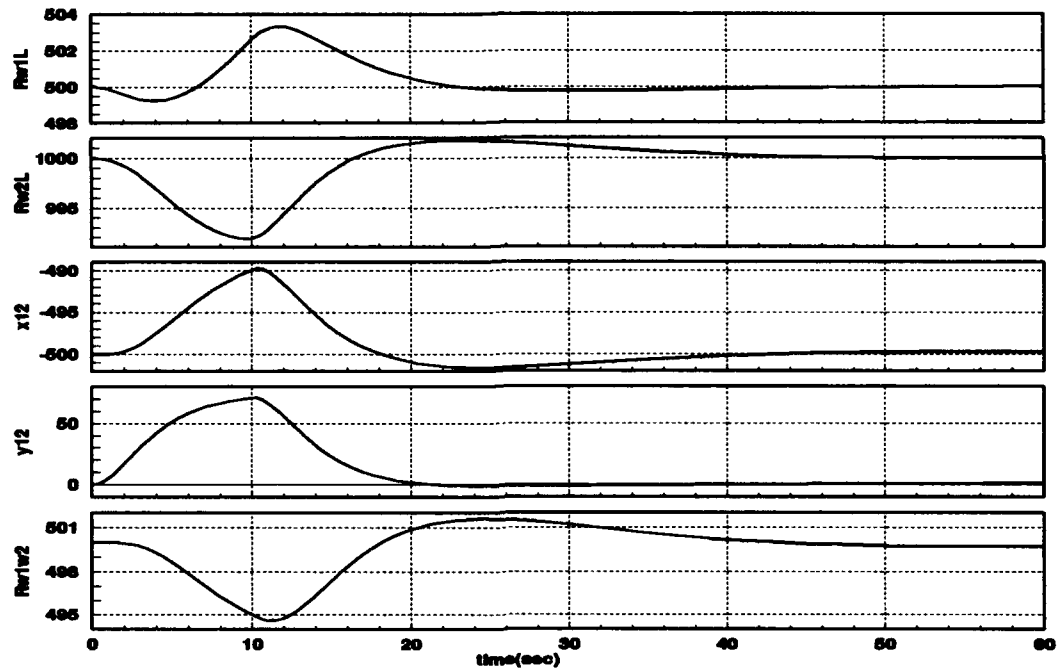


Figure 4.3. Trail Formation, Two Wing Aircraft, +30 Degrees Heading Change, Separation Distances

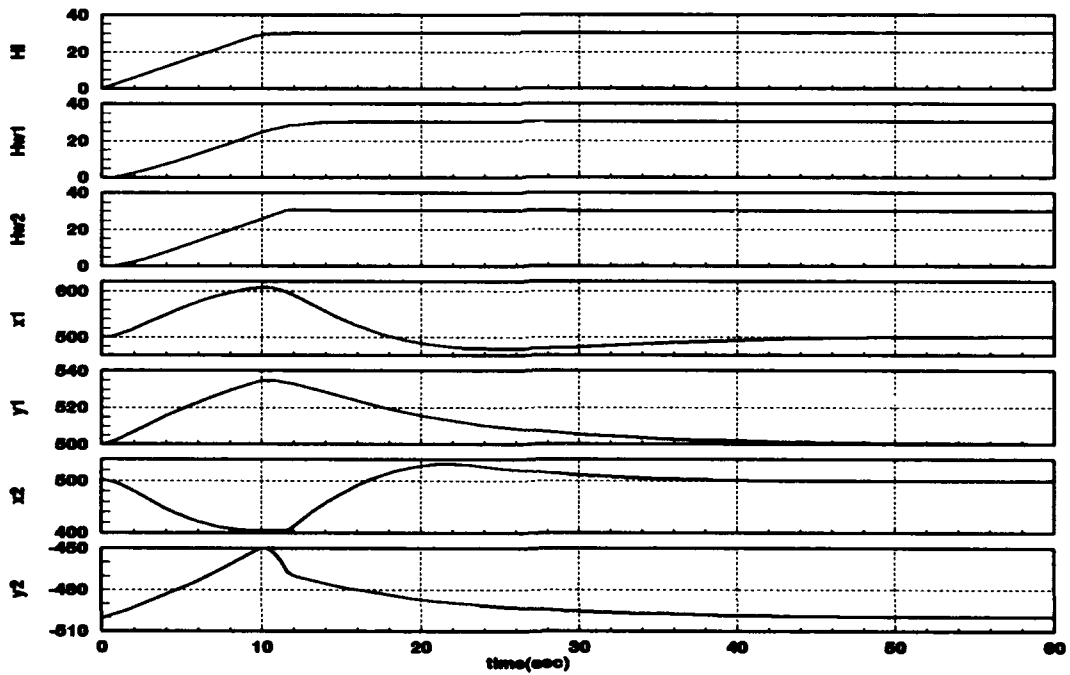


Figure 4.4. Lissajous Figure of Wing₂'s Trajectory in Wing₁'s Reference Frame, for a +30 Degrees Heading Change in Trail Formation

4.3.2 Diamond Formation Heading Change The time response plots of a two wing aircraft diamond formation through a 30 degree heading change maneuver is shown in Figure 4.5. The radial separation distances is shown in Figure 4.6. Of special note is the separation of the two wing aircraft. The minimum distance between the two aircraft is just under 996 ft. There is little deviation from the nominal 1000 feet separation during this maneuver.

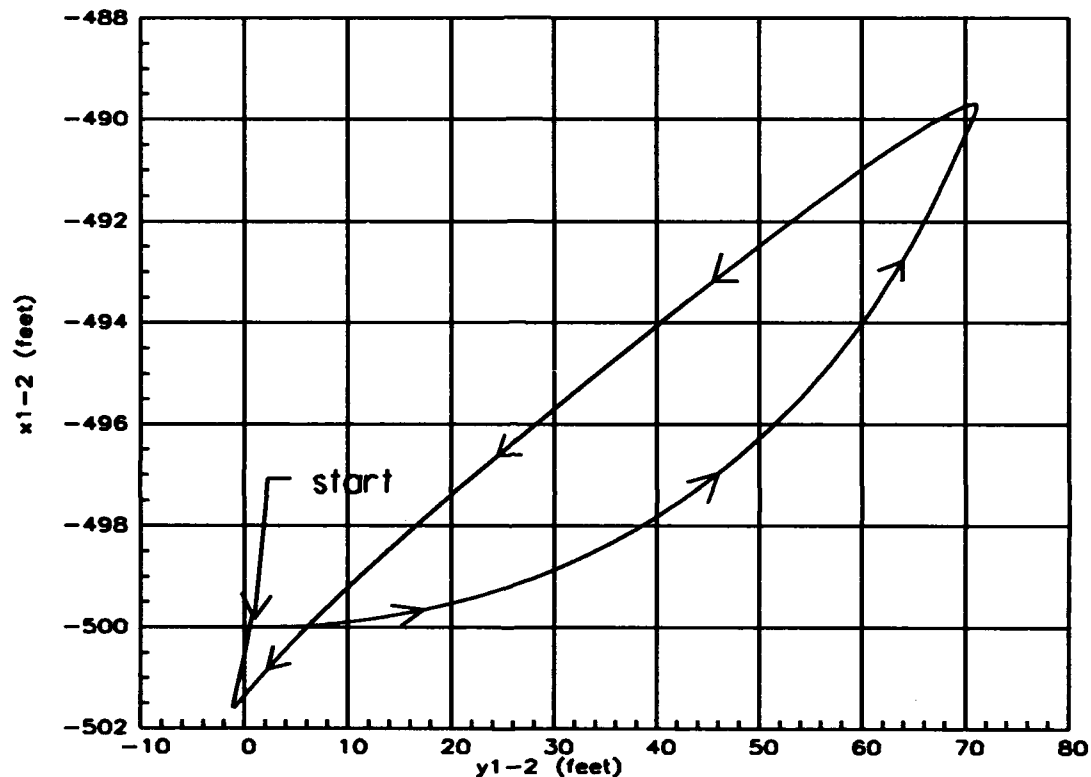


Figure 4.5. Diamond Formation, Two Wing Aircraft, +30 Degrees Heading Change Time Response

The relatively high tracking performance of the formation controllers on each aircraft is able to maintain the distance between all aircraft. This is also illustrated in Figure 4.7. In this figure, a Lissajous figure containing wing₂'s trajectory with respect to wing₁ is displayed. The next plot, Figure 4.8, displays the flight path of each aircraft during the 30 degree heading change. This inertial perspective illustrates how each wing aircraft is able to track the lead. The small circles represent five second intervals. They can be used to roughly show the changing position of each aircraft.

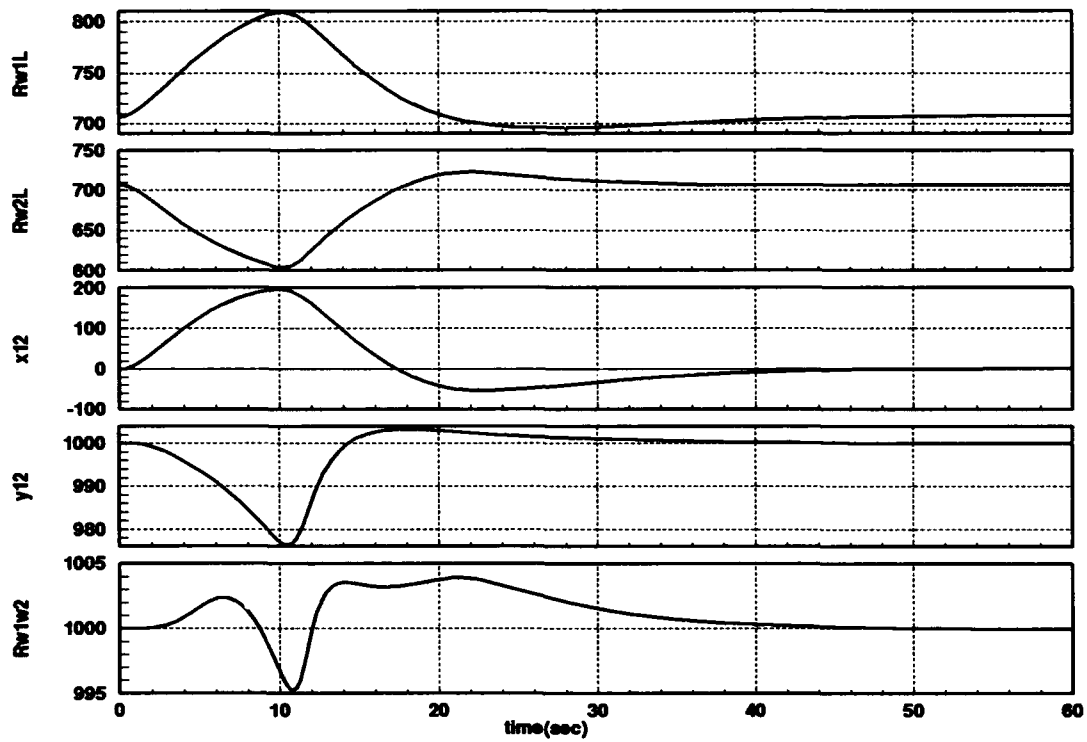


Figure 4.6. Trail Formation, Two Wing Aircraft, +30 Degrees Heading Change, Separation Distances

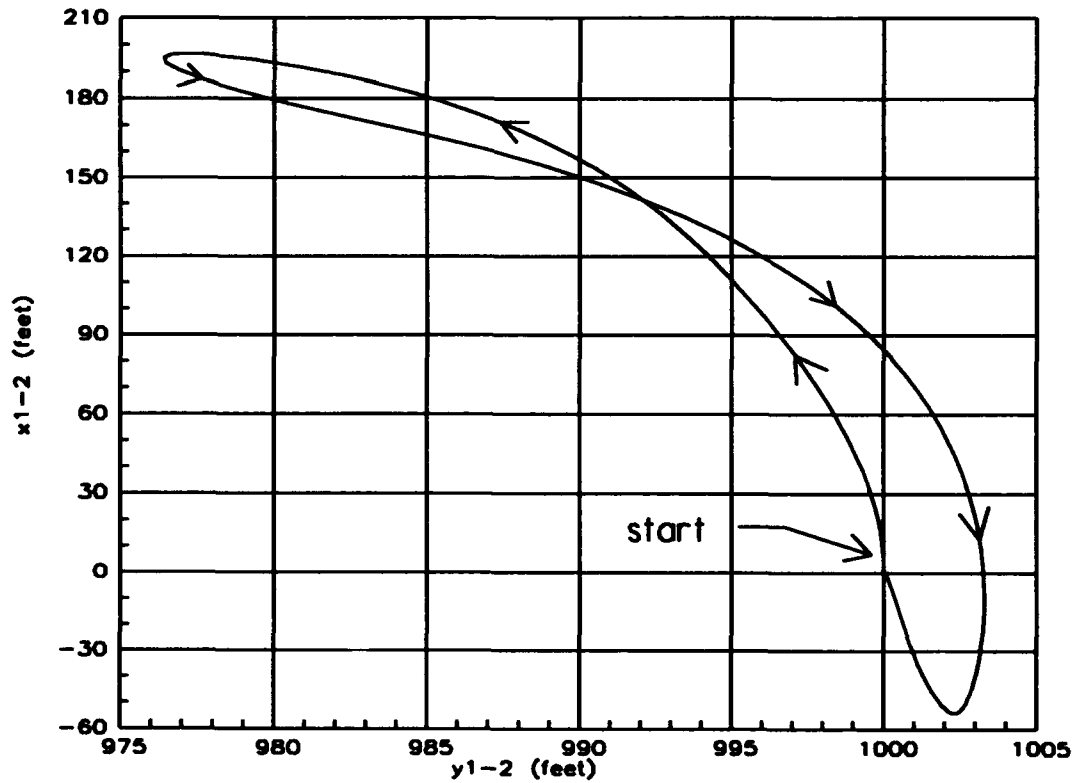


Figure 4.7. Lissajous Figure of Wing₂'s Trajectory in Wing₁'s Reference Frame, for a +30 Degree Heading Change in Diamond Formation

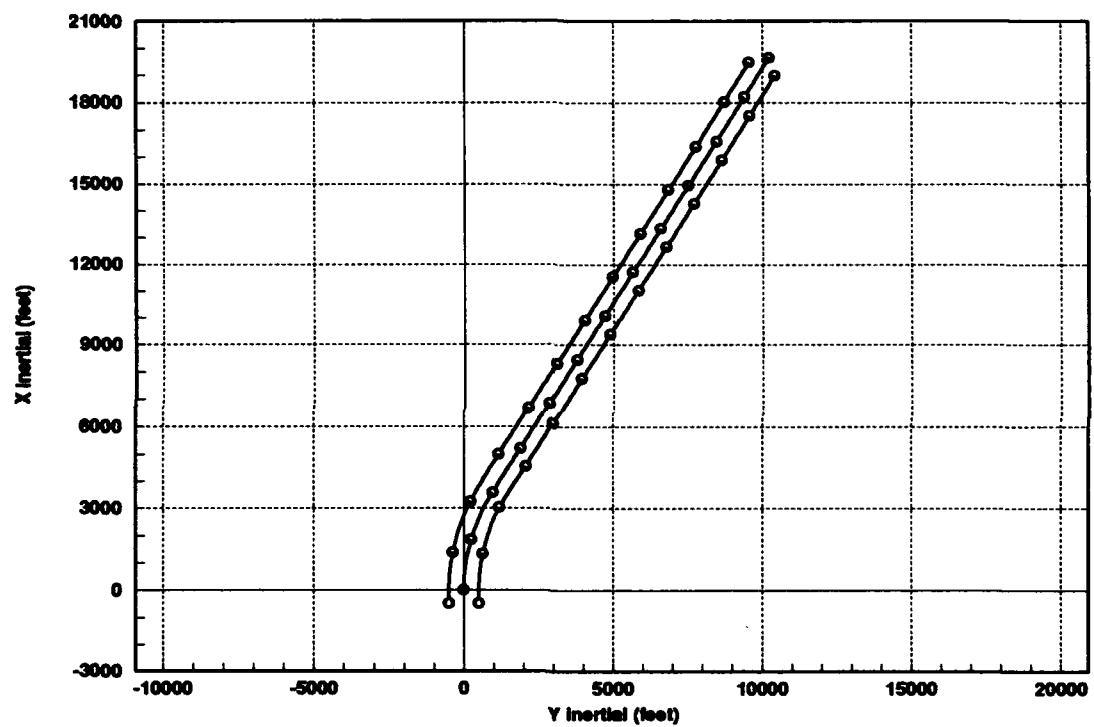


Figure 4.8. Diamond Formation, +30 Degrees Heading Change, Inertial Flight Paths

4.4 Summary

In this chapter, a second wing aircraft is added to the flight control problem. This second aircraft is equipped with a formation flight controller identical to the first wing aircraft. In order to properly maintain the formation of the two wing aircraft, the separation between these aircraft must be maintained. Even though this separation distance is not directly measured and controlled, the ability of each wing aircraft to successfully track the leader, is sufficient to maintain the formation, and guarantee the separation of wing₁ and wing₂. The wing tracking errors due to the heading change are small in magnitude compared to the formation geometry. This is verified by the 30 degree heading change computer simulations. Consequently, the formation flight control system developed for the single wing aircraft can successfully be used for multi-wing aircraft formations. This is true as long as the individual tracking errors of each aircraft are small compared to the size of the formation.

V. Analytical Formation Flight Controller Synthesis

The formation flight controller entails output feedback and proportional plus integral control. This combination produces output decoupling and tracking of the command inputs by the corresponding outputs. Unfortunately the non-linear rate limiters in the aircraft models and trigonometric functions in the kinematic equations preclude the exclusive use of linear control design methods. Hence, both the proportional and integral gains in the PI controller are determined using the formation flight control simulation and a trial and error method. Numerous computer simulations are performed while modifying these gains and observing the tracking ability of the control system. This method produces successful results, but considerable labor is expended in determining the PI controller gains.

A linearized plant model is desirable since pole placement techniques can be used to analytically determine initial controller gain values. These initial values are then experimentally refined using the full non-linear computer simulation. This chapter presents the derivation of a linear and parametrized MIMO plant used to analytically determine the optimal PI control gains for the formation flight control problem. In this chapter, analysis is restricted to the planar velocity and heading channels.

5.1 Theoretical Development

The linear model for the formation flight control problem is developed as follows: First, the formation geometry is outlined and the key geometric parameters are identified. Linearized equations for both the aircraft models and kinematics are developed. These equations are then non-dimensionalized and presented in state space form. The separate x and y-channels are identified, decoupled, and augmented using the PI control law. These augmented state equations are then analyzed for steady state error and stability. Finally, the characteristic equation of these augmented plants are used in determining the optimal control laws (gains). The formation geometry is illustrated in Figure 5.1. The key parameters are the separation $l = \sqrt{x_o^2 + y_o^2}$, and the formation angle α . Equations (5.1) through

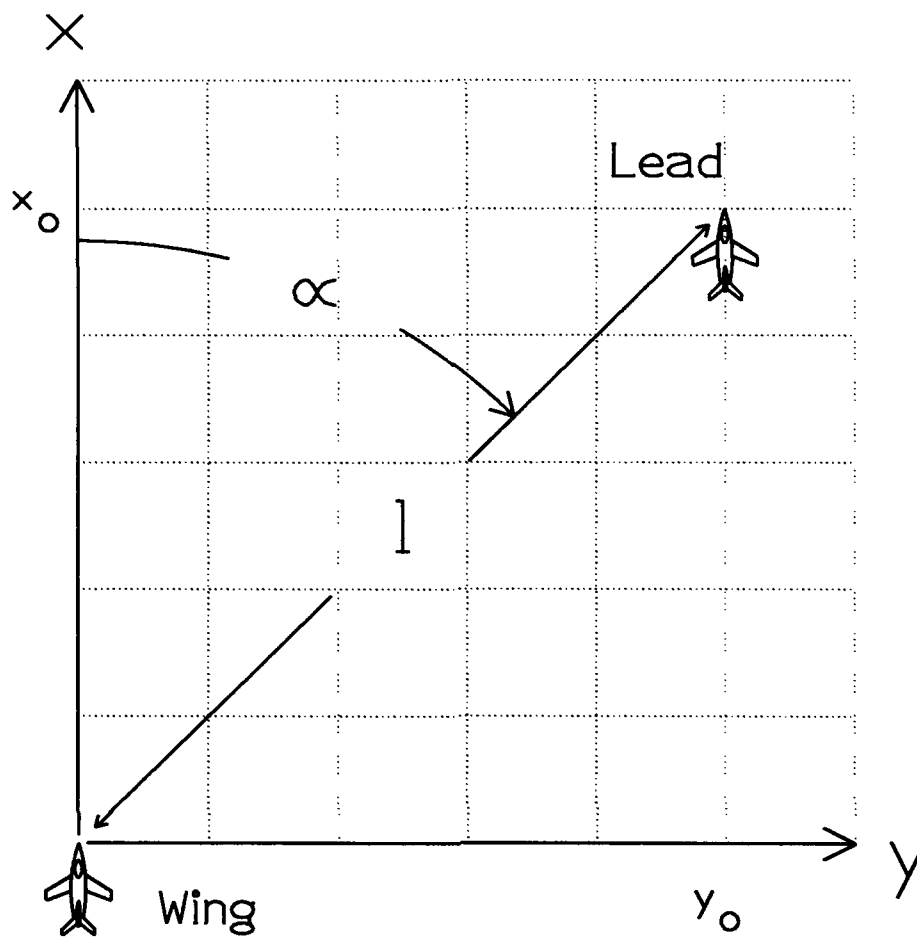


Figure 5.1. Formation Geometry

(5.2) relate the Cartesian separation distances to these two parameters,

$$x_o = l \cos \alpha \quad (5.1)$$

$$y_o = l \sin \alpha \quad (5.2)$$

where

x_o = nominal x-separation

y_o = nominal y-separation

α = separation angle

First order aircraft models are used in this analysis. This simplifies the final equations and provides a means of comparing the final results with the results developed by Dargatzis (2)[4-1-4-22] and Rohs (9). Equations (5.3) to (5.5) define the first order C-130 aircraft models developed in Rohs research (9)[28-35].

$$\dot{V}_W = -\frac{1}{\tau_{V_W}} V_W + \frac{1}{\tau_{V_W}} V_{Wc} \quad (5.3)$$

$$\dot{\psi}_W = -\frac{1}{\tau_{\psi_W}} \psi_W + \frac{1}{\tau_{\psi_W}} \psi_{Wc} \quad (5.4)$$

$$\dot{h}_W = -\frac{1}{\tau_{h_W}} h_W + \frac{1}{\tau_{h_W}} h_{Wc} \quad (5.5)$$

where

τ_{V_W} = wing's first order velocity time constant

τ_{ψ_W} = wing's first order heading time constant

The kinematic equations describing the separation between the lead and the wing aircraft are given by(2)[Eqs. 3.15 and 3.16]

$$\dot{x} = V_L \cos \psi_E + \dot{\psi}_W y - V_W \quad (5.6)$$

$$\dot{y} = V_L \sin \psi_E - \dot{\psi}_W x \quad (5.7)$$

Incorporating small angle approximations and the small perturbations method into Eqs. (5.6) and (5.7) yields

$$\dot{x} = V_L + \dot{\psi}_W y_o - V_W \quad (5.8)$$

$$\dot{y} = V_L \psi_E - \dot{\psi}_W x_o \quad (5.9)$$

Substituting Eqs. (5.1) through (5.4) into Eqs (5.8) and (5.9) yields

$$\dot{x} = V_L + \left[-\frac{1}{\tau_{\psi_W}} \psi_W + \frac{1}{\tau_{\psi_W}} \psi_{Wc} \right] l \sin \alpha - V_W \quad (5.10)$$

$$\dot{y} = V_L (\psi_L - \psi_W) - \left[-\frac{1}{\tau_{\psi_W}} \psi_W + \frac{1}{\tau_{\psi_W}} \psi_{Wc} \right] l \cos \alpha - V_W \quad (5.11)$$

The next step in the development of the linear MIMO plant model is the parametrization (non-dimensionalization) of all variables. Define the following variables

$$l = \sqrt{x_o^2 + y_o^2} \quad (5.12)$$

$$\bar{t} = \frac{l}{V} \quad (5.13)$$

where

l = characteristic length, nominal formation separation

\bar{t} = characteristic time

V_o = nominal formation velocity

These variables are used to non-dimensionalize the Eqs (5.10) and (5.11). Non-dimensional variables and parameters are defined using the characteristic length and time. These variables and parameters are identified using the ^ symbol and are displayed below.

$$\begin{aligned} \hat{x} &= \frac{x}{l} & \hat{y} &= \frac{y}{l} & \hat{x}_o &= \frac{x_o}{l} = \cos \alpha \\ \hat{y}_o &= \frac{y_o}{l} = \sin \alpha & \hat{V}_w &= \frac{V_w}{V_o} & \hat{V}_{wc} &= \frac{V_{wc}}{V_o} \\ \hat{\tau}_{Vw} &= \frac{\tau_{Vw}}{\bar{t}} & \hat{\tau}_{\psi w} &= \frac{\tau_{\psi w}}{\bar{t}} & \hat{V}_L &= \frac{V_w}{V_o} \end{aligned} \quad (5.14)$$

where

\hat{x} = non-dimensional x-separation error

\hat{y} = non-dimensional y-separation error

\hat{x}_o = non-dimensional nominal x-separation

\hat{y}_o = non-dimensional nominal y-separation

\hat{V}_w = non-dimensional wing velocity

\hat{V}_{wc} = non-dimensional wing velocity command

$\hat{\tau}_{Vw}$ = non-dimensional wing velocity time constant

$\hat{\tau}_{\psi w}$ = non-dimensional wing heading time constant

\hat{V}_L = non-dimensional lead velocity

The above non-dimensional parameters are substituted into Equations (5.3), (5.4), (5.10) and (5.11) in order to form the following linear non-dimensional differential equations.

$$\dot{\hat{x}} = -\hat{V}_W - \frac{\sin \alpha}{\hat{\tau}_{\psi_W}} \psi_W + \frac{\sin \alpha}{\hat{\tau}_{\psi_W}} \psi_{Wc} + \hat{V}_L \quad (5.15)$$

$$\dot{\hat{V}}_W = -\frac{1}{\hat{\tau}_{v_W}} \hat{V}_W + \frac{1}{\hat{\tau}_{v_W}} \hat{V}_{Wc} \quad (5.16)$$

$$\dot{\hat{y}} = \left[\frac{\cos \alpha}{\hat{\tau}_{\psi_W}} - 1 \right] \psi_W - \frac{\cos \alpha}{\hat{\tau}_{\psi_W}} \psi_{Wc} + \psi_L \quad (5.17)$$

$$\dot{\psi}_W = -\frac{1}{\hat{\tau}_{\psi_W}} \psi_W + \frac{1}{\hat{\tau}_{\psi_W}} \psi_{Wc} \quad (5.18)$$

The above differential equations are rearranged into state variable form. Thus, the MIMO plant is represented by the following equations.

$$\dot{X} = AX + BU + \Gamma D \quad (5.19)$$

$$Y = CX \quad (5.20)$$

where the state and output matrices are

$$X = \begin{bmatrix} \hat{x} \\ \hat{V}_W \\ \hat{y} \\ \psi_W \end{bmatrix}, \quad A = \begin{bmatrix} 0 & -1 & 0 & -\frac{\sin \alpha}{\hat{\tau}_{\psi_W}} \\ 0 & -\frac{1}{\hat{\tau}_{v_W}} & 0 & 0 \\ 0 & 0 & 0 & \frac{\cos \alpha}{\hat{\tau}_{\psi_W}} - 1 \\ 0 & 0 & 0 & -\frac{1}{\hat{\tau}_{\psi_W}} \end{bmatrix}, \quad B = \begin{bmatrix} 0 & \frac{\sin \alpha}{\hat{\tau}_{\psi_W}} \\ \frac{1}{\hat{\tau}_{v_W}} & 0 \\ 0 & -\frac{\cos \alpha}{\hat{\tau}_{\psi_W}} \\ 0 & \frac{1}{\hat{\tau}_{\psi_W}} \end{bmatrix}, \quad \Gamma = \begin{bmatrix} 1 & 0 \\ 0 & 0 \\ 0 & 1 \\ 0 & 0 \end{bmatrix}, \quad (5.21)$$

$$C = \begin{bmatrix} 1 & 0 & 0 & 0 \\ 0 & 0 & 0 & 0 \end{bmatrix}, \quad D = \begin{bmatrix} \hat{V}_L \\ \psi_L \end{bmatrix}, \quad U = \begin{bmatrix} \hat{V}_{Wc} \\ \psi_{Wc} \end{bmatrix}, \quad Y = \begin{bmatrix} \hat{x} \\ \hat{y} \end{bmatrix} \quad (5.22)$$

where

D = disturbance input matrix

Γ = disturbance input vector

In the next two sections, the y and x-channels are identified and decoupled. The PI control law is applied to these decoupled state equations to form the closed loop state equations.

5.1.1 Y-Channel The y-channel is decoupled from the x-channel by partitioning the $X \in \mathbb{R}^4$ state vector as shown in Eq (5.23).

$$X = [(\hat{x}, \hat{V}_W), (\hat{y}, \psi_W)]' \quad (5.23)$$

Hence, the decoupled y-channel state equation is:

$$\begin{bmatrix} \dot{\hat{y}} \\ \dot{\psi}_W \end{bmatrix} = \begin{bmatrix} 0 & \frac{\cos \alpha}{\hat{\tau}_{\psi_W}} - 1 \\ 0 & -\frac{1}{\hat{\tau}_{\psi_W}} \end{bmatrix} \begin{bmatrix} \hat{y} \\ \psi_W \end{bmatrix} + \begin{bmatrix} -\frac{\cos \alpha}{\hat{\tau}_{\psi_W}} \\ \frac{1}{\hat{\tau}_{\psi_W}} \end{bmatrix} \psi_{Wc} + \begin{bmatrix} 1 \\ 0 \end{bmatrix} \psi_L \quad (5.24)$$

The wing aircraft's heading is commanded in response to a formation separation change in the y direction. The PI control law operates on the lateral separation error \hat{y} and is

$$\psi_{Wc} = \hat{k}_{yp} \hat{y} + \hat{k}_{yi} \int_0^t \hat{y} dt \quad (5.25)$$

where

\hat{k}_{yp} = non-dimensional, y-separation error, proportional gain

\hat{k}_{yi} = non-dimensional, y-separation error, integral gain

Differentiating Eq (5.25) yields

$$\dot{\psi}_{Wc} = \hat{k}_{yi} \hat{y} + \hat{k}_{yp} \dot{\hat{y}} \quad (5.26)$$

and inserting in Eq (5.26) the expression for $\dot{\hat{y}}$, yields

$$\dot{\psi}_{Wc} = \hat{k}_{yi} \hat{y} + \hat{k}_{yp} \left(\frac{\cos \alpha}{\hat{\tau}_{\psi_W}} - 1 \right) \psi_W - \hat{k}_{yp} \frac{\cos \alpha}{\hat{\tau}_{\psi_W}} \psi_{Wc} + \hat{k}_{yp} \psi_L \quad (5.27)$$

The augmented state equations incorporating the PI controller are

$$\dot{X}_y = A_y X_y + \Gamma_y d_y \quad (5.28)$$

$$Y_y = C_y X_y \quad (5.29)$$

i.e.,

$$\begin{bmatrix} \dot{\hat{y}} \\ \dot{\psi}_W \\ \dot{\psi}_{Wc} \end{bmatrix} = \begin{bmatrix} 0 & \frac{\cos \alpha}{\hat{\tau}_{\psi W}} - 1 & -\frac{\cos \alpha}{\hat{\tau}_{\psi W}} \\ 0 & -\frac{1}{\hat{\tau}_{\psi W}} & \frac{1}{\hat{\tau}_{\psi W}} \\ \hat{k}_{yi} & \hat{k}_{yp} \left(\frac{\cos \alpha}{\hat{\tau}_{\psi W}} - 1 \right) & -\hat{k}_{yp} \frac{\cos \alpha}{\hat{\tau}_{\psi W}} \end{bmatrix} \begin{bmatrix} \hat{y} \\ \psi_W \\ \psi_{Wc} \end{bmatrix} + \begin{bmatrix} 1 \\ 0 \\ \hat{k}_{yp} \end{bmatrix} \psi_L \quad (5.30)$$

$$Y_y = \begin{bmatrix} 0 & 1 & 0 \end{bmatrix} \begin{bmatrix} \hat{y} \\ \psi_W \\ \psi_{Wc} \end{bmatrix} = [\psi_W] \quad (5.31)$$

where

X_y = augmented y-channel state vector

A_y = augmented y-channel state transition matrix

Γ_y = augmented y-channel disturbance input matrix

D_y = augmented y-channel disturbance input vector

Y_y = augmented y-channel output vector

C_y = augmented y-channel output matrix

Note: The two y-channel parameters in Eqs (5.30) and (5.31) are the formation angle α , and the heading time constant $\hat{\tau}_{\psi W}$.

(i) Statics Consider a lead heading change (disturbance) input, $\psi_L(\bar{t})$. The steady state response to a unit step disturbance is

$$\hat{y}(\bar{t})_{ss} = \lim_{s \rightarrow 0} s(SI - A_y)^{-1} \Gamma_y \frac{1}{s} = -A_y^{-1} \Gamma_y = \begin{bmatrix} 0 \\ 1 \\ 1 \end{bmatrix} \quad (5.32)$$

The wing aircraft must be able to track the lead aircraft with zero steady state error. This zero steady state tracking error requirement is stated below,

$$\text{At } \hat{t} \rightarrow \infty, \hat{y}(\infty) = 0, \psi_W(\infty) = \psi_{Wc}(\infty) = \psi_L = D_y = 1, \quad (5.33)$$

i.e.,

$$-\Gamma_y = A_y \begin{bmatrix} 0 \\ 1 \\ 1 \end{bmatrix} = \begin{bmatrix} -1 \\ 0 \\ -\hat{k}_{yi} \end{bmatrix} \quad (5.34)$$

Now Eq (5.33) implies that Eq (5.34) satisfies this requirement, as long as A_y is invertible. A necessary condition for the augmented state matrix A_y to be invertible is that the integral gain \hat{k}_{yi} must be non-zero.

(ii) Dynamics The system characteristic equation for the y-channel augmented state equation is shown in Eq (5.35). A Routh stability analysis is performed to determine stability(3)[185-191]. The Routhian array for the characteristic equation is shown in Table 5.1.

$$\det(SI - A_y) = \hat{\tau}_{\psi_W} s^3 + (\hat{k}_{yp} \cos \alpha + 1) s^2 + (\hat{k}_{yp} + \hat{k}_{yi} \cos \alpha) s + \hat{k}_{yi} = 0 \quad (5.35)$$

s^3	$\hat{\tau}_{\psi_W}$	$(\hat{k}_{yp} + \hat{k}_{yi} \cos \alpha)$
s^2	$(\hat{k}_{yp} \cos \alpha + 1)$	\hat{k}_{yi}
s^1	$\frac{(\hat{k}_{yp} \cos \alpha + 1)(\hat{k}_{yp} + \hat{k}_{yi} \cos \alpha) - \hat{\tau}_{\psi_W} \hat{k}_{yi}}{(\hat{k}_{yp} \cos \alpha + 1)}$	
s^0	\hat{k}_{yi}	

Table 5.1. Y-Channel Routhian Array

After applying the Routh criterion, the following stability conditions relating the system parameters and PI controller gains are obtained:

$$\hat{\tau}_{\psi_w} > 0 \quad (5.36)$$

$$\hat{k}_{yp} > -\frac{1}{\cos \alpha} \quad (5.37)$$

$$\hat{k}_{yp} + \hat{k}_{yi} \cos \alpha > \frac{\hat{\tau}_{\psi_w} \hat{k}_{yi}}{\hat{k}_{yp} \cos \alpha + 1} \quad (5.38)$$

$$\hat{k}_{yi} > 0 \quad (5.39)$$

The above conditions reveal the close relationship between the formation geometry, controller gains and stability parameters. This relationship is critical to the assignment of the PI controller gains. In the next section, a similar analysis is performed on the x-channel.

5.1.2 X-Channel The x-channel is decoupled from the y-channel; see Eq (5.23). The decoupled x-channel state equation is shown below. The $d(t)$ signal in Equation (5.40) is considered a disturbance input. This disturbance perturbs the x-channel due to a wing heading change and a lead aircraft velocity change; the disturbance signal is defined in Equation (5.41).

$$\begin{bmatrix} \dot{\hat{x}} \\ \dot{\hat{V}}_w \end{bmatrix} = \begin{bmatrix} 0 & -1 \\ 0 & -\frac{1}{\hat{\tau}_{v_w}} \end{bmatrix} \begin{bmatrix} \hat{x} \\ \hat{V}_w \end{bmatrix} + \begin{bmatrix} 0 \\ \frac{1}{\hat{\tau}_{v_w}} \end{bmatrix} \hat{V}_{wc} + \begin{bmatrix} 1 \\ 0 \end{bmatrix} \left(V_L + \frac{\sin \alpha}{\hat{\tau}_{\psi_w}} (\psi_{wc} - \psi_w) \right) \quad (5.40)$$

$$d(t) = \hat{V}_L + \frac{\sin \alpha}{\hat{\tau}_{\psi_w}} (\psi_{wc} - \psi_w) \quad (5.41)$$

The wing aircraft's velocity is commanded in response to a formation separation change in the x direction. The PI control law is given by

$$\hat{V}_{wc} = \hat{k}_{xp} \hat{x} + \hat{k}_{xi} \int_0^t \hat{x} dt \quad (5.42)$$

where

\hat{k}_{xp} = non-dimensional, x-separation error, proportional gain

\hat{k}_{xi} = non-dimensional, x-separation error, integral gain

Differentiating Eq (5.42) yields

$$\dot{\hat{V}}_{wc} = \hat{k}_{xi}\hat{x} + \hat{k}_{xp}\dot{\hat{x}} \quad (5.43)$$

Inserting into Eq (5.43) the $\dot{\hat{x}}$ expression from Eq (5.40) gives

$$\dot{\hat{V}}_{wc} = \hat{k}_{xi}\hat{x} - \hat{k}_{xp}\hat{V}_w + \hat{k}_{xp}d \quad (5.44)$$

The augmented state equations comprised of Eq (5.40) and the PI controller (Eq (5.44)), are displayed in Eqs. (5.45) through (5.48).

$$\dot{X}_x = A_x X_x + \Gamma_x D_x \quad (5.45)$$

$$Y_x = C_x X_x \quad (5.46)$$

i.e.,

$$\begin{bmatrix} \dot{\hat{x}} \\ \dot{\hat{V}}_w \\ \dot{\hat{V}}_{wc} \end{bmatrix} = \begin{bmatrix} 0 & -1 & 0 \\ 0 & -\frac{1}{\tau_{vw}} & \frac{1}{\tau_{vw}} \\ \hat{k}_{xi} & -\hat{k}_{xp} & 0 \end{bmatrix} \begin{bmatrix} \hat{x} \\ \hat{V}_w \\ \hat{V}_{wc} \end{bmatrix} + \begin{bmatrix} 1 \\ 0 \\ \hat{k}_{xp} \end{bmatrix} d \quad (5.47)$$

$$Y_x = \begin{bmatrix} 0 & 1 & 0 \end{bmatrix} \begin{bmatrix} \hat{x} \\ \hat{V}_w \\ \hat{V}_{wc} \end{bmatrix} = [\hat{V}_w] \quad (5.48)$$

where

X_x = augmented x-channel state vector

A_x = augmented x-channel state transition matrix

Γ_x = augmented x-channel disturbance input matrix

D_x = augmented x-channel disturbance input vector

Y_x = augmented x-channel output vector

C_x = augmented x-channel output matrix

Note: The primary x-channel parameter in Eq (5.47) is the velocity time constant $\hat{\tau}_{V_w}$.

(i) Statics Consider a unit step disturbance input. Similar to the y-channel "static" analysis, the steady state response to a unit step disturbance is

$$\hat{x}(t)_{ss} = \lim_{s \rightarrow 0} s(Si - A_x)^{-1} \Gamma_x \frac{1}{s} = -A_x^{-1} \Gamma_x = \begin{bmatrix} 0 \\ 1 \\ 1 \end{bmatrix} \quad (5.49)$$

Again, the wing aircraft must be able to track the lead aircraft with zero steady state error. This zero steady state tracking error requirement is stated by

$$\text{At } t \rightarrow \infty, \hat{x}(\infty) = 0, \hat{V}_w(\infty) = \hat{V}_{w_c}(\infty) = \hat{V}_L = D_y = 1, \quad (5.50)$$

i.e.,

$$-\Gamma_x = A_x \begin{bmatrix} 0 \\ 1 \\ 1 \end{bmatrix} = \begin{bmatrix} -1 \\ 0 \\ -\hat{k}_{xi} \end{bmatrix} \quad (5.51)$$

Equation (5.49) implies that Eq (5.51) satisfies this requirement, as long as A_x is invertible. Hence, a necessary condition for the augmented state matrix, A_x , to be invertible is that the integral gain \hat{k}_{xi} must be non-zero. This is in line with the results from the y-channel analysis.

(ii) Dynamics The system characteristic equation for the x-channel augmented state equation is shown in Eq (5.52). A Routh stability analysis is again performed to determine stability(3)[185-191]. The Routhian array for the characteristic equation is shown in Table 5.2.

$$\det(SI - A_x) = \hat{\tau}_{V_w} s^3 + s^2 + \hat{k}_{xp} s + \hat{k}_{xi} = 0 \quad (5.52)$$

After applying the Routh criterion, the following stability conditions on both the system parameters and PI controller gains are obtained:

$$\begin{array}{c|cc}
s^3 & \hat{\tau}_{VW} & \hat{k}_{xp} \\
s^2 & 1 & \hat{k}_{xi} \\
s^1 & (\hat{k}_{xp} - \hat{\tau}_{VW} \hat{k}_{xi}) & \\
s^0 & \hat{k}_{xi} &
\end{array}$$

Table 5.2. X-Channel Routhian Array

$$\hat{\tau}_{VW} > 0 \quad (5.53)$$

$$\hat{k}_{xp} > \hat{k}_{xi} \hat{\tau}_{VW} \quad (5.54)$$

$$\hat{k}_{xi} > 0 \quad (5.55)$$

The above equations tie in the type of aircraft, controller gains, and stability parameters. This relationship is critical to the assignment of the PI controller gains. Hence the following holds:

Proposition 1 *The necessary and sufficient conditions for formation flight control are the employment of integral feedback, and satisfaction of the conditions stated in Eqs (5.36)–(5.39) and Eqs (5.53)–(5.55).* \square

The next section makes use of both the Y and X-Channels analyses, i.e., Eqs (5.36)–(5.39) and Eqs (5.53)–(5.55), to assign the optimal PI controller parameters.

5.2 Pole Placement through Controller Gain Adjustment: Residues of the Step Response for Preliminary Identification of Dominant Dynamics

The closed-loop MIMO state equations developed for the formation flight control problem in the previous section are used to design the PI controller. The controller is designed in two steps. In the first step, the controller gains are determined for the linear state equations using pole placement. The second step involves applying these gains to the non-linear formation control system model. Computer simulations are performed to fine

tune these gains for the best tracking response. The poles, residues and controller gains presented in this section are all dimensional.

A SISO closed-loop transfer function, Eq (5.56), is obtained for both the Y and X-channels by optimizing the wing aircraft's heading and velocity response respectively. Using the stability and steady state conditions, from the previous section, a transient analysis is performed in order to optimize the output time response. The dominant dynamics are identified by checking the residues of the output response. The controller gains are then adjusted to produce the fastest poles with the largest residues.

$$G(s) = C_{cl}[sI - A_{cl}]^{-1}\Gamma_{cl} \quad (5.56)$$

Computer simulations using the non-linear control system are performed using these gains. The rate-limiters in the aircraft models tend to produce an underdamped oscillatory response for high integral gains values. This response is caused by the increase in tracking error induced by the presence of the rate-limiters. Figure 5.2 shows an example of this build up. Indeed, integral action is needed for tracking. At the same time, integral feedback adversely interacts with the saturation. Hence, an interesting trade off situation has arisen, which, however, is not fully investigated in this thesis.

In the next two sections, this analysis is conducted on both the Y and X channels in order to develop an optimum set of gains. This analysis is performed using the C-130A first order models developed by Dargan(2) and Rohs(9). The two aircraft are arranged in a diamond formation as shown in Figure 5.1. The key dimensional parameters needed for this analysis are contained in Table 5.3.

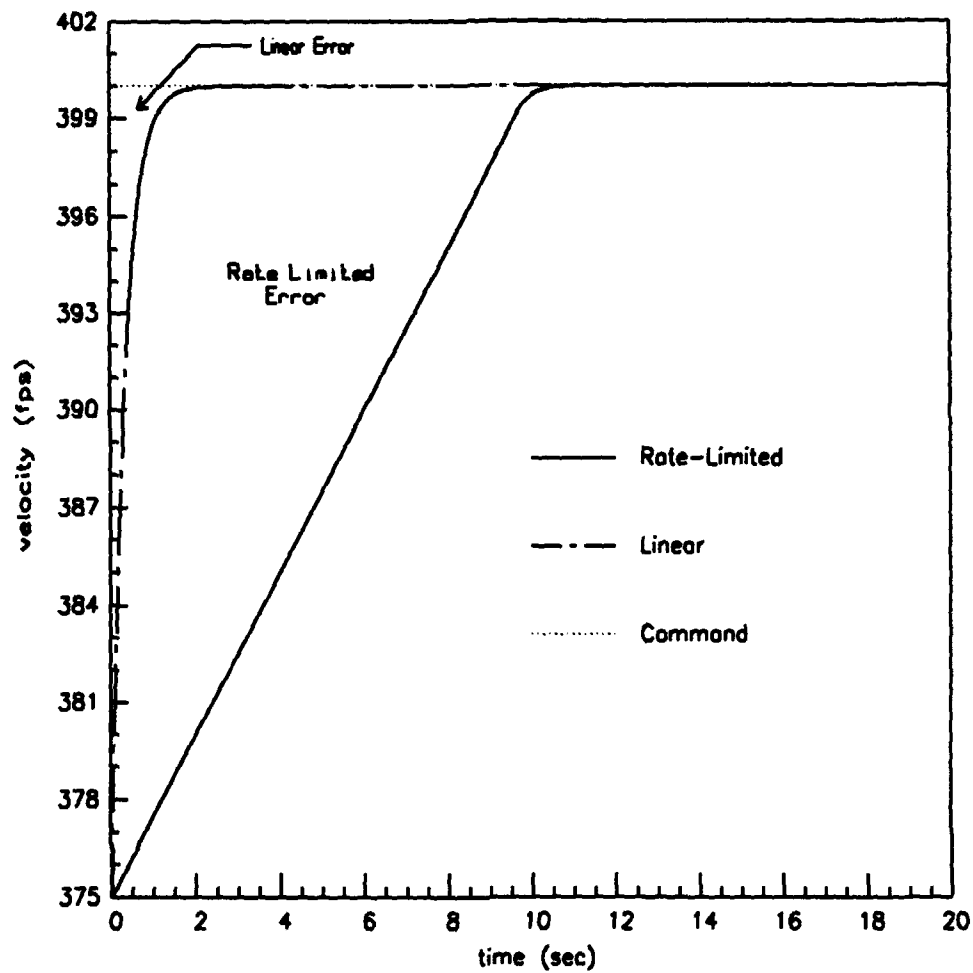


Figure 5.2. Comparison of Linear and Rate-Limited Velocity Responses

Table 5.3. Formation and Aircraft Parameters

Parameter	Description	Value	Units
V	Nominal Velocity	375	fps
x_o	x-separation	500	feet
y_o	y-separation	500	feet
α	formation angle	45	degs
l	separation	707	feet
$\tau_{\psi w}$	Hdg time constant	$\frac{1}{1.5}$	secs
τ_{Vw}	Vel time constant	$\frac{1}{3}$	secs

5.2.1 Y-Channel Gains The Y-Channel controller gains are selected by optimizing the wing aircraft's heading response to a lead aircraft's step heading change. The Laplace representation of the output response is

$$\psi_W(s) = G(s)\psi_L(s) = \begin{bmatrix} 0 & 1 & 0 \end{bmatrix} [sI - A_y]^{-1} \Gamma_y \frac{1}{s} = \frac{1}{s} + \frac{r_2}{s + p_2} + \frac{r_3}{s + p_3} + \frac{r_4}{s + p_4} \quad (5.57)$$

Both k_{yi} and k_{yp} are varied, and the resulting poles and residues of Eq (5.57) are determined using computer simulations. The ratio of $\frac{k_{yz}}{k_{yi}}$ is fixed, while k_{yp} is varied from 0.001 to 10. Figure 5.3 displays the poles and residues for $\frac{k_{yz}}{k_{yi}} = 100$. The best response is attained for values of $k_{yp} \geq 0.1$. The pole p_2 is no longer the dominant pole since its associated residue is nearly zero.

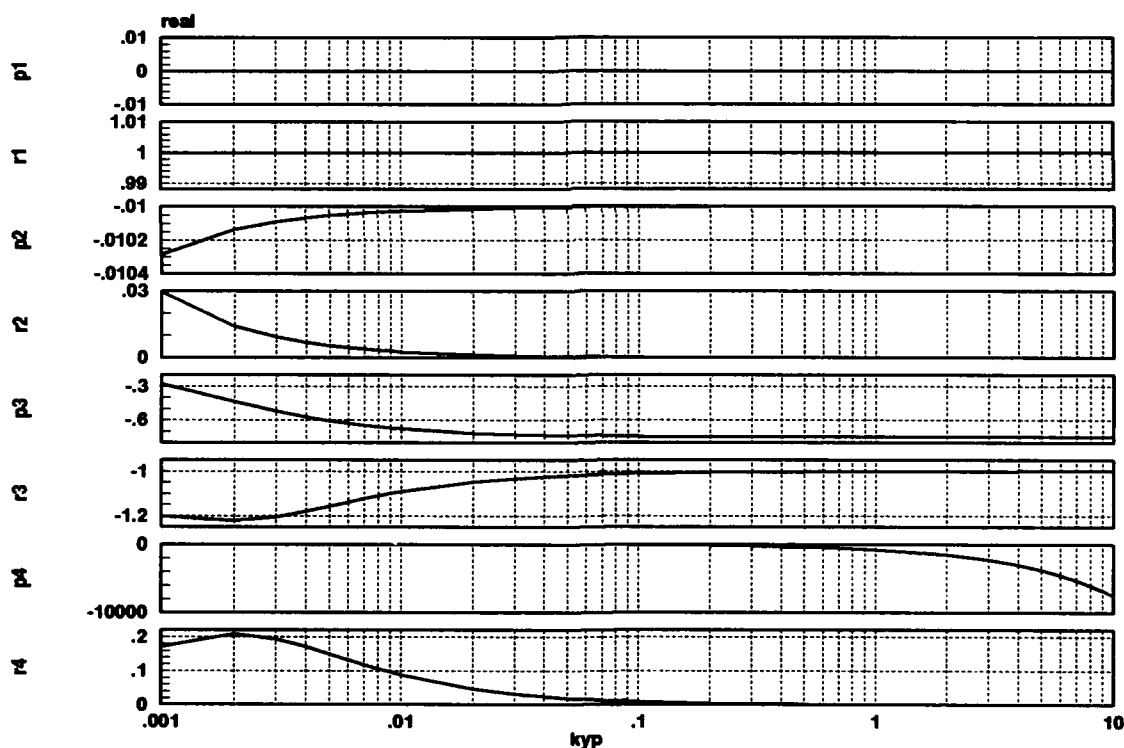


Figure 5.3. Y-Channel, Wing's Heading Step Response, Poles and Residues versus Controller Gains, $\frac{k_{yz}}{k_{yi}} = 100$

Selecting $k_{yp} = 1$ and $k_{yi} = 0.01$ results in the following poles and residues:

$$\psi_w(s) = \frac{1}{s} + \frac{0.0001}{s + .01} + \frac{-1.0010}{s + .7492} + \frac{.0010}{s + 750.7408} \quad (5.58)$$

The output time response is obtained through the inverse Laplace transform of Eq (5.58). Other ratios of $\frac{k_{yz}}{k_{yi}}$ may be selected but numerous computer simulations have shown this to be a near optimum value.

5.2.2 X-Channel Gains The x-channel controller gains are selected by optimizing the wing aircraft's response to a lead aircraft's step velocity change. The disturbance input in Eq (5.41) is confined to the lead aircraft's velocity by setting both the heading and commanded heading to zero. The wing's velocity response to a step input is shown in Eq (5.59).

$$V_w(s) = G_x(s)D_x(s) = [010][sI - A_x]^{-1}\Gamma_x \frac{1}{s} = \frac{1}{s} + \frac{r_2}{s + p_2} + \frac{r_3}{s + p_3} + \frac{r_4}{s + p_4} \quad (5.59)$$

The poles and residues of Eq (5.59) are again determined using computer simulation. The ratio of $\frac{k_{yz}}{k_{yi}}$ is fixed while k_{xp} is varied from 0.001 to 10. Figure 5.4 displays the poles and residues for $\frac{k_{yz}}{k_{yi}} = 100$. A fast response is attained for values of $k_{xp} \geq 0.7$. The pole p_2 is not dominant since it's associated residue is much less than the other three residues.

Selecting $k_{xp} = 0.75$ and $k_{xi} = 0.0075$ results in the following output poles and residues:

$$V_w(s) = \frac{1}{s} + \frac{0.0138}{s + 0.0101} + \frac{-6.6677}{s + 1.3719} + \frac{5.6538}{s + 1.6179} \quad (5.60)$$

The next section compares the controller gains determined using the above analysis against those developed in previous research(2)[4-1-4-13]. This comparison is done using the non-linear formation control system model.

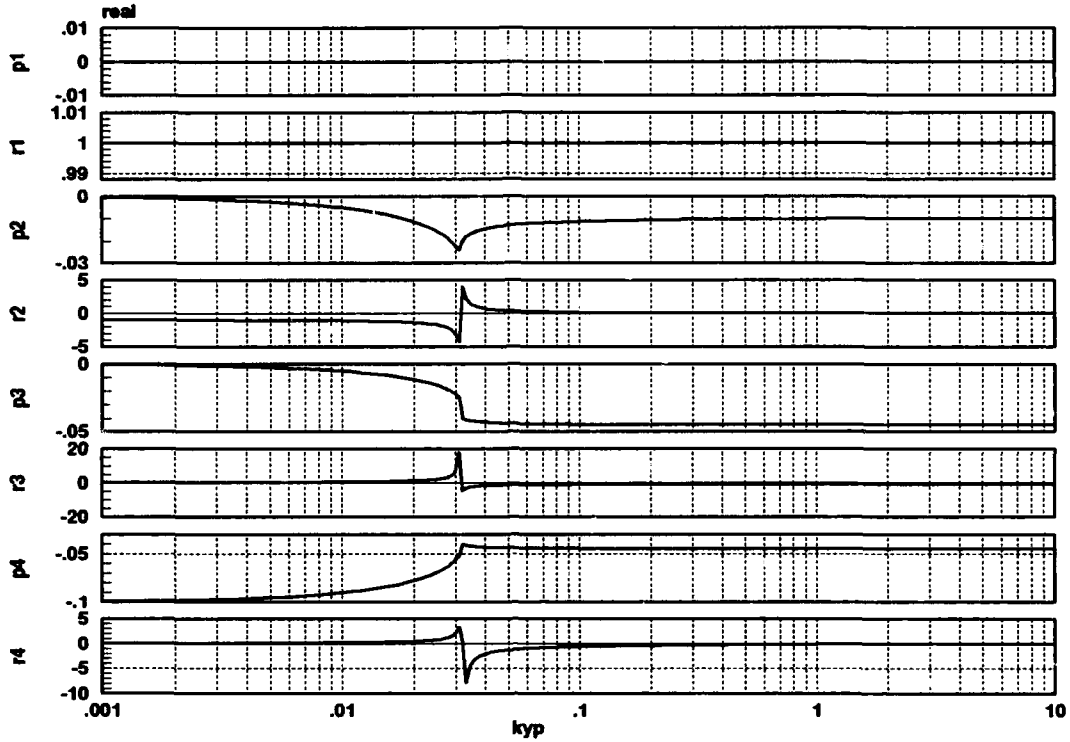


Figure 5.4. X-Channel, Wing's Velocity Step Response, Poles and Residues versus Controller Gains, $\frac{k_{yz}}{k_{yi}} = 100$

5.3 Performance Evaluations

Two different computer simulations are performed to evaluate the controller designed in the previous two sections. A diamond formation consisting of a single wing aircraft is commanded to have first a velocity change, and then a heading change. The wing aircraft's time response is compared against values developed in previous research(2)[4-1-4-13]. Table 5.4 summarizes the PI controller values used in the evaluations. No mixer is used in this evaluation.

Table 5.4. PI Controller Gains

Parameter	New	Previous
k_{yp}	1	.2
k_{yi}	.01	.009
k_{xp}	.75	.2
k_{xi}	.0075	.015

5.3.1 Diamond Formation Heading Change The response for a 10 degree heading change from a diamond formation is shown in Figure 5.5. This figure shows a slightly faster response of the wing aircraft in tracking the lead aircraft. There is a significantly reduced error in the y-separation during the maneuver. The better tracking is offset by a slight increase in the wing's velocity.

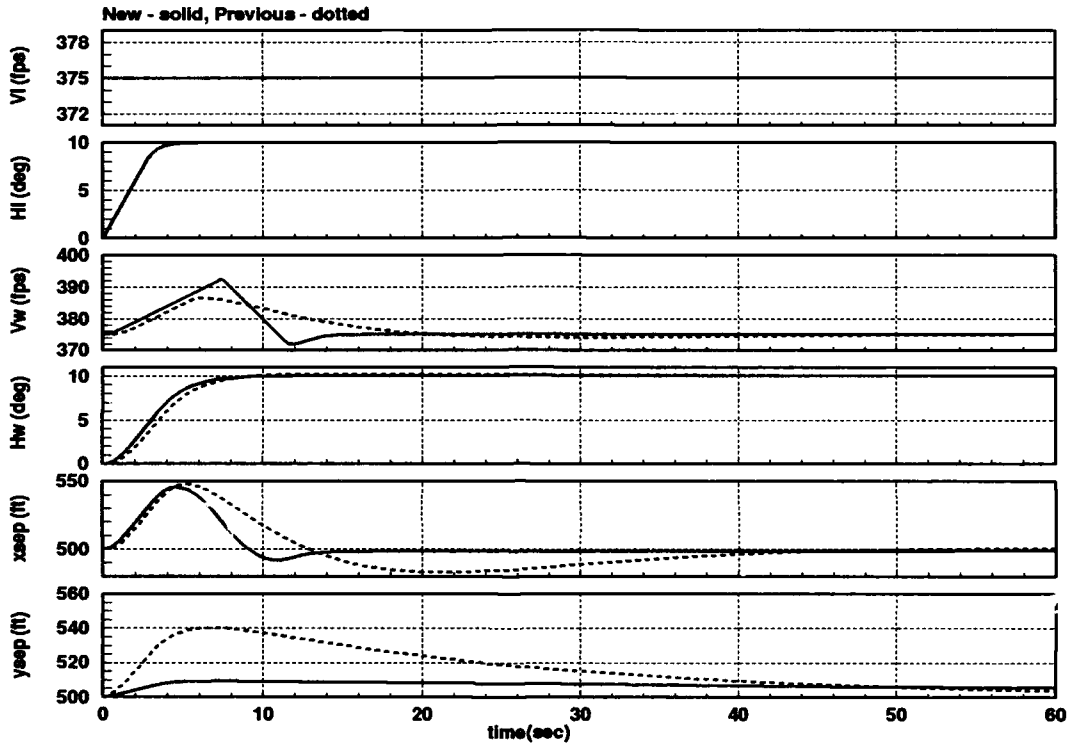


Figure 5.5. Diamond Formation, 10 Degrees Heading Change, Time Response Comparison

5.3.2 Diamond Formation Velocity Change The response for a 400 feet per second velocity command is shown in Figure 5.6. This figure shows a faster response of the wing aircraft in tracking the lead aircraft. The new controller gains result in virtually zero overshoot, since the output poles are overdamped and the integral gain is relatively small. This low integral gain adversely affects the y-separation, resulting in a high settling time. In terms of the velocity response, the new gains definitely result in a better response. The integral gain k_{zi} could be increased to decrease the y-separation settling time.

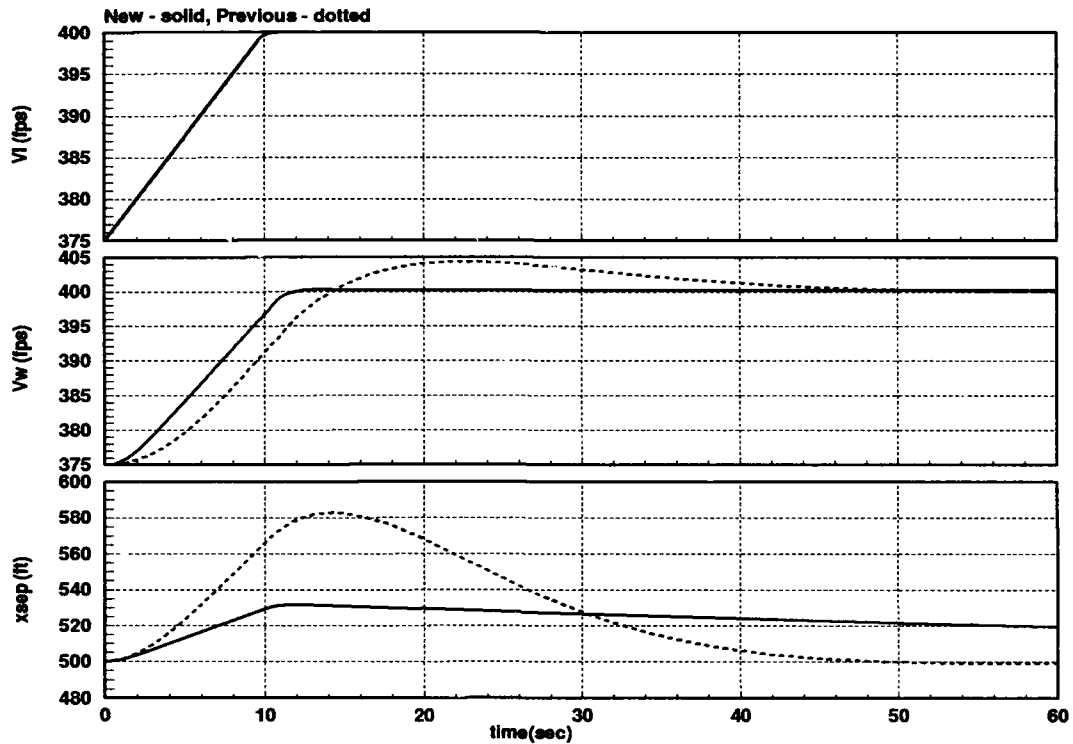


Figure 5.6. Diamond Formation, 375 to 400 fps Velocity Change, Time Response Comparison

5.4 Summary

An analytical analysis of the formation flight control problem produced a linear four-dimensional state space model using small angle approximations and small perturbations. The X and Y-Channels are decoupled and augmented using a PI control law. Further analysis of these augmented closed-loop equations substantiated the requirement for integral feedback to achieve zero steady-state error. Application of Routh's stability criterion identified the interrelationship of formation geometry, aircraft models, and controller gains on stability. Simple pole placement is used to select an optimum set of PI controller gains. The performance evaluation shows that these gains produce a fast time response with zero steady state error. While the analytical analysis result in acceptable PI controller gains, additional refinement of these values is still needed to produce the best tracking response in the non-linear computer simulation.

VI. Energy Conserving Maneuvers

Horizontal and constant velocity lead aircraft maneuvers force the wing aircraft to adjust its speed to maintain the formation. Consequently, the wing aircraft is constantly accelerating and decelerating during level flight formation turns. Conserving the wing aircraft's energy, will reduce fuel consumption. In addition, it is advantageous from a reliability and maintainability point of view to have the engine operate at a constant throttle setting. Hence, the vertical separation requirement between the lead and the wing aircraft is relaxed in order to allow for energy conserving maneuvers. This allows the wing aircraft to dive to increase its velocity, or to zoom to slow down. The next section presents the theoretical analysis outlining a wing energy conserving formation control strategy. As in the previous chapter, first order aircraft models are used. A performance evaluation of the energy-conserving formation flight control system follows this analysis.

6.1 Theoretical Development

The wing aircraft's specific energy is the sum of its kinetic and potential energy per unit mass:

$$e_w = \frac{1}{2}V_w^2 + gh_w, \quad (6.1)$$

where

g = acceleration of gravity

e_w = wing aircraft's specific energy

Differentiating Eq (6.1) and setting \dot{e}_w equal to zero results in Eq (6.2). This equation is the fundamental relationship for energy conservation.

$$\dot{e}_w = V\dot{V}_w + g\dot{h}_w = 0 \quad (6.2)$$

Rearranging this equation and substituting the first order aircraft model

$$\dot{h}_w = -\frac{1}{\tau_{hw}}h_w + \frac{1}{\tau_{hw}}h_{wc}, \quad (6.3)$$

yields

$$\dot{V}_W = \left(\frac{g}{V_o \tau_{h_W}} \right) h_W - \left(\frac{g}{V_o \tau_{h_{Wc}}} \right) h_{Wc} \quad (6.4)$$

As seen in Eq (6.4), the wing aircraft's velocity is controlled by using an altitude change command.

The following equations display the definitions needed to non-dimensionalize Eq (6.4).

$$\begin{aligned} \hat{h}_W &= \frac{h_W}{l} & \hat{h}_{Wc} &= \frac{h_{Wc}}{l} \\ \hat{\tau}_{\psi_W} &= \frac{\tau_{\psi_W}}{t} \end{aligned} \quad (6.5)$$

Furthermore,

$$\dot{\hat{V}}_W = \frac{\xi}{\hat{\tau}_{\psi_W}} \hat{h}_W - \frac{\xi}{\hat{\tau}_{\psi_W}} \hat{h}_{Wc} \quad (6.6)$$

and the nondimensional parameter

$$\xi = \frac{gl}{V_o^2} \quad (6.7)$$

where

ξ = altitude to velocity proportionality constant

A PI controller is designed to command the wing's altitude in response to a change in x-separation. The appropriate equations are listed below. The disturbance input $d(t)$ is defined in Eq (5.41).

$$\hat{h}_{Wc} = \hat{k}_{xzp} \hat{x} + \hat{k}_{xzi} \int_0^t \hat{x} dt \quad (6.8)$$

where

\hat{k}_{xzp} = non-dimensional, 3-D x-separation error, proportional gain

\hat{k}_{xzi} = non-dimensional, 3-D x-separation error, integral gain

Differentiating Eq (6.8) yields:

$$\dot{\hat{h}}_{Wc} = \hat{k}_{xzi} \hat{x} + \hat{k}_{xzp} \dot{\hat{x}} \quad (6.9)$$

Inserting the $\dot{\hat{x}}$ from Eq (5.6) and $d(t)$ from Eq (5.42) into Eq (6.8) yields

$$\dot{\hat{h}}_{Wc} = \hat{k}_{zzi}\hat{x} + \hat{k}_{zsp}\xi\hat{h}_W + \hat{k}_{zsp}d \quad (6.10)$$

The closed loop X channel state space equations incorporating energy conservation and proportional plus integral feedback are shown in Eqs (6.11) to (6.12).

$$\dot{X} = A_{xz}X_{xz} + \Gamma_{xz}D_{xz} \quad (6.11)$$

$$\begin{bmatrix} \dot{\hat{x}} \\ \dot{\hat{h}}_W \\ \dot{\hat{h}}_{Wc} \end{bmatrix} = \begin{bmatrix} 0 & \xi & 0 \\ 0 & -\frac{1}{\tau_{hW}} & \frac{1}{\tau_{hW}} \\ \hat{k}_{zzi} & \hat{k}_{zsp} & 0 \end{bmatrix} \begin{bmatrix} \hat{x} \\ \hat{h}_W \\ \hat{h}_{Wc} \end{bmatrix} + \begin{bmatrix} 1 \\ 0 \\ \hat{k}_{zsp} \end{bmatrix} d \quad (6.12)$$

$$Y_{xz} = C_{xz}X_{xz} = \begin{bmatrix} 0 & -\xi & 0 \end{bmatrix} \begin{bmatrix} \hat{x} \\ \hat{h}_W \\ \hat{h}_{Wc} \end{bmatrix} = [\hat{V}_W] \quad (6.13)$$

where

X_{xz} = augmented x-channel state vector

A_{xz} = augmented x-channel state transition matrix

Γ_{xz} = augmented x-channel disturbance input matrix

D_{xz} = augmented x-channel disturbance input vector

Y_{xz} = augmented x-channel output vector

C_{xz} = augmented x-channel output matrix

Given a unit step disturbance input, the wing aircraft must be able to track the lead with zero steady state error. The steady state response to a unit step disturbance is

$$\lim_{s \rightarrow 0} s(SI - A_{xz})^{-1}\Gamma_{xz}\frac{1}{s} = -A_{xz}^{-1}\Gamma_{xz} = \begin{bmatrix} 0 \\ 1 \\ 1 \end{bmatrix} \quad (6.14)$$

Zero steady state error is verified by rearranging Eq (6.14). Equation (6.15) verifies that this requirement is satisfied as long as A_{xz} is invertible.

$$-\Gamma_{xz} = A_{xz} \begin{bmatrix} 0 \\ 1 \\ 1 \end{bmatrix} = \begin{bmatrix} -1 \\ 0 \\ -\hat{k}_{xzi} \end{bmatrix} \quad (6.15)$$

Analysis of the matrix A_{xz} in Eq (6.12) shows that a necessary condition for the augmented state matrix, A_{xz} , to be invertible is that the integral gain \hat{k}_{xzi} must be non-zero. This reaffirms **Proposition 1**, in Chapter V, that integral feedback is a necessary and sufficient condition for formation flight control.

The system characteristic equation for the X-Channel augmented state equation is shown in Eq (6.16). A Routh stability analysis is performed to determine stability. The Routhian array for the characteristic equation is shown in Figure 6.1.

$$\det(sI - A_{xz}) = \hat{\tau}_{hw} s^3 + s^2 - \hat{k}_{xzp} \xi s - \hat{k}_{xzi} \xi = 0 \quad (6.16)$$

After applying the Routh criterion, the following stability constraints on both the system

s^3	$\hat{\tau}_{hw}$	$-\hat{k}_{xzp}\xi$
s^2	1	$-\hat{k}_{xzi}\xi$
s^1	$(-\hat{k}_{xzp}\xi + \hat{\tau}_{hw}\hat{k}_{xzi}\xi)$	
s^0	$\hat{k}_{xzi}\xi$	

Table 6.1. X-Channel Routhian Array

parameters and PI controller gains result.

$$\hat{\tau}_{hw} > 0 \quad (6.17)$$

$$\hat{k}_{xzi} > \frac{\hat{k}_{xzp}}{\hat{\tau}_{hw}} \quad (6.18)$$

$$\hat{k}_{xzi} < 0 \quad (6.19)$$

The above equations impose the requirement for negative controller gains in order to maintain stability. This inverse relationship is easily visualized, since the wing aircraft

must descend to speed up and climb to slow down. The next section uses an analysis of the X-Channel to assign the optimum PI controller parameters.

6.2 X-Channel Controller Gain Adjustment

The X-Channel controller gains are selected by optimizing the wing aircraft's response to a lead aircraft's velocity change. When the heading and the commanded heading are equal, the disturbance input given by Eq (5.41) is reduced to the lead aircraft's velocity. The wing's velocity response to a step input is

$$V_W(s) = \begin{bmatrix} 0 & -\xi & 0 \end{bmatrix} [sI - A_{xz}]^{-1} \Gamma_{xz} \frac{1}{s} = \frac{1}{s} + \frac{r_2}{s + p_2} + \frac{r_3}{s + p_3} + \frac{r_4}{s + p_4} \quad (6.20)$$

The poles and residues of Eq (6.20) are again determined using computer simulation. The ratio of $\frac{k_{xzp}}{k_{xzi}}$ is fixed while k_{xzp} is varied from 0.001 to 100. Figure 6.1 displays the poles and residues for $\frac{k_{xzp}}{k_{xzi}} = 100$. A fast response is attained for a value of $k_{xzp} \leq -2$. Again, the pole, p_2 , is a less dominant pole since it's associated residue is much smaller less than the residues of the other poles. Selecting $k_{xzp} = -3$ and $k_{xzi} = -0.03$ results in the response shown in Eq (6.21). Even though the selected poles are complex, they provide a faster response than selecting real poles.

$$V_W(s) = \frac{1}{s} + \frac{0.0432}{s + 0.0104} - \frac{1.4561\angle -135.7624 \text{ deg}}{s + 0.2448 - j0.2510} - \frac{1.4561\angle +135.7624 \text{ deg}}{s + 0.2448 + j0.2510} \quad (6.21)$$

In the next section, a set of controller gains which produces a good response is determined, using the above analysis, and through computer simulation.

6.3 Performance Evaluations

Two different computer simulations are performed to evaluate the controller designed in the previous section. A diamond formation consisting of a single wing aircraft is commanded to perform a 30 degree "side step" heading change. The second maneuver is a 90 degree heading and formation change. Table 6.2 summarizes the PI controller values used in the evaluations. No mixer is used in this evaluation.

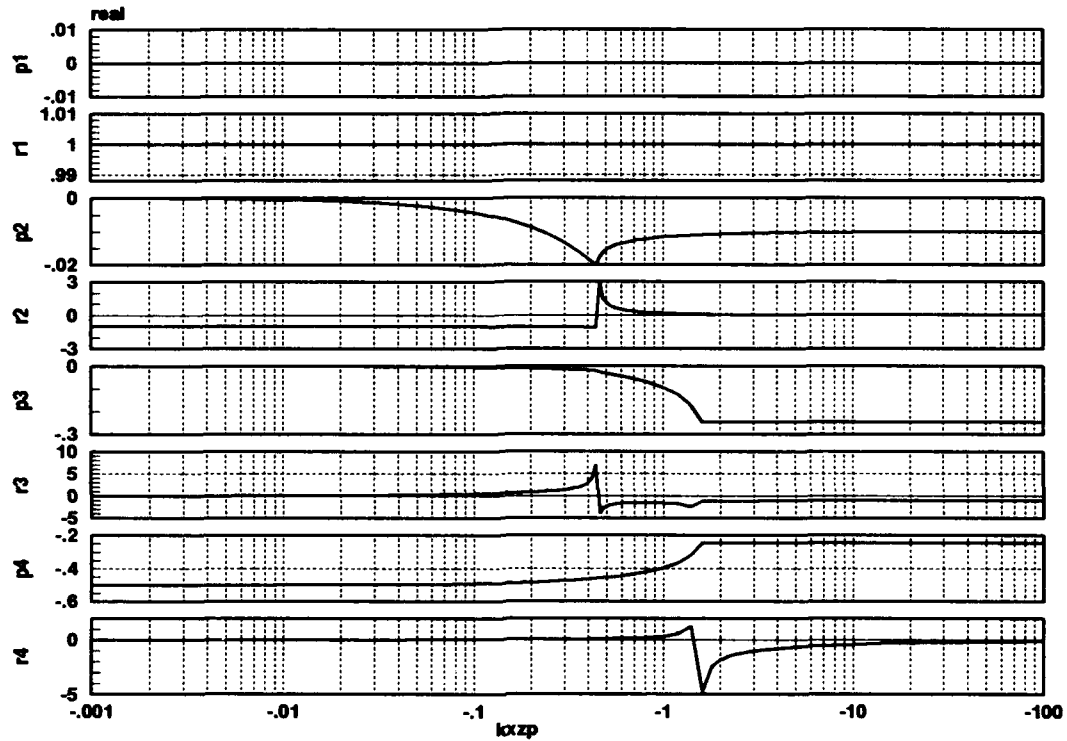


Figure 6.1. X-Channel Design for Energy Conservation, Wing's Velocity Step Response, Poles and Residues versus Controller Gains, $\frac{k_{xsp}}{k_{xsi}} = 100$

6.3.1 Diamond Formation Side Step Maneuver The side step heading change maneuver consists of two consecutive equal but opposite 10deg heading commands. The purpose of this maneuver is to return the formation back to its original heading after the initial command. Figure 6.2 displays the time responses for this maneuver. During the initial 10deg heading change, the wing aircraft must descend, increasing its velocity, in order to track the lead. As the lead aircraft executes the -10deg heading change during the second part of the maneuver, the wing ascends, bleeding off its airspeed.

Table 6.2. PI Controller Gains

Parameter	Value
k_{yp}	1
k_{yi}	0.01
k_{xsp}	-0.3
k_{xsi}	-0.03

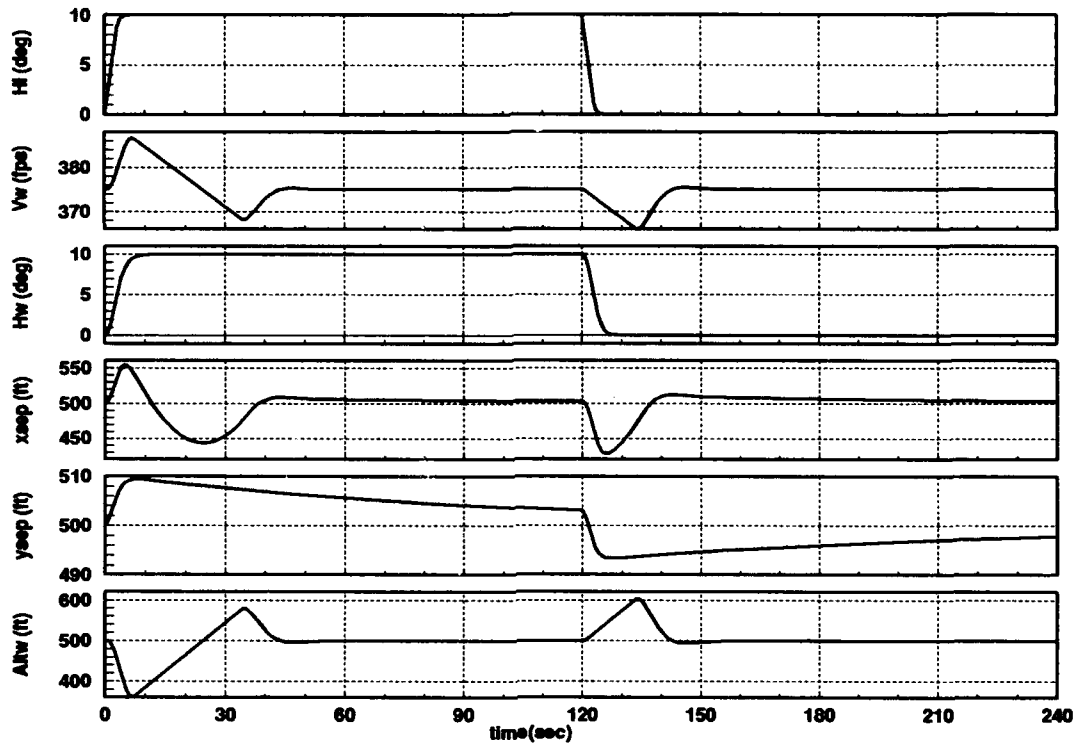


Figure 6.2. Diamond Formation 10 Degree Side Step Heading Change

6.3.2 Diamond Formation 90 Degree Heading Change and Formation Transposition As seen in the side step heading change, the wing aircraft must increase its velocity in order to follow the lead aircraft for a positive heading change. If the lead is to make a 90 degree heading change, a considerable amount of energy is required to increase the wing's velocity and track the lead aircraft along the outside path. Figure 6.3 illustrates an alternative trajectory for the wing aircraft. In this case, the wing aircraft conserves its energy by decreasing its altitude, which increases its velocity, and then executes a formation change to the opposite side of the lead aircraft as is often an operational practice. The wing then climbs to bleed off the excess velocity and resumes formation holding on the other side of the lead.

A design is accomplished in which the gains are changed from those in Table 7.1. The PI controller gains are reduced to $k_{xip} = -0.5$ and $k_{xii} = -0.005$ to facilitate this maneuver. The time responses for this maneuver are shown in Figure 6.4. Figure 6.5 displays the inertial flight paths for both aircraft. The circular dots are placed at five

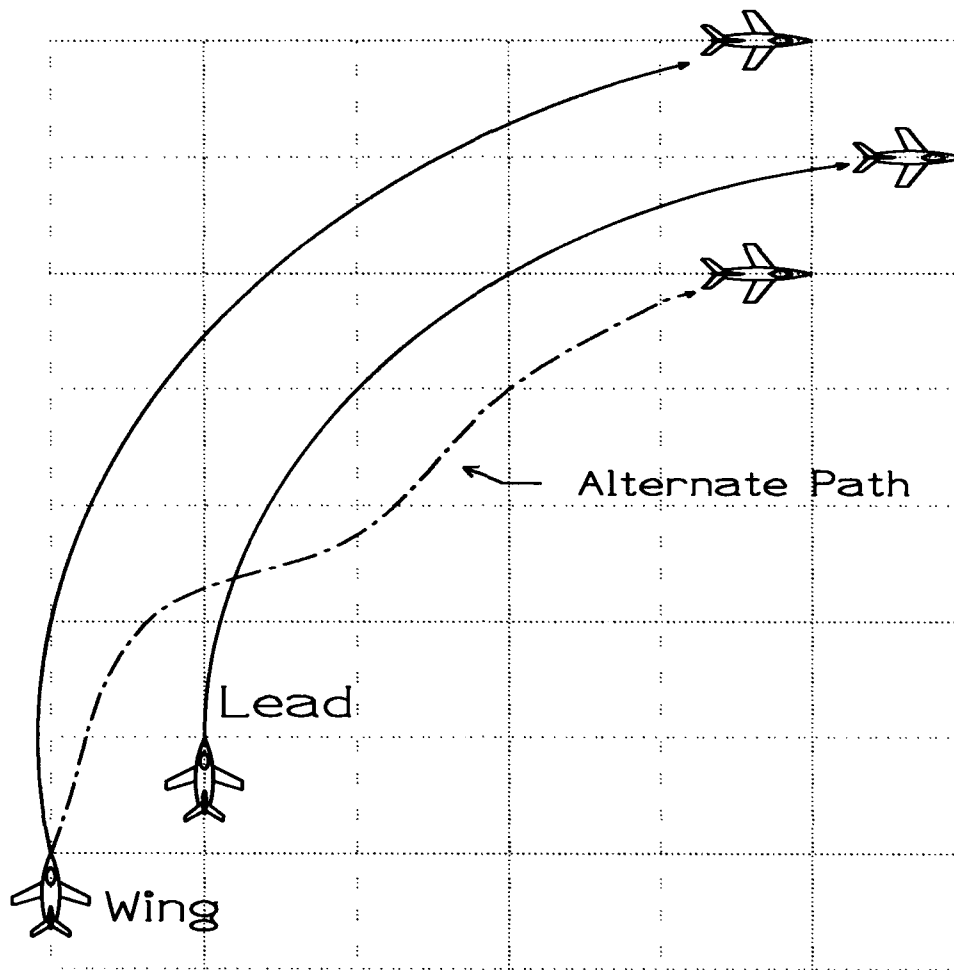


Figure 6.3. Diamond Formation 90 Degree Heading and Formation Change utilizing Energy Conservation, Flight Path Illustration

second intervals. Even though the wing's path crosses the lead's, there is no collision because they are at different altitudes. This is illustrated in the final plot, which displays a three dimensional view of this maneuver.

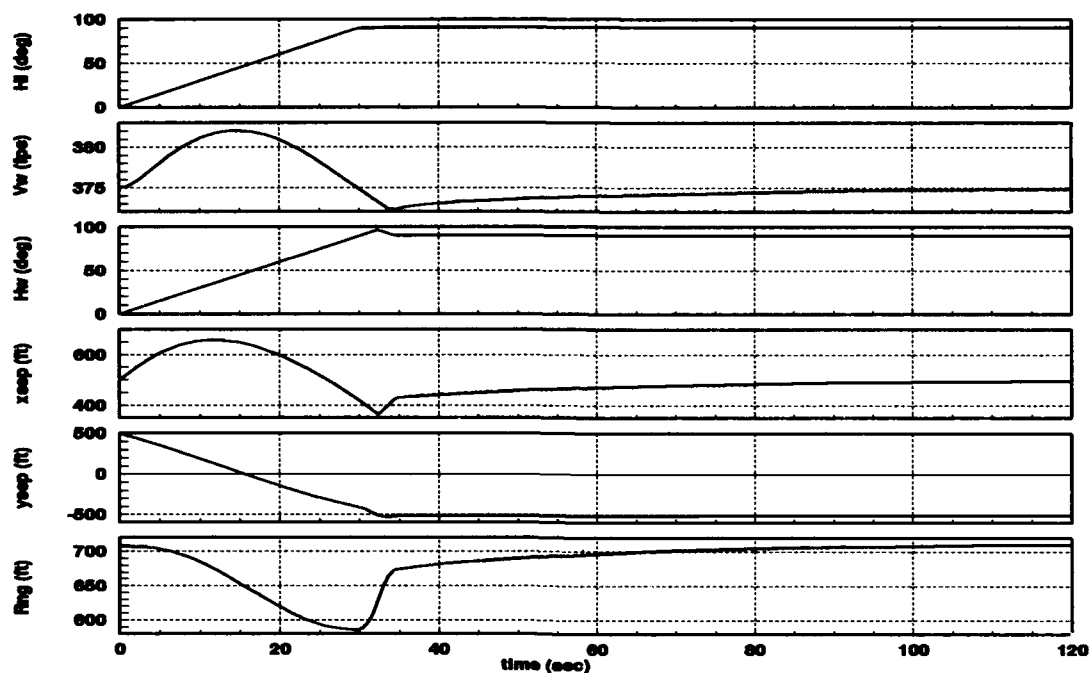


Figure 6.4. Diamond Formation 90 Degree Heading and Formation Change Utilizing Energy Conservation; Time Responses

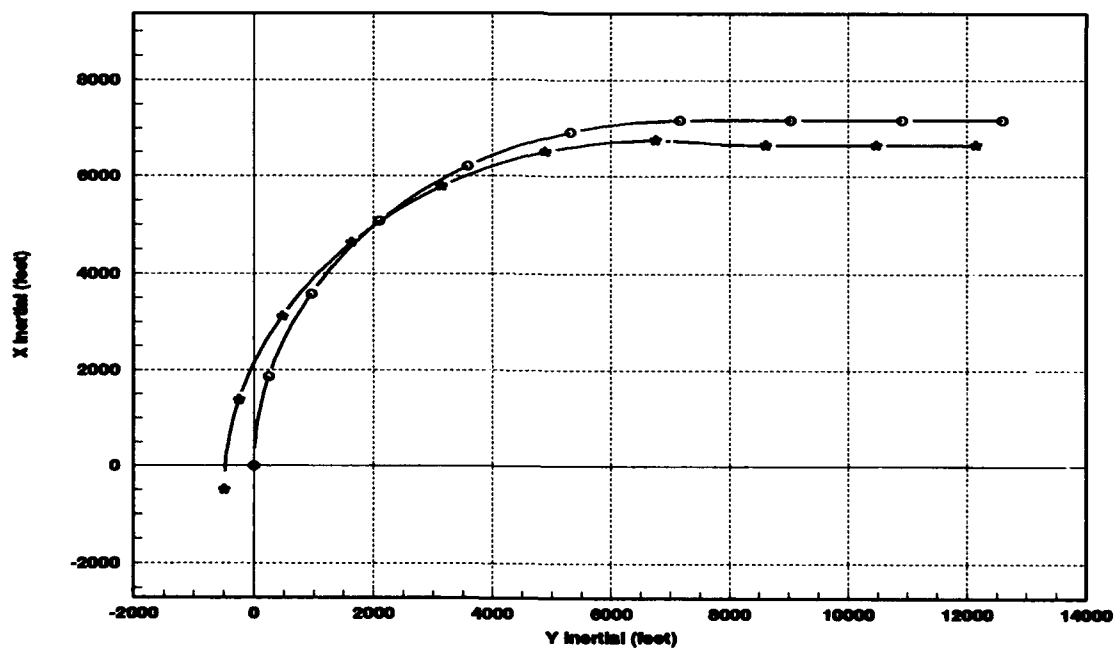


Figure 6.5. Diamond Formation 90 Degree Heading and Formation Change Utilizing Energy Conservation, Flight Path in Inertial Frame

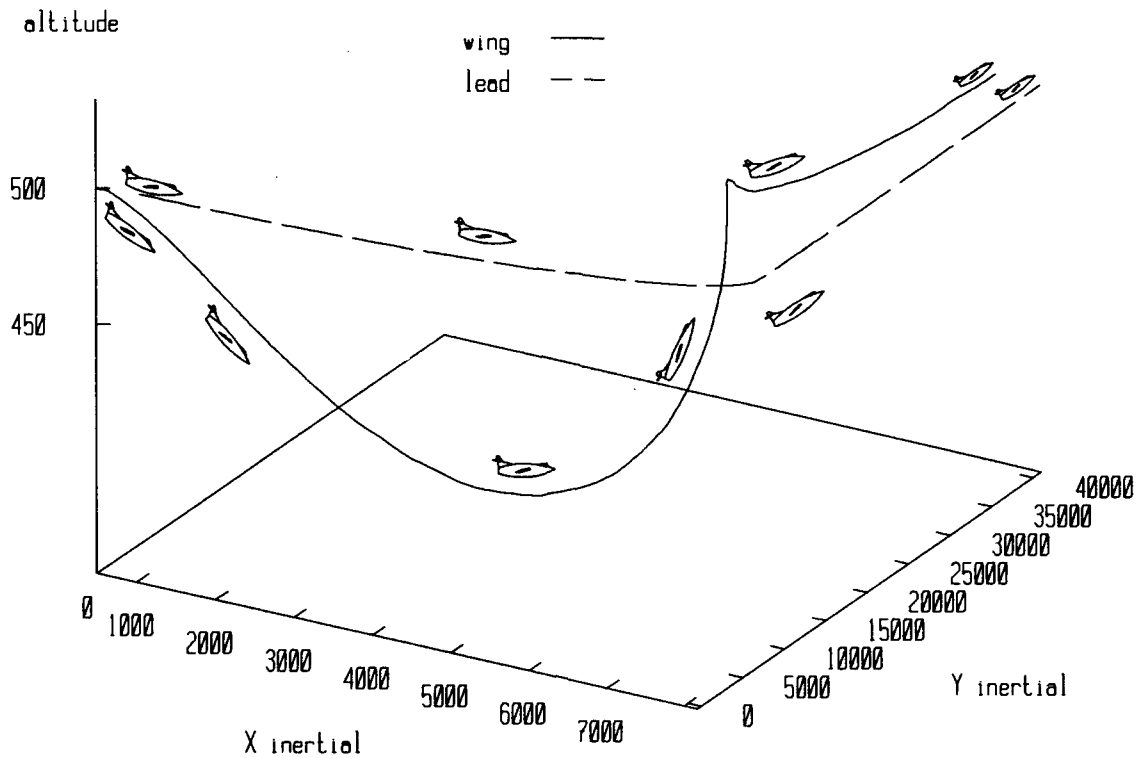


Figure 6.6. Diamond Formation 90 Degree Heading and Formation Change Utilizing Energy Conservation; 3-D Flight Path in Inertial Frame

6.4 Summary

This chapter introduces the concept of energy conservation into formation flight control. By maintaining the wing aircraft's energy constant, fuel consumption is reduced during horizontal maneuvers. Linearized equations are developed that facilitate the synthesis of the control law needed to implement this concept. A PI controller is used to command the wing aircraft in response to separation changes caused by the lead aircraft. The controller successfully maintains the formation through a side step maneuver while maintaining the wing's energy constant. A second maneuver consisting of a 90 degree heading change is also simulated. An alternate trajectory is chosen for the wing aircraft in order to conserve energy.

VII. Automated Formation Flight Control Simulation using Second-Order C-130 Aircraft Models

In this chapter, the second order aircraft models developed in Appendix B are used in the computer simulation. The formation flight control system as described in Chapter II, Section 2.5.2, implementing a PI controller and linear mixer is evaluated. This control system was designed in previous research using first order aircraft models. The purpose of this chapter is to evaluate the effects on the system response due to the new aircraft models. Of special interest is the transient time response of the wing aircraft during a formation maneuver. The new aircraft models incorporate an onset delay in both the heading and the altitude channels. Both the PI controller and linear mixer gains need to be adjusted in order to compensate for this time delay. In the next section, the formation control system is simulated using the PI controller and gains developed in Dargan's research (2)[4-14-4-22].

7.1 Initial Performance Evaluation

The formation flight control system utilizing the PI controller and linear mixer, as illustrated in Figure 2.7, produce a fast time response and zero steady-state error, when simulated using first-order aircraft models(2)[Fig 4.12]. The new aircraft models, as shown in Figure 2.2, display a slower time response than the first order models. Even though the velocity channel remains a first order transfer function, its time constant is much larger than in the previous model. This results in a longer time response. Computer simulations consisting of formation velocity, heading and altitude change are evaluated. Table 7.1 lists the key parameters used in the following simulations. Note, the mixer is not used for the altitude channel.

7.1.1 Velocity Change Performance Evaluation The simulation as described in Table 7.1 is commanded a step velocity change input from a nominal velocity of 375 feet per second to 400 feet per second. The time response plots for this input are shown in Figure 7.1. While the lead aircraft's velocity response exhibits a first order overdamped response, the wing's response is clearly second order and underdamped. The x-separation is also underdamped, and has a large overshoot. Clearly these responses are less desirable

Table 7.1. Initial Performance Evaluation Parameters

Parameter	Value
Lead Aircraft	C-130B
Wing Aircraft	C-130B
PI Controller Gains	
X Channel	$k_{xp} = .17, k_{xi} = .02$
Y Channel	$k_{yp} = .5, k_{yi} = .5$
Z Channel	$k_{zp} = 1, k_{zi} = .5$
Linear Mixer Gains	
X Channel	$k_x = 2, k_v = 5$
Y Channel	$k_y = 1, k_\psi = 10$
Z Channel	$k_z = 1$
Formation	Diamond
x separation	500 feet
y separation	500 feet
y separation	0 feet
Nominal Velocity	375 fps
hline Nominal Heading	0 degrees
Nominal Altitude	500 feet

than the time responses using first order aircraft models. On the positive side, the system is stable, with zero steady state error. The previous aircraft model time responses are shown as dotted lines.

7.1.2 Heading Change Performance Evaluation The formation control system response to a 30 degree heading change is displayed in Figure 7.2. Again the second order aircraft models result in a less than optimal time responses. Even though there is minimal degradation in the wing's heading response, the wing's velocity and the x and y separation responses are highly oscillatory. Again, on the positive side, the system is stable with zero steady state error.

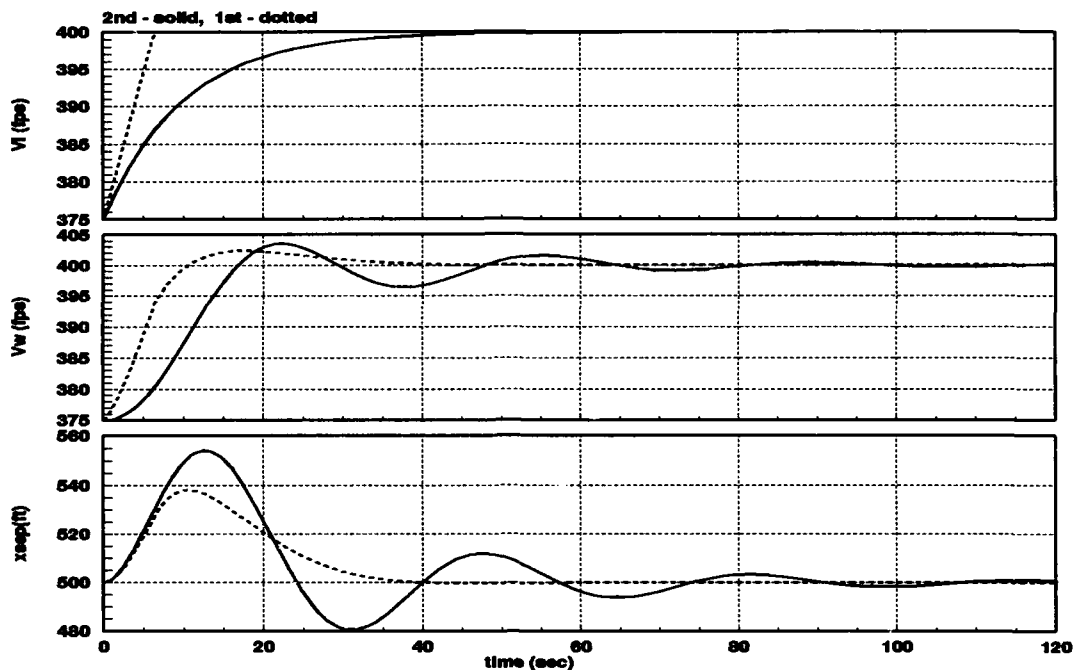


Figure 7.1. Time Response Plots to a 400 fps Velocity Command, 1st and 2nd Order Aircraft, Initial Gains

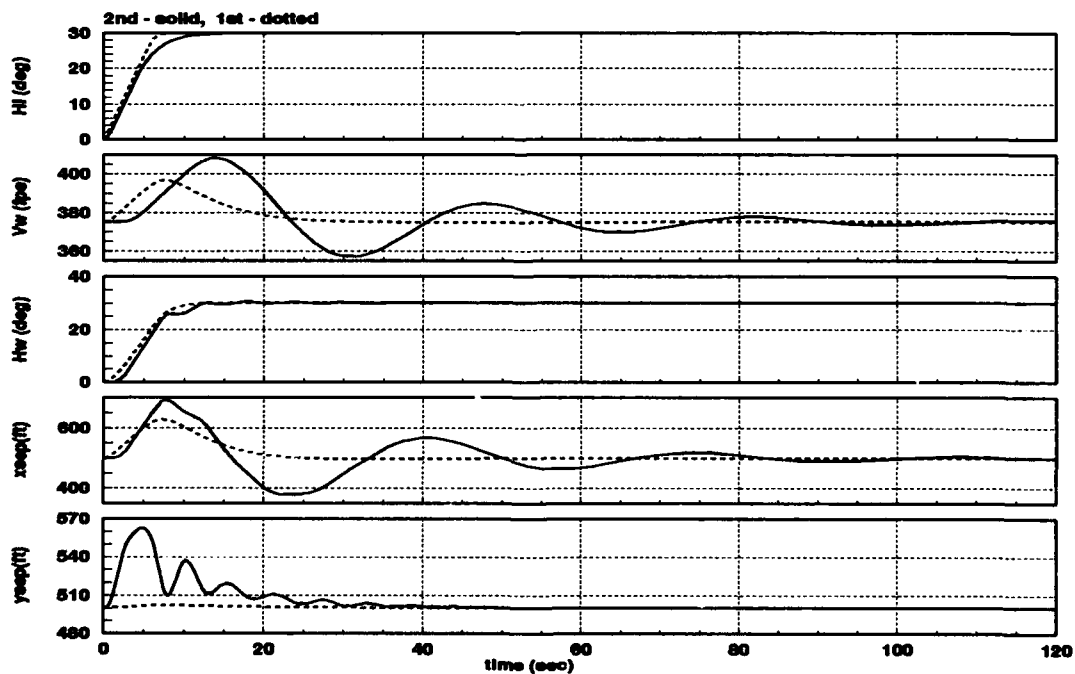


Figure 7.2. Time Response Plots to a 30 Degrees Heading Command, 1st and 2nd Order Aircraft, Initial Gains

7.1.3 Altitude Change Performance Evaluation The formation control system response to 550 feet altitude change is shown in Figure 7.3. The altitude response is clearly the best of the three channels. There is a slightly noticeable oscillation present in both the wing's altitude response and z separation. This response compares favorably with the first order system response. Consequently, the system is stable with zero steady state error.

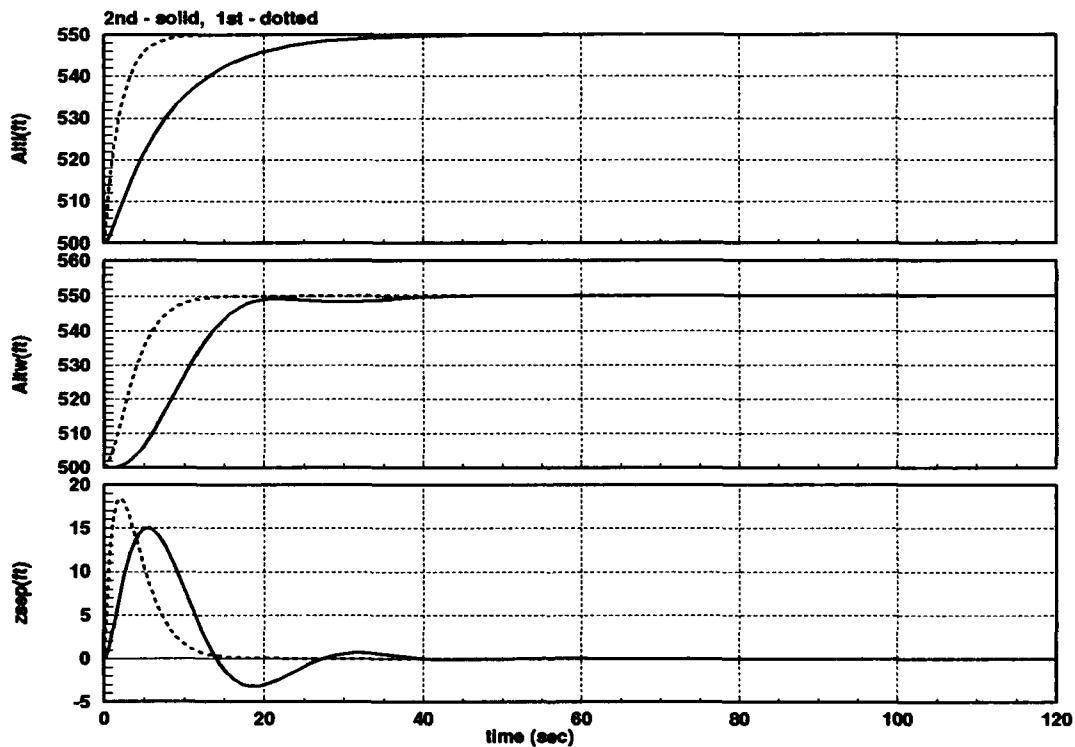


Figure 7.3. Time Response Plots for a 550 feet Altitude Change Command, 1st and 2nd Order Aircraft, Initial Gains

7.2 Performance Evaluation using Modified PI Controller and Linear Mixer Gains

The computer simulations in the previous section clearly indicate that the new, predominantly second-order and slower aircraft models, yield formation control system responses that are not as good as those provided by the first-order aircraft models. The mixer and controller parameters determined using the first order aircraft models no longer produce satisfactory performance using the slower, second order models. Consequently, the PI controller and mixer gains are adjusted to improve the formation control system time response. The controller gains are adjusted in order to reduce the oscillations and instability caused by the previous values. These new values are shown in Table 7.2.

Table 7.2. Adjusted PI Controller and Mixer Performance Parameters

Parameter	Value
PI Controller Gains	
X Channel	$k_{xp} = 0.8, k_{xi} = 0.08$
Y Channel	$k_{yp} = 10, k_{yi} = 0.8$
Z Channel	$k_{zp} = 1, k_{zi} = 0.3$
Linear Mixer Gains	
X Channel	$k_x = 1, k_v = 5$
Y Channel	$k_y = 1, k_\psi = 0$
Z Channel	$k_z = 1$

Both the X and Y-Channel gains are increased significantly in order to optimize the response. The linear mixer is the key in smoothing out the wing's velocity response. However, the heading error gain, k_ψ , is disabled since it has very little effect on the time response. The integral PI controller gain in the Z channel is reduced in order to dampen the response. The same computer simulations performed in the previous section are repeated using these new parameters.

7.2.1 Velocity Change Performance Evaluation The nominal formation parameters as described in Table 7.1, in addition to the PI controller and linear mixer gains listed in Table 7.2, are used in this evaluation. Again a step velocity change input from a nominal velocity of 375 feet per second to 400 feet per second is simulated. The time

response plots for this input are shown in Figure 7.4. The previous first order responses are again repeated on the same plot for comparison. Even though the new aircraft model responses are naturally slower than the previous models, they exhibit smooth response with no overshoot. As expected, the new aircraft models do not reach the rate limiters as is clearly the case in the old models.

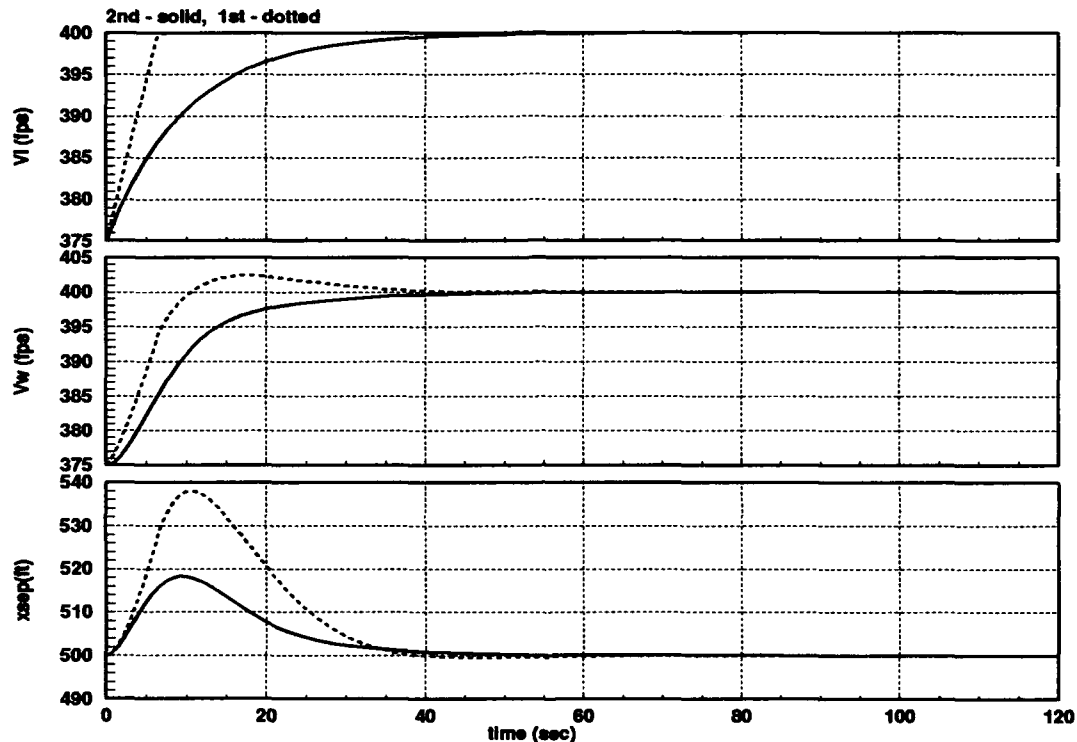


Figure 7.4. Time Response plots of a 400 fps Velocity Command, Diamond Formation, 1st and Second Order Models and Initial Controller Gains

7.2.2 Heading Change Performance Evaluation The formation response to a 30 degree heading change is shown in Figure 7.5. After implementing the new set of PI controller gains, both the first and second order system responses are very similar. Both the lead and wing aircraft saturate their respective rate limiters during the maneuver. Consequently, their time responses are similar. This may indicate an inconsistency between the rate limit values, and the transfer functions used to model the heading channel. The y-separation response for the second order model displays a high frequency oscillation not

seen in the heading response. Changing the proportional or integral gains is effective in dampening this oscillation.

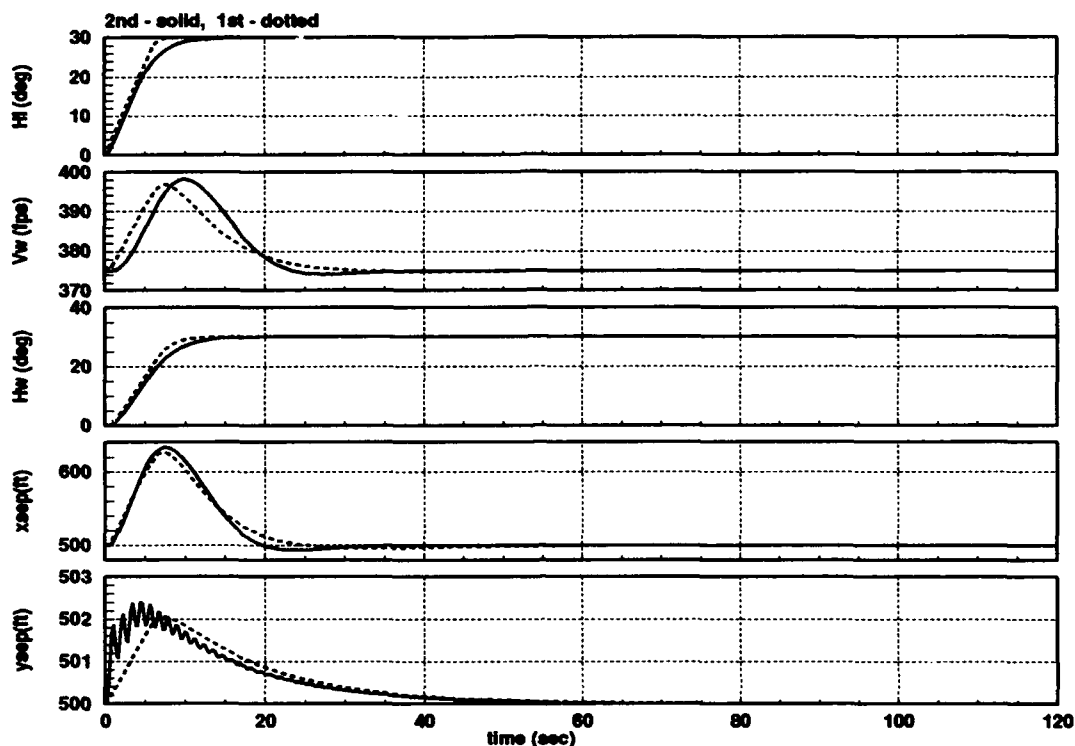


Figure 7.5. Time Response plots of a 30 Degree Heading Command, Diamond Formation, 1st and Second Order Models and Modified Controller Gains

7.2.3 Altitude Change Performance Evaluation The formation control system response to a 550 feet altitude change command is shown in Figure 7.3. The slight decrease in k_{zi} removes the light oscillation present in the earlier second order response. Other than the speed of the response, both altitude models exhibit similar time responses.

7.3 Summary

This chapter provides a preliminary evaluation of the performance of the formation flight control system utilizing the new, second-order and slower aircraft models. Computer simulation of three separate formation maneuvers illustrated the effects of the new and "slower" aircraft models on the control system response. Both the velocity and heading channels display an oscillatory response with poor settling time. The least degradation

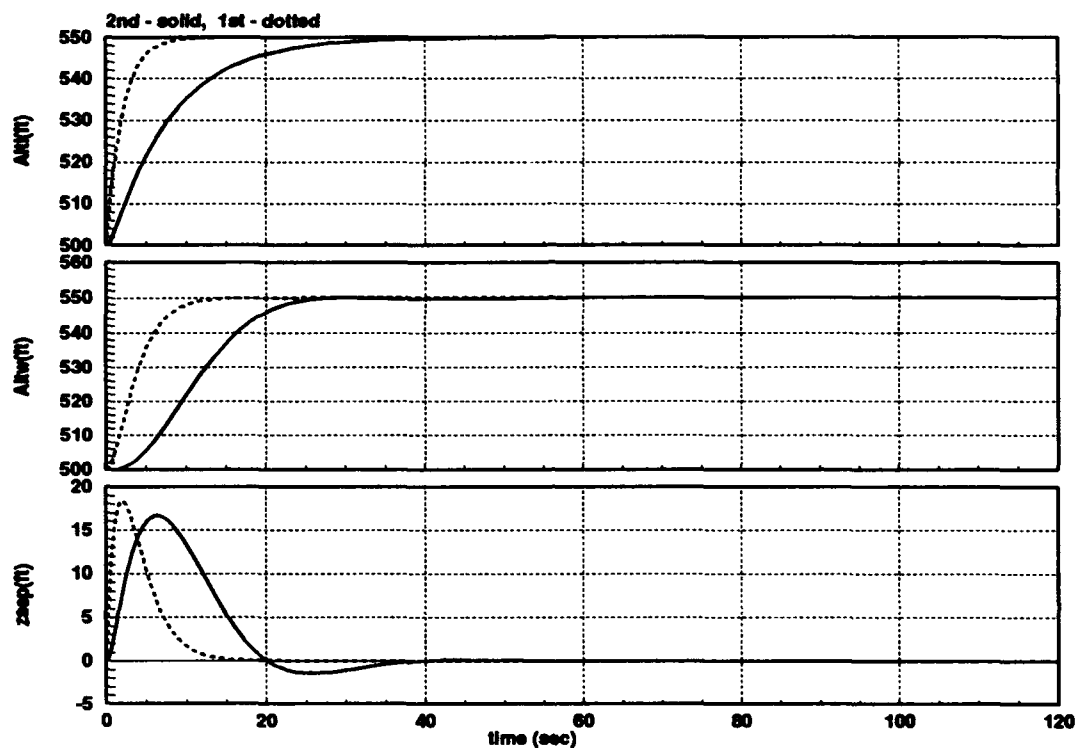


Figure 7.6. Time Response plots of a 550 feet Altitude Command, Diamond Formation, 1st and Second-Order Models and Initial Controller Gains

is in the altitude channel. Consequently, the same control system parameters can not be used for first and second-order models. An adjustment of both the PI controller and mixer gains results in satisfactory transient responses with zero steady state error. Except for the heading channel, the new aircraft models exhibit satisfactory and more realistic time responses.

VIII. Analysis and Conclusions

8.1 Analysis of Results

The objective of this research is to continue the development of an automated formation flight control system through an analytical analysis of the control problem, investigation of energy preserving formation flight control strategies, development of more realistic aircraft models, improved visualization tools, and computer simulation. These objectives have been met.

8.2 Display of Lead Aircraft's Trajectory as a Means of Evaluating the Formation Flight Control System's Performance

Computer simulation is used to evaluate the design of the formation control system. Normally, the time response plots of each aircraft's velocity, heading, altitude, and separations distances are evaluated after each computer simulation. As shown in Chapter III, a graphical method of displaying the lead aircraft's trajectory in the wing aircraft's reference frame is developed. Analogous to Lissajous figures used to visualize two dimensional oscillations, this method is a valuable tool in evaluating the tightness and speed of the formation control system.

8.3 Two Wing Aircraft Formation Flight Control

Using first-order aircraft models, an aircraft formation consisting of two wing aircraft, is simulated in Chapter IV. Each wing aircraft uses both PI control and a mix of separation and maneuver errors to track the leader. The wing aircraft successfully tracks the lead aircraft through 30 degree formation heading changes. No coordination/communication between the wing aircraft is used. Consequently, multiple wing aircraft formations are feasible as long as the formation separation distance restrictions are maintained. These restrictions are based on each aircraft's tracking error which are determined using single wing aircraft computer simulations.

8.4 Analytical Formation Flight Controller Synthesis

In previous research efforts, the key parameters in the formation control system were developed using a trial and error method. These parameters included the PI controller and linear mixer gains. This method produced successful results, yet required considerable effort and numerous computer simulations.

An analytical approach to determining the optimal control gains is developed in Chapter V. Using first-order aircraft models, a linearized and parameterized MIMO plant is developed and augmented using the PI control law. Steady state analyses of the closed-loop state matrix reveals the necessary and sufficient condition of integral feedback control for formation flight control. A Routh stability analysis on the closed loop characteristic equation shows the close relationship between the formation geometry, controller gains and system stability.

A two step process is developed, using the above analysis, to determine the PI controller gains. In the first step, pole placement is used to select a preliminary set of controller gains. Computer simulations of the non-linear formation flight control system are then performed in order to fine-tune these preliminary gains. Fine tuning through computer simulation is still needed to take into account the non-linear rate limiters present in the aircraft models. When compared with the controller gains developed using a purely trial and error approach, these new values perform somewhat better. The development of the linear closed loop state space equations provides valuable insight into the formation flight control problem and aids in determination of PI controller gains.

8.5 Energy Conservation of Wing Aircraft

The primary need for energy conservation of the wing aircraft is to reduce fuel consumption during large formation heading changes. If the wing is positioned in a diamond formation, an initial increase in velocity is required to track the lead along the "outer track" trajectory during a heading change. This is followed by a speed reduction as the wing aircraft settles back into formation once the maneuver is complete. The opposite is true for the "inside track" trajectory of the diamond formation. Instead of using the

throttle to first increase and then decrease velocity, the wing aircraft descends to increase velocity, and then ascends to decrease its velocity, while preserving its total energy.

An analytical approach is used to design a formation flight control system using an altitude change to conserve the wing's energy during velocity changes. A formation control system based on a PI controller and first-order aircraft models is designed. Pole placement through analysis of the systems step response is used to select the controller gains. Computer simulations show that the control system maintains the formation throughout the heading maneuver, while maintaining the wing's energy constant. Wing transpositions during heading change maneuvers are also considered.

8.6 Computer Simulation of Formation Flight Control System using Second-Order Aircraft Models

Up to this point, first-order aircraft autopilot models have been used to model the flight performance of the C-130 aircraft. The development of second-order aircraft models is addressed in Appendices A and B. New aircraft models based on computer simulation of C-130 longitudinal and lateral autopilots are designed. The new models incorporate second-order transfer functions in both the velocity and heading channels. The second-order transfer functions better model the time delay present in the autopilot's step response. In addition, the new and "slower" aircraft models exhibit a more realistic and linear behavior, by not immediately saturating the rate limits during command inputs.

In Chapter VII, computer simulation of velocity, heading and altitude formation maneuvers show that the new models affect the response of the control system as expected. Both the velocity and heading channels initially display unacceptable transient oscillations in their time response. The control system designed with the previous aircraft models no longer produce satisfactory results with the new aircraft. A fine tuning of the controller gains results in acceptable performance using the new second-order models.

8.7 Conclusions

The following conclusions are drawn from the results of this study.

1. An analytical analysis of the formation flight control problem revealed the necessary and sufficient condition of integral feedback in order to control a formation of aircraft with zero steady state error. Important stability conditions, linking the aircraft and formation geometry parameters were derived.
2. A linearized MIMO plant model mathematically describing the formation flight control problem can be used, through pole placement techniques, as an valuable tool in selecting the optimal PI controller gains. The presence of non-linear elements in the aircraft models and kinematic equations requires the use of a trial and error method to fine tune the controller gains.
3. The formation flight control system developed using the first order aircraft models, can successfully track formation maneuver commands using the new second-order models, after adjustment of both the PI controller and linear mixer gains. The slower second-order models exhibit a more realistic time response by not immediately saturating the non-linear rate limiters.
4. The formation flight control system designed to control single wing aircraft formations can be successfully used to control multiple wing aircraft formations. As long as the formation separation distances are established in accordance with the tracking error of the lead aircraft, no communication/coordination between the wing aircraft is needed.
5. The display of the lead aircraft's trajectory in the wing aircraft's rotating reference frame provides a graphical means of evaluating the performance of the formation flight control system. Similar to Lissajous figures used to display two dimensional oscillation, this trajectory is used to evaluate the tightness, speed and tracking error of the control system.

8.8 Recommendations for Further Study

Additional research in the area of formation flight control is needed in several areas. This work will in part address the limitations and assumptions made for this research. These areas are described below.

1. An analytical analysis of the formation control design problem using second-order models should be accomplished.
2. More extensive computer simulations using the second-order models should be accomplished in order to further validate the formation control system.
3. Additional research should be done on the multiple wing formation flight control problem.
4. A method of quantifying the effect of the non-linear rate limiters on the control system response in order to eliminate the trial and error procedure used to select the controller gains should be accomplished.
5. Actual sensor models should be used in the formation control system to allow evaluation of particular sensors in particular, the measurements update rate is an important parameter.
6. Noise should be incorporated into the sensor model to evaluate its interaction with the controller's gains and its effect on formation stability.

8.9 Summary

The results of this research show that a PI controller developed for automated maneuvering flight can successfully maintain a multiple wing aircraft formation without collisions among the aircraft. An analytical analysis of the formation control design problem affirmed the requirement of integral feedback to control a formation of aircraft with zero state error. A control system can be designed to conserve the energy of the wing aircraft during large heading changes. Finally, second-order transfer functions better model the C-130 aircraft.

Appendix A. Second-Order Aircraft Models and Large Aircraft Flying Qualities

An integral part of the formation flight control problem entails the adequate modeling of the formation aircraft dynamics (see also (10)). These aircraft models are based on wind tunnel data, actual flight test data, or high fidelity computer simulation of the aircraft equations of motion. For the purpose of formation flight control, a balanced, accurate, yet simplified representation of each formation aircraft is needed. Thus, a mathematical method of modeling the aircraft dynamics as a low order transfer function is desired.

The technical report titled "Second - Order System Models of High - Order Plants," by M. Pachter J. J. D'Azzo and L. E. Buzogany presents an analytical approach in modeling high order dynamical systems (6). The response of the system to a unit step function input is used as a means of evaluation. The system, in this case, is the actual aircraft control system, subjected to either a step velocity, heading, or altitude change.

The order of the transfer function model is determined by the dynamic behavior of the aircraft response. Large aircraft exhibit a time lag, or physical delay, in response to a step input. A first-order transfer function is inadequate in modelling the time delay, since it includes only an initial positive rate of change. A second-order transfer function is desirable, since it incorporates both a finite rate of change and a "time delay" (6)[1]. The next two sections present the theoretical background and procedure used to derive equivalent second-order aircraft models.

A.1 Theoretical Background

First and second-order system responses to a step function input differ in one significant aspect. The initial response of the first-order system has a positive slope at $t = 0$, while the second-order system has invariably a zero slope at $t = 0$ (6)[1]. An overdamped second-order system is given by,

$$\frac{y(s)}{u(s)} = \frac{ab}{(s+a)(s+b)} \quad (A.1)$$

where the parameters $a, b \in R_+$. Figure A.1 displays the response of an overdamped second-order system to a unit step input.

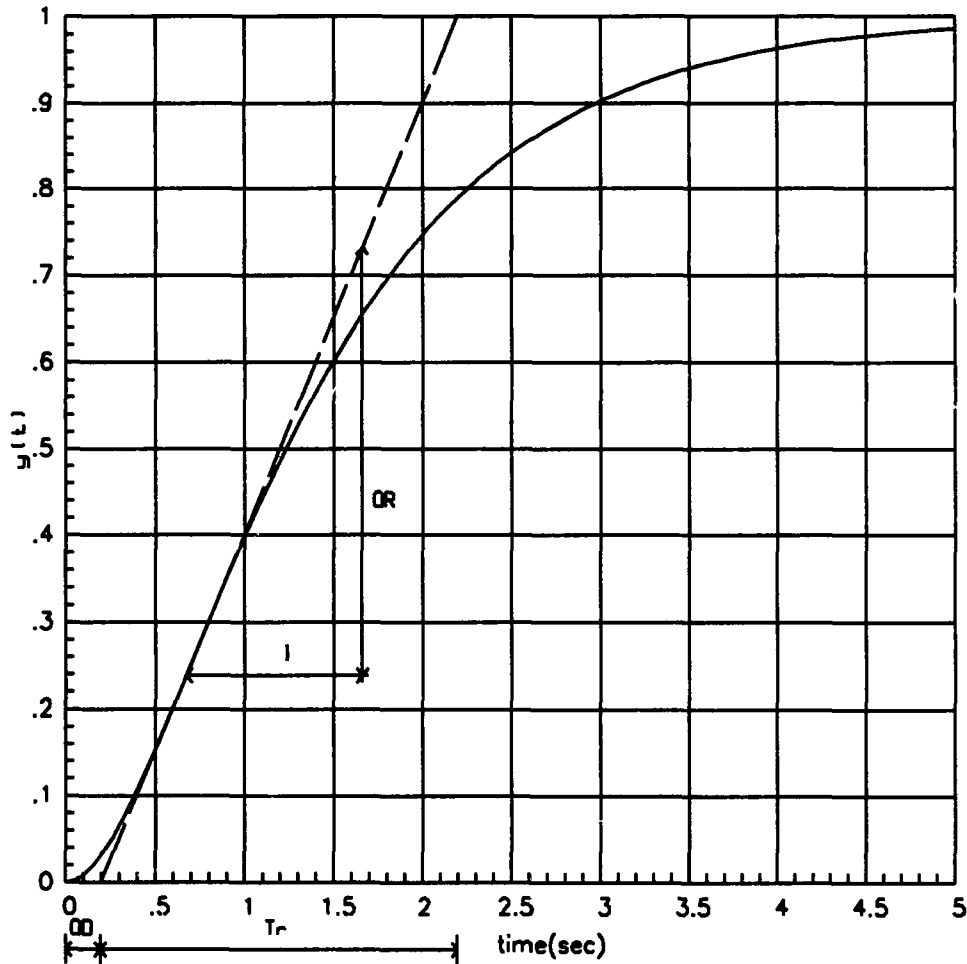


Figure A.1. Overdamped Second Order Step Response, $a=2$, $b=1$

The quantities labeled Onset Delay(OD), and Onset Rate(OR), completely determine the response of the second-order system. The Onset Rate is the maximum slope of the system response. The Onset Delay is determined by the point of intersection of the time axis, and a line tangent to the curve at the maximum rate. The values of OR and OD, can be empirically determined from flight performance data, or they can be analytically determined using analysis (6)[7]. The product of OR and OD of second-order systems of the form

$$\frac{\omega_n^2}{s^2 + 2\zeta\omega_n s + \omega_n^2} \quad (\text{A.2})$$

where

ω_n = undamped natural frequency

ζ = damping ratio

results in a universal function $f(x)$, as defined on the next page.

$$f(x) = OD \times OR \quad (A.3)$$

$$= x^{\frac{1}{1-x}} \left(1 + \frac{1}{x} - \frac{1}{1-x} \ln x \right) - 1, \quad 0 < x < 1. \quad (A.4)$$

where

$$x = \frac{b}{a}. \quad (A.5)$$

Note that

$$f(0) = 0 \quad (A.6)$$

$$f(1) = \frac{3}{e} - 1 \approx 0.1036 \quad (A.7)$$

The function $f(x)$, and parameter x , are helpful in determining the values of a and b . Given values of OR and OD, the parameter x is determined from a solution of Eq (A.4), or graphically using Figure A.2. Once x is determined, Eqs (A.8) and (A.5) are used to determine a and b .

$$a = ORx^{\frac{1}{1-x}} \quad (A.8)$$

An important restriction on the determination of a second-order approximation is the maximum value of $f(x) = OR \times OD$, as defined in Eq (A.7). If $f(x)$ exceeds this value, than a second-order approximation is no longer possible. Obviously, in this case, the data came from a higher order system. A similar analysis can be performed for an underdamped second-order system (6)[5-6].

The next section presents a design example in deriving a second-order model for the altitude response of a C-130 aircraft.

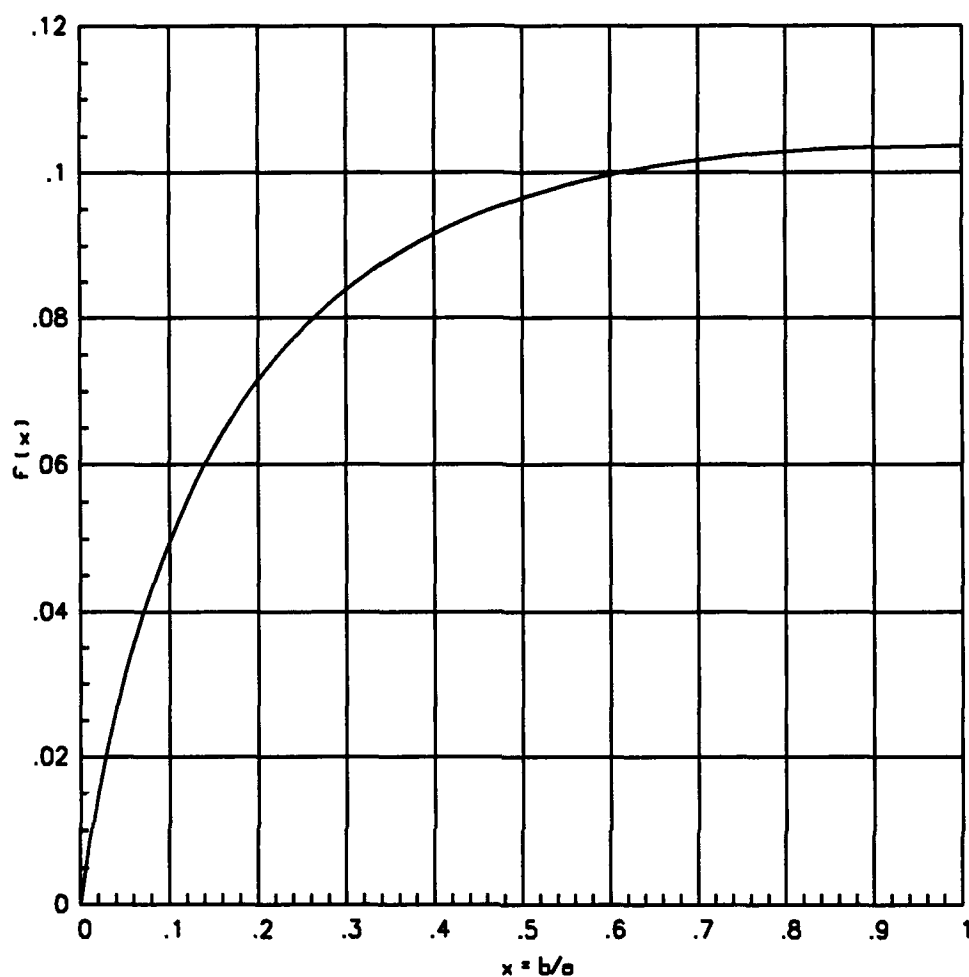


Figure A.2. Overdamped Function OR x OD

A.2 Design Example

This section illustrates the application of this method to design a second-order transfer function approximation of the altitude response of the C-130 aircraft. The altitude response is derived using a computer simulation of a six degree of freedom linear state space model, equipped with an Altitude Hold Autopilot. This autopilot is described in detail in Appendix B.

The first step in the design is to obtain the step response (see Figure A.3) and the determination of the two parameters, OD and OR. Since an analytical computer model is available, OD and OR can be analytically determined. Thus, OR and OD respectively, are

Table A.1. C-130 Altitude Response 2nd Order Parameters

Parameter	Value
t^*	.8 seconds
$h(t^*)$	4.08 feet
OR	.1044 feet/second
OD	.409 seconds
OR x OD	.0427 feet
x	.08
a_h	1.625
b_h	.13

are shown in Eqs (A.9) and (A.10).

$$OR = \frac{dh}{dt}(t^*) \quad (A.9)$$

$$OD = t^* - \frac{h(t^*)}{OD} \quad (A.10)$$

where

OR = onset rate

OD = onset delay

$h(t)$ = altitude response of the C-130 to a step input

t^* = time of the maximum rate of change of $h(t)$

The unknowns, t^* and $h(t^*)$, are determined directly from the time response plots of $h(t)$ and $\frac{dh(t)}{dt}$. The time response plots for the altitude channel of the C-130 are displayed in Figure A.3. The unknown parameters extrapolated from Figure A.3, are displayed in Table A.1. OR and OD are calculated using Equations (A.9) and (A.10).

The product, OR x OD, is checked against Eqs (A.6) and (A.7) in order to justify the use of the second-order approximation. The value of $x = \frac{b}{a}$, is determined analytically using Eq (A.4) or graphically using Figure A.2. Eqs (A.8) and (A.5) are used to determine a_h and b_h . The resulting second-order transfer function approximation of the altitude response of the C-130 is

$$\frac{h(s)}{h_c(s)} = \frac{.211}{(s + .13)(s + 1.625)} \quad (A.11)$$

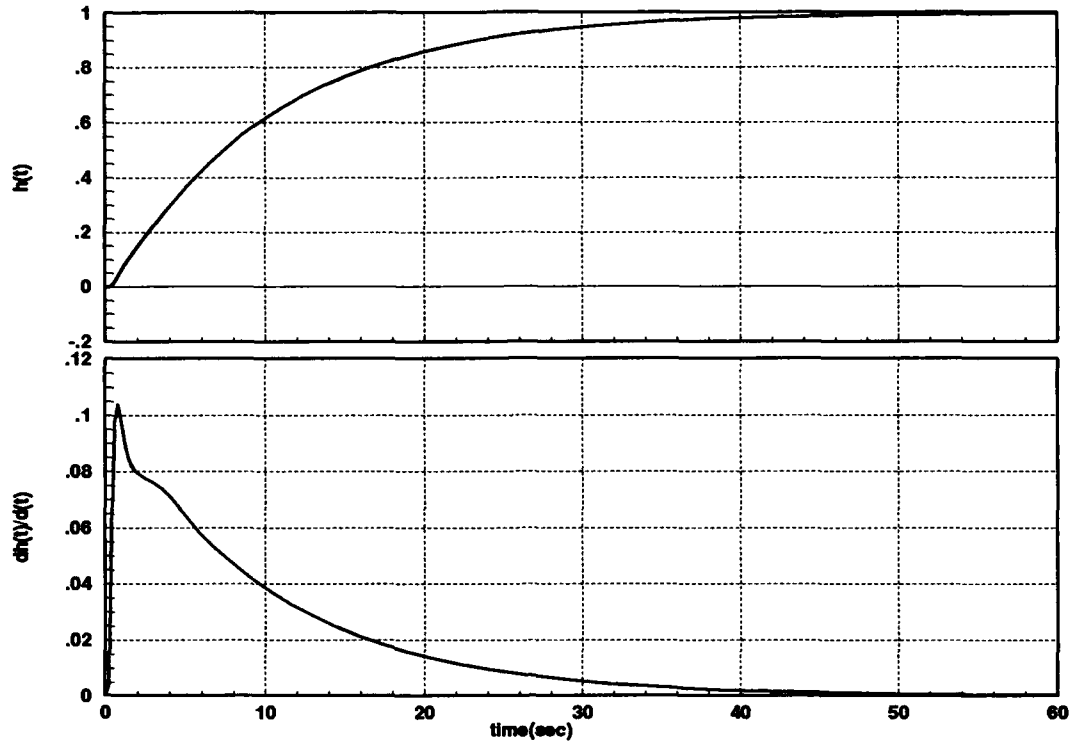


Figure A.3. C-130 Time Response Step Altitude Change

The actual transfer function derived from the linear state space model and Altitude Hold autopilot is

$$\begin{aligned}
 h(s) = & \frac{-0.0007s^{12} - 0.002s^{11} + 0.025s^{10} + 0.253s^9 + 1.053s^8 + 2.724s^7 + 4.847s^6 + 5.742s^5 + 4.725s^4 + 2.199s^3 + 0.596s^2 + 0.081s + 0.004}{0.004s^{14} + 0.051s^{13} + 0.425s^{12} + 2.381s^{11} + 9.275s^{10} + 25.85s^9 + 52.883s^8 + 79.645s^7 + 85.883s^6 + 64.78s^5 + 30.3s^4 + 8.77s^3 + 1.456s^2 + 0.122s + 0.004} \\
 & \text{(A.12)}
 \end{aligned}$$

A comparison of the actual altitude response and the second-order approximation is shown in Figure A.4. There is a close correlation of the two time responses with maximum difference of about 10 feet at 15 seconds. The second-order transfer function does an acceptable job in modelling the actual response, while providing the benefits of reduced order modeling.

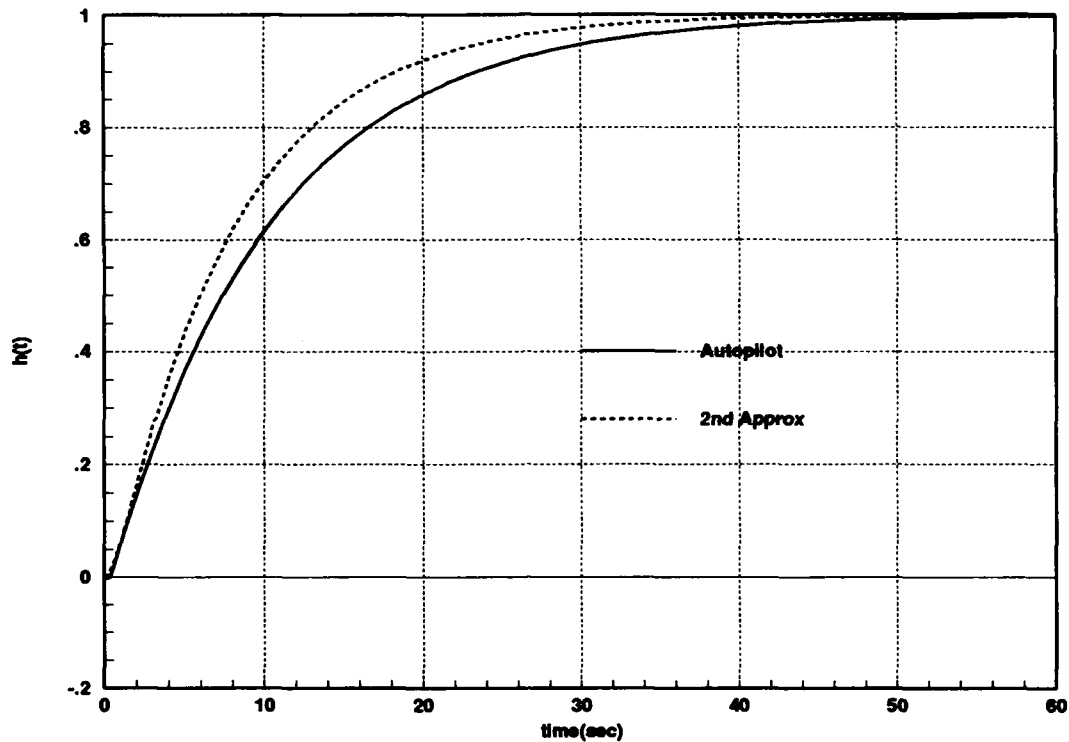


Figure A.4. C-130 Altitude Time Response Comparison

A.3 Summary

The use of accurate yet simple models of the formation aircraft is a key factor in the solution of the formation flight control problem. Second order transfer functions are desired in order to model the time delay present in most physical systems. The analysis presented in the technical report "Second - Order System Models of High - Order Plants," by M. Pachter, J. J. D'Azzo and L. E. Buzogany contains valuable tools in the development of second-order models(6). These tools are used in the design example in modelling the 14th order altitude response of the C-130 aircraft as a second-order transfer function.

Appendix B. C-130 Aircraft Models and Longitudinal and Lateral Autopilots

An important factor which is critical to the design of a formation flight control system is the modelling of the aircraft, as stated in Appendix A. The aircraft model becomes integrated into the system plant, and thus directly impacts the response of the system and performance of the flight controller. The analytical analysis in Chapter VI presents the relationship between the aircraft parameters, formation geometry, controller gains and stability. Hence, a realistic aircraft model is required to have confidence in the results obtained through this analysis and computer simulations.

A second consideration in developing accurate models is the level of complexity needed to simulate the aircraft. The previous research used first-order models based on empirical data and aircraft time responses. These models represent C-130 aircraft equipped with lateral and longitudinal autopilots. The separate velocity, heading, and altitude channels were assumed to be uncoupled. While, the first-order models incorporated an initial rate of change, they could not simulate the onset delay present in many physical systems. Using second-order models, both the onset rate and onset delay are incorporated. Higher order models could be used, but the increased amount of analysis and computer resources needed would offset any advantages gained.

Closed-loop aircraft models incorporating installed autopilots and performance data needed to derive the second-order aircraft models are difficult to acquire. An alternative approach, for use in this study, is to design basic autopilots around available, bare aircraft state space models. Computer simulations and system identification techniques are then used to derive the reduced order models used in the formation flight control system simulation. The latter approach is used to develop the second order aircraft models for the C-130 aircraft. Linear six degree of freedom state space aircraft equations supplied by Lockheed Aerospace are used (4).

Basic longitudinal and lateral autopilots are designed around these linear aircraft equations using root locus techniques. The time responses of these autopilots are then

analyzed in order to derive decoupled reduced order models of the aircraft. Table B.1 lists the flight conditions and key aircraft parameters used in the model development.

Table B.1. Aircraft Flight Conditions and Parameters

Parameter	Value	Description
Type	C-130H	Aircraft Type
GWT	12,000 lbs	Gross Weight
ALT	500 feet	Altitude
V	306 fps	Trim Velocity

The complete linear six degree of freedom state space model data supplied by Lockheed is attached in Appendix A.2. The following assumptions are used to simplify the design of the autopilots:

1. The aircraft body axis is assumed to be closely aligned with the stability axis for small values of α , angle of attack, and β , sideslip(1)[604-611].
2. Velocity, heading and altitude step inputs are separately applied to the closed-loop aircraft in order to identify the individual transfer function models.
3. The autopilots are optimized for command inputs of 10 fps, 10 degrees, and 100 ft for the velocity, heading and altitude channels respectively.

In the following sections, the design of the C-130 autopilots and model development is presented.

B.1 Longitudinal Autopilot and Reduced Order Models

A Mach-Hold autopilot is designed as shown in Figure B.1. Pitch-rate feedback is used in the inner-loop, while proportional plus rate feedback is used for the outer loop. The gains are optimized for proper damping and output time response. The autopilot time responses for a 10 fps input is shown in Figure B.2.

The velocity response u of the Mach-Hold autopilot closely resembles a first order response(1)[101]. In this case, a first-order transfer function best models the velocity channel of the C-130 aircraft. Figure B.3 compares the first-order approximation, with the

actual autopilot velocity response. These plots shows that the first-order transfer function shown in Eq (B.1), very accurately models the aircraft performance.

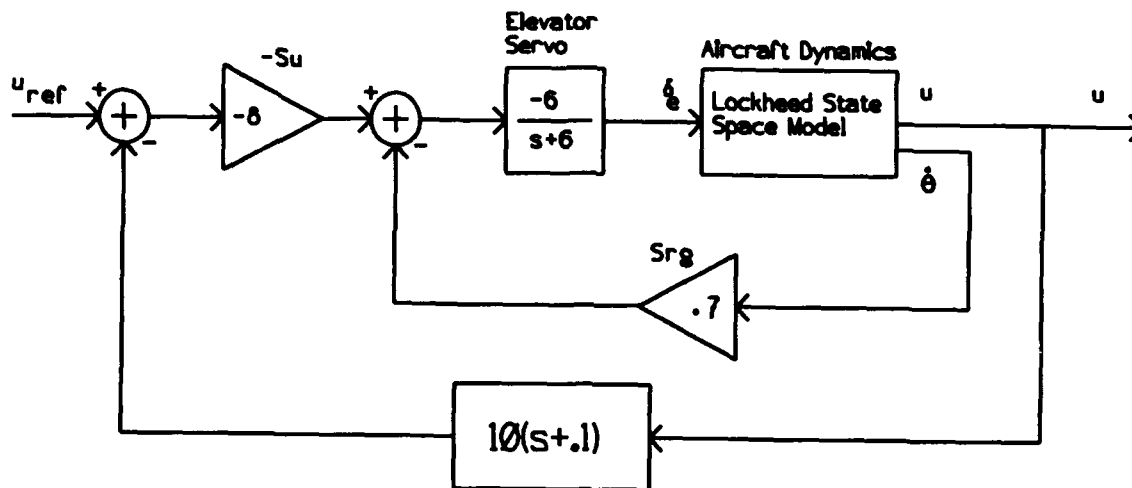


Figure B.1. C-130 Mach-Hold Autopilot Design

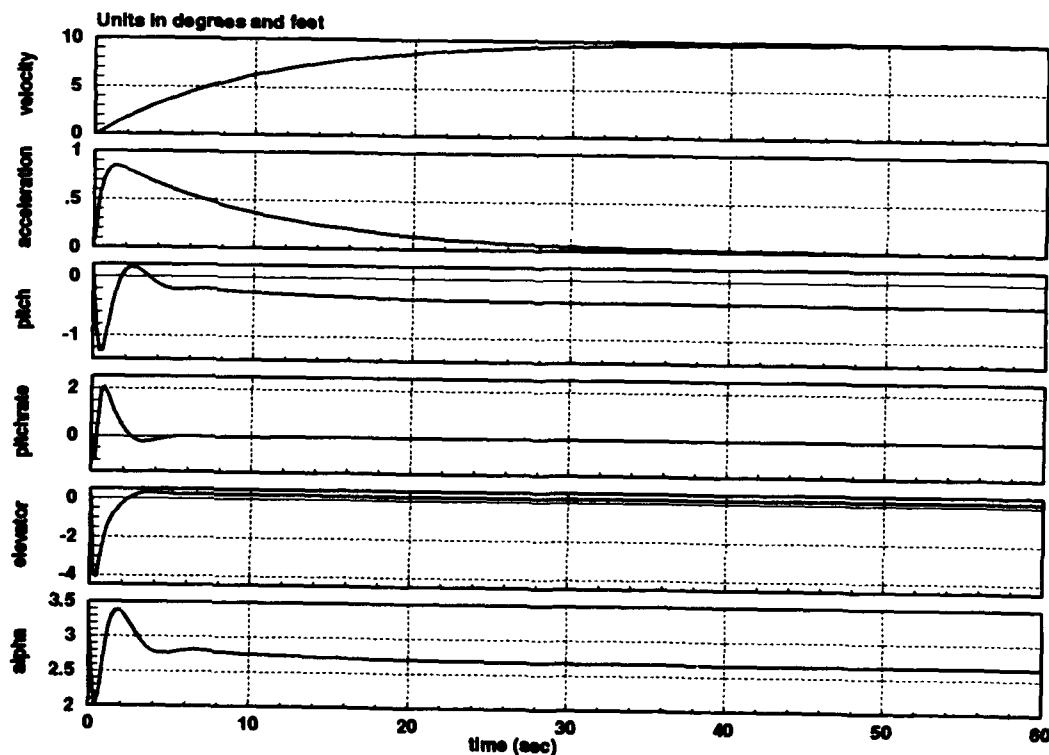


Figure B.2. Mach-Hold Autopilot response to 10 fps Command Input

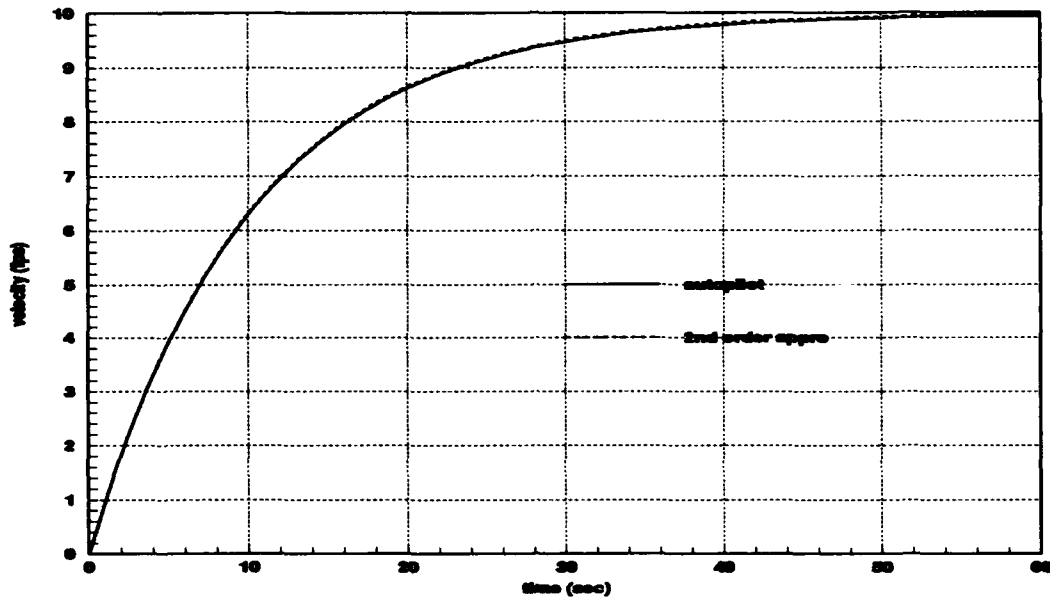


Figure B.3. Time Response Comparison of Mach-Hold Autopilot and First-Order Approximation

$$\frac{u(s)}{u_{ref}(s)} = \frac{\tau_V}{s + \tau_V} = \frac{.1}{s + .1} \quad (B.1)$$

An Altitude-Hold autopilot is designed as shown in Figure B.4. The aircraft's flight path angle, and thus altitude, is commanded using throttle control. A second-order cascade compensator is designed to stabilize the inner loop and to provide sufficient damping. Proportional plus rate feedback is again used to provide the best altitude tracking. The Altitude-Hold autopilot's response to a 100 feet step altitude change is shown in Figure B.5.

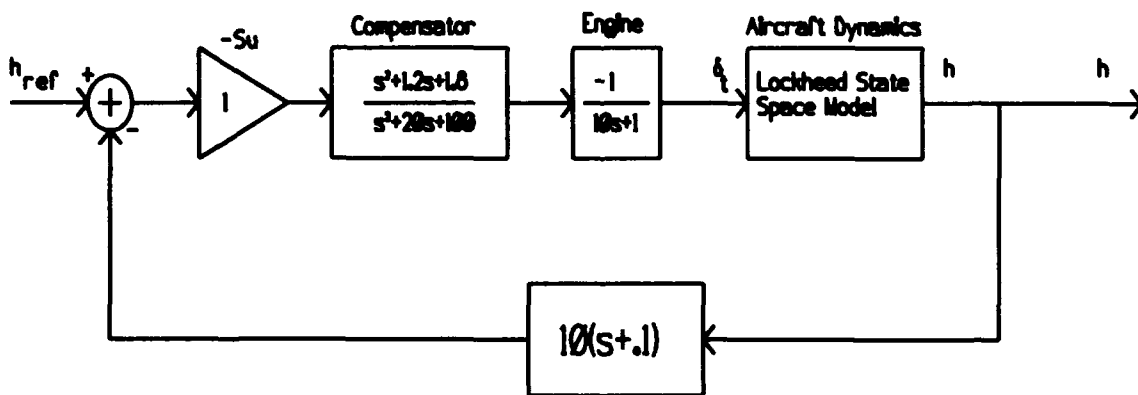


Figure B.4. Altitude-Hold Autopilot Control System Design

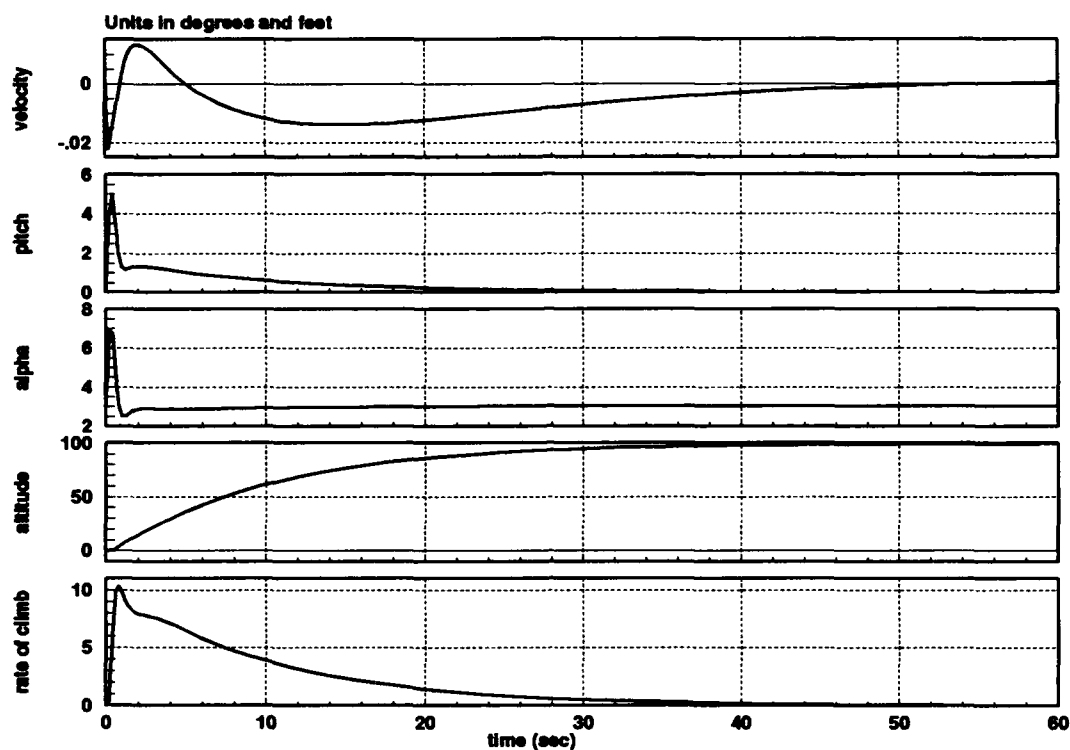


Figure B.5. Time Response of the Altitude-Hold Autopilot to a 10 feet Step Altitude Command

The altitude response of the autopilot is clearly second-order or greater. An over-damped, second-order approximation of the altitude response is developed using techniques described in Appendix A. Table B.2 list the parameters used to determine the second-order model.

Table B.2. Altitude-Hold 2nd Order Parameters

Parameter	Value
Onset Rate	10.436 feet/second
Onset Delay	0.409 seconds
a_h	1.625
b_h	0.13

The second-order transfer function approximating the time response of the Altitude-Hold autopilot is

$$\frac{h(s)}{h_{ref}(s)} = \frac{a_h b_h}{(s + a_h)(s + b_h)} = \frac{0.211}{(s + 1.625)(s + 0.13)} \quad (B.2)$$

A comparison of the altitude time response from the Altitude-Hold autopilot and the second-order approximation is shown in Figure B.6. This figure shows a close correlation between the two time responses.

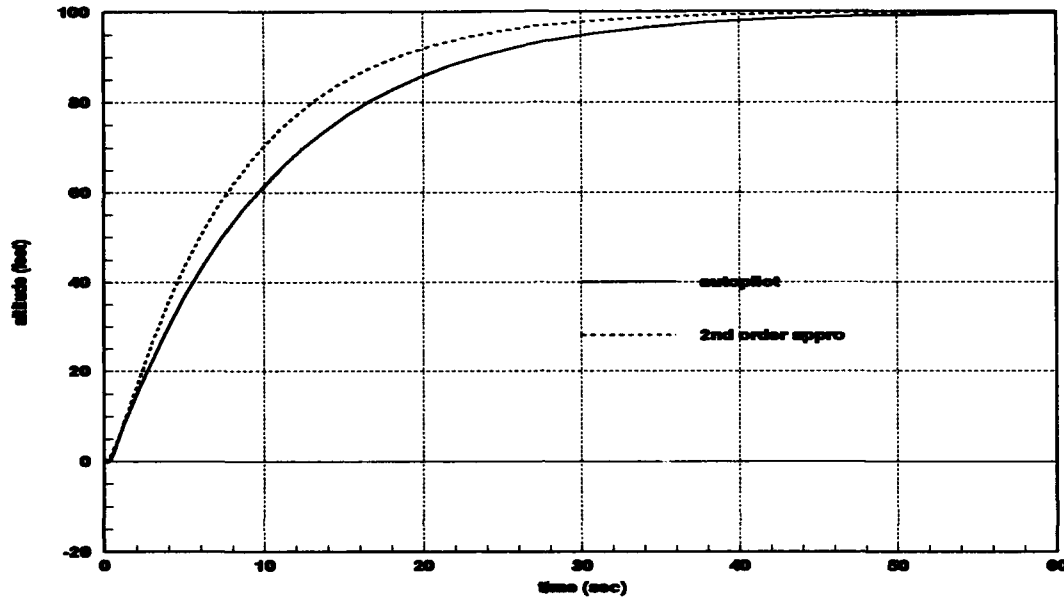


Figure B.6. Time Response Comparison of Altitude-Hold Autopilot and Second Order Approximation

B.2 Lateral Autopilot and Reduced Order Model

A lateral directional control autopilot is designed as shown in Figure B.7(1)[176-188]. Yaw rate feedback and a washout filter are used to dampen the dutch roll. Sideslip feedback is used to provide rudder coordination. Since a bank angle command is used to turn the aircraft, a roll angle control system is designed around the coordinated aircraft. A limiter is used to limit the bank angle commanded in response to a heading error. The outer loop utilizes proportional feedback in order to command the heading error.

The response of the directional autopilot to a 10 degree heading change is shown in Figure B.8. The sideslip, roll, and actuator deflections are all within reasonable limits.



The heading response of the Lateral Directional autopilot clearly exhibits characteristics of a high order system. A second-order transfer function is designed to best fit this response. While there is not an exact correlation of the two responses, the second-order transfer function better models the transient characteristics than a first-order transfer function. The second-order model is shown in Eq (B.3), and the heading response comparison in Figure B.9.

B-7

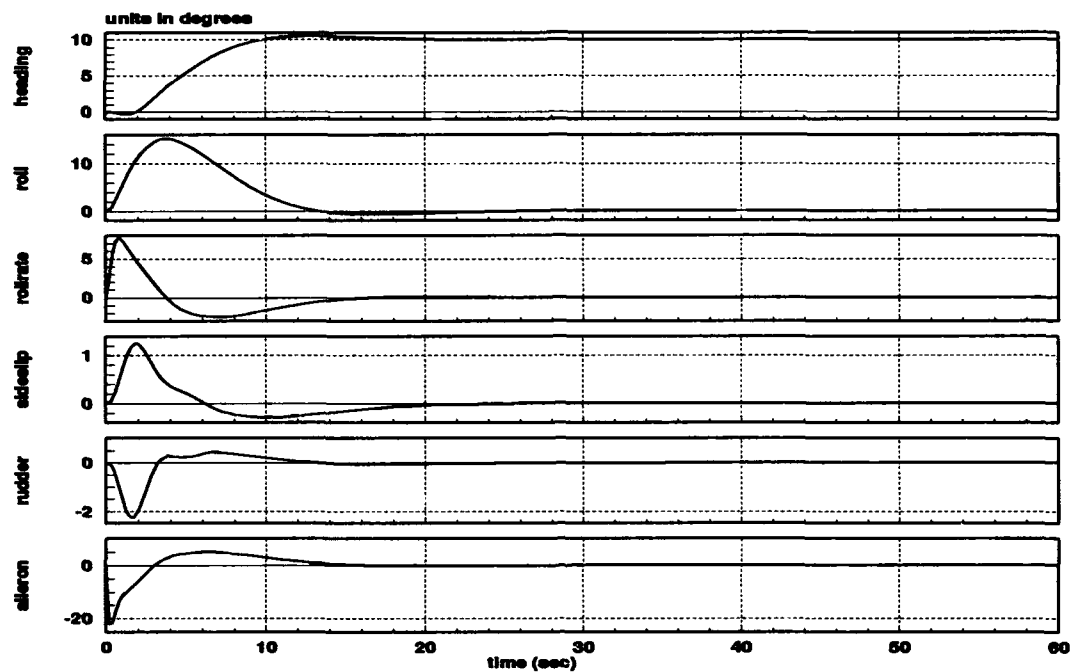


Figure B.8. Time Response of the Lateral Directional Autopilot to a 10 Degree Heading Command

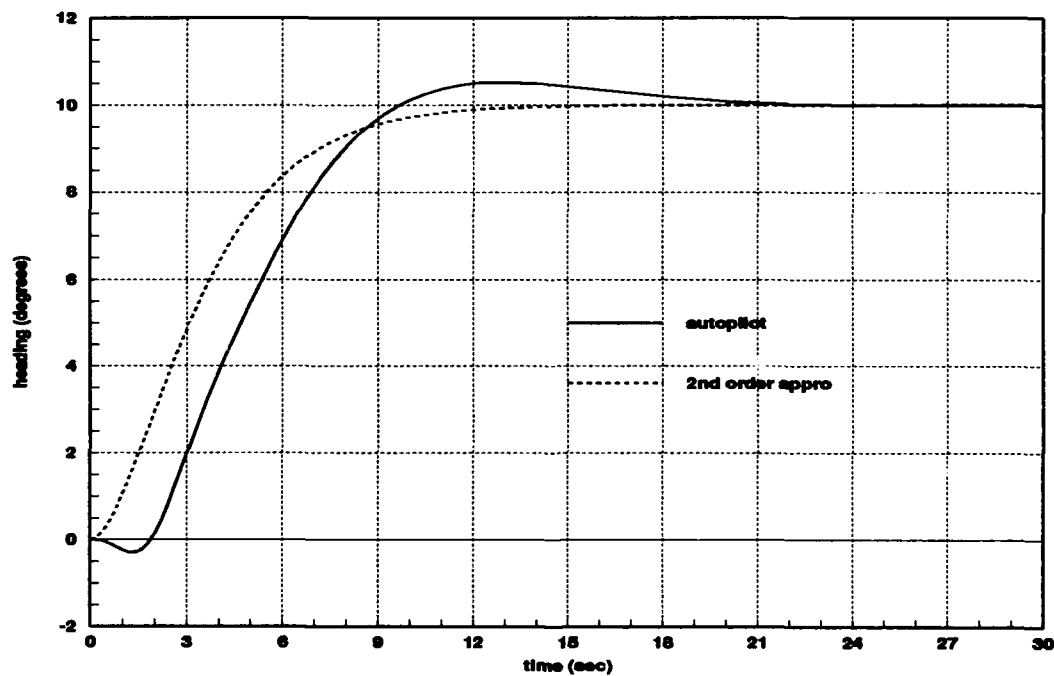


Figure B.9. Time Response Comparison of Lateral Directional Autopilot and Second-Order Model Heading Response

B.3 Summary

Lateral and longitudinal autopilots are designed around linear, six degree of freedom state space models of the C-130 Aircraft. The time responses of these autopilots to step command inputs are used to derive decoupled, reduced order models of the aircraft. These models are used in the continued development of a formation flight control system. Equations (B.4) through (B.6) summarize the final transfer functions used to model the C-130's velocity, altitude and heading channels, respectively. Figure B.10 contains the final system build diagram including the three autopilots for reference.

$$\frac{V(s)}{V_c(s)} = \frac{0.1}{(s + 0.1)} \quad (\text{B.4})$$

$$\frac{h(s)}{h_c(s)} = \frac{0.211}{(s + 1.625)(s + 0.13)} \quad (\text{B.5})$$

$$\frac{\psi(s)}{\psi_c(s)} = \frac{0.296}{(s + 0.544)(s + 0.544)} \quad (\text{B.6})$$

12-NOV-92

Continuous SuperBlock	Ext. Inputs	Ext. Outputs
C 130 Autopilot	0	7

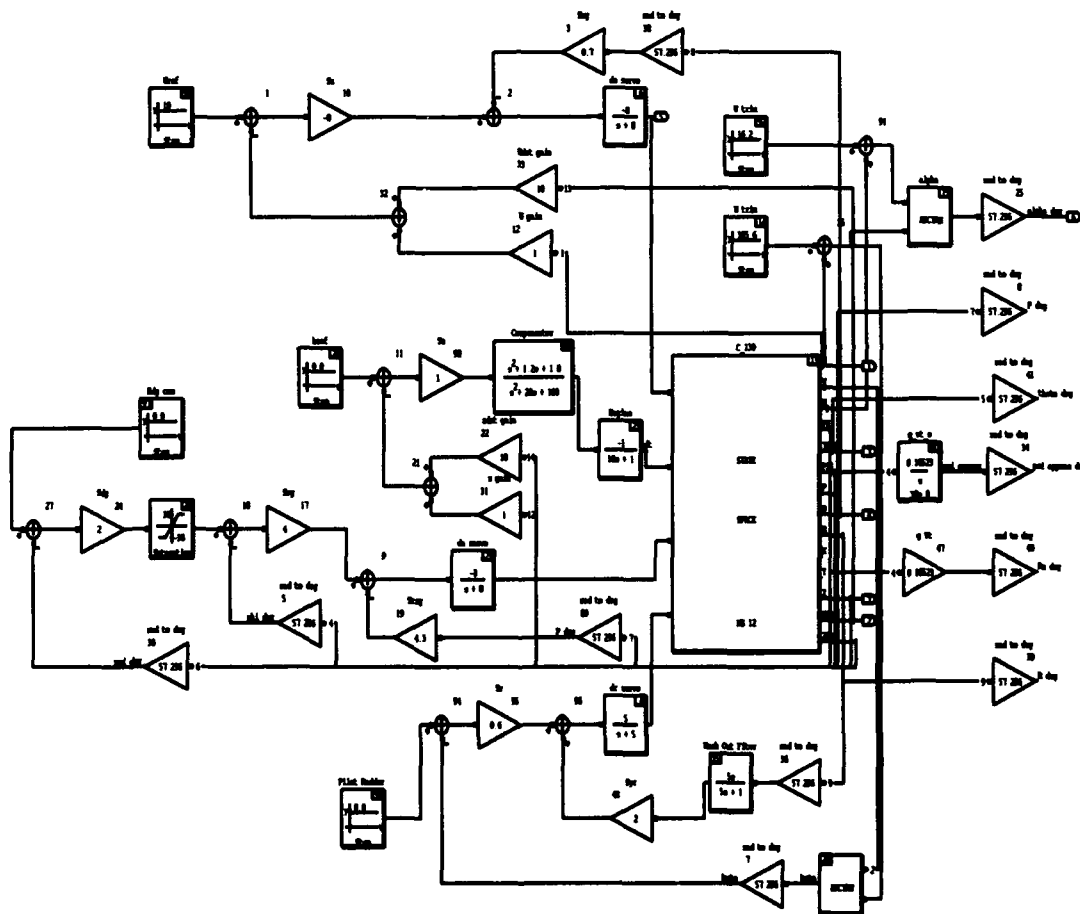


Figure B.10. MatrixX System Build Diagram of C-130 Autopilots

Bibliography

1. Blakelock, John H. *Automatic Control of Aircraft and Missiles* (Second Edition). John Wiley and Sons, Inc., 1991.
2. Dargan, John L. *Proportional Plus Integral Control of Aircraft for Automated Maneuvering Formation Flight*. MS thesis, Air Force Institute of Technology, Wright-Patterson AFB OH, December 1991.
3. D'Azzo, John J. and Constantine Houpis. *Linear Control System Analysis and Design*. McGraw-Hill, NY 1988.
4. McCarty, J.M. and F.B. Green, "C-130, LINEAR SIX DEGREE OF FREEDOM STATE SPACE MODELS." LOCKHEED AERONAUTICAL SYSTEMS COMPANY, Marietta, GA 1992.
5. Meyer, R.T. and E.G. Husband. "Large Aircraft Flying Qualities Revisited," *AIAA paper*, (90-2847):456-463 (1990).
6. Pachter, Meir J., et al. "Second - Order System Models of High - Order Plants." Submitted for Publication, September 1992.
7. Porter, B. and A. Bradshaw. "Design of Linear Multivariable Continuous-Time Tracking Systems," *Int. J. Syst. Sci*, 5, 1155-1164 (1974).
8. Porter, B. and A. Bradshaw. "Singular Perturbation Methods in the Design of Tracking Systems Incorporating Inner-Loop Compensators and High-Gain Error-Actuated Controllers," *Int. J. Syst. Sci*, 12, 1193-1205 (1981).
9. Rohs, Paul. *A Fully Coupled, Automated Formation Control System for Dissimilar Aircraft in Maneuvering, Formation Flight*. MS thesis, Air Force Institute of Technology, Wright-Patterson AFB OH, March 1991.
10. Trosen, Dennis. *Aerial Refueling Control System*. MS thesis, Air Force Institute of Technology, Wright-Patterson AFB OH, December 1992. In preparation.

Vita

Captain Louis E. Buzogany was born in Cleveland, Ohio and attended Lake Catholic High School in Menter, Ohio. He attended Ohio State University and recieved a Bachelor of Science Degree in Electrical Engineering. Upon graduation, he was commissioned a Second Lieutenant in the United States Air Force and was assigned to the 1000th Satellite Operations Group, Offutt AFB, NE from May 1986 to May 1991.

While at Offutt AFB, he performed duties as a Satellite Mission Planner and was responsible for planning satellite missions for the Defense Metereological Satellite Program. In May 1991 he was selected to attend the Air Force Institute of Technology, Wright Patterson AFB, OH in persuance of a Master of Science Degree in Electrical Engineering.

Permanent address: 7101 Sandpiper Ct.
Painesville, Ohio 44077

REPORT DOCUMENTATION PAGE			NSN 7540-01-280-5500	
1. AGENCY USE ONLY (Leave blank)			2. REPORT DATE 15 December 1992	
			3. REPORT TYPE AND DATES COVERED Master's Thesis	
4. TITLE AND SUBTITLE AUTOMATED CONTROL OF AIRCRAFT IN FORMATION FLIGHT			5. FUNDING NUMBERS	
6. AUTHOR(S) Louis E. Buzogany Captain, USAF				
7. PERFORMING ORGANIZATION NAME(S) AND ADDRESS(ES) Air Force Institute of Technology WPAFB OH 45433-6583			8. PERFORMING ORGANIZATION REPORT NUMBER AFIT/GE/ENG/92D-07	
9. SPONSORING/MONITORING AGENCY NAME(S) AND ADDRESS(ES) Wright Laboratories, FIGS, Wright-Patterson AFB, OH 45433			10. SPONSORING/MONITORING AGENCY REPORT NUMBER	
11. SUPPLEMENTARY NOTES				
12a. DISTRIBUTION/AVAILABILITY STATEMENT Distribution unlimited			12b. DISTRIBUTION CODE	
13. ABSTRACT (Maximum 200 words) In this study, an automated formation control system for an aircraft formation comprised of one lead and multiple wing aircraft is analyzed. Second-order models of the C-130 aircraft are developed in order to accurately model the flying qualities of large aircraft. This automated formation control system is capable of controlling the C-130 aircraft in maneuvering formation flight, thus reducing the wing's pilot workload. During formation flight, the wing aircraft continuously measures the lead aircraft's relative position with an ideal on-board position sensor. This information, in addition to Proportional Plus Integral feedback control, is used to maintain the aircraft in formation. The control of each wing aircraft is assumed to be independent of other wing aircraft. Other than for nominal formation separation commands, no continuous communication is assumed between the formation aircraft. An analytical analysis of the formation control problem reveals that integral control is needed to achieve zero steady state error in the separation distances (after a formation maneuver is executed). This conclusion is confirmed using computer simulations. An analytical method of selecting the Proportional Plus Integral parameters is developed by identifying the dominant system dynamics and residues of the step response. In an attempt to reduce the fuel consumption of the wing aircraft during formation heading change maneuvers, an alternate control system is designed to conserve the energy of the wing aircraft. The resulting automated formation control system effectively maintains the formation of aircraft through a combination of velocity, heading, and altitude changes. There is zero steady state error for all maneuver and separation distance change responses. Additionally, the separation transients are such that no collisions occur between the aircraft. Both analytical equations and computer simulation generated time responses are provided for reference.				
14. SUBJECT TERMS flight control, automated, formation, C-130			15. NUMBER OF PAGES 125	
			16. PRICE CODE	
17. SECURITY CLASSIFICATION OF REPORT Unclassified	18. SECURITY CLASSIFICATION OF THIS PAGE Unclassified	19. SECURITY CLASSIFICATION OF ABSTRACT Unclassified	20. LIMITATION OF ABSTRACT UL	